# The Institute of Paper Science and Technology

Atlanta, Georgia

## Doctor's Dissertation

**An Overall Model of the Combustion of a Single Droplet of Kraft Black Liquor**

**Katherine A. Kulas**



**January, 1990**

# AN OVERALL MODEL OF THE COMBUSTION OF A SINGLE DROPLET OF KRAFT BLACK LIQUOR

A Thesis Submitted by

Katherine A. Kulas

B.S. 1984, University of New Hampshire

M.S. 1986, Lawrence University

in partial fulfillment of the requirements
of The Institute of Paper Science and Technology
for the degree of Doctor of Philosophy
Atlanta, Georgia



January, 1990

ABSTRACT

Kraft black liquor burns through four distinct stages - drying, volatiles burning, char burning, and inorganic reactions. This thesis presents three models, one for each of the first three burning stages. The models were designed to run sequentially. The output from the drying model is input to the volatiles burning model, and the output from the volatiles burning model is input to the char burning model. Each model was verified with data obtained from the convective single particle reactor (SPR).

Drying was modeled as an external heat transfer limited process. The drop temperature and mass were predicted by simultaneous mass and energy balances around the drop. The model was verified by comparing predicted and measured drop temperatures as a function of time. Low gas temperatures (550°C and 650°C) were used to exagerate the drying time. The predicted drop temperature was within 10% of the measured drop temperature. Model predictions were approximately the same when either an assumed average surface area or the measured dynamic surface area were used in the heat transfer calculations.

Volatiles burning was also modeled as an external heat transfer limited process. A volatiles combustion flame was not observed surrounding single particles burning at typical furnace conditions (<10% $O_2$) in the SPR. Combustion of volatiles near or in the surface pores was included in the model. Volatiles burning ends when the particle has swollen to its maximum size, and this diameter can be empirically predicted from the initial dry mass. As the break point between drying and volatiles burning is impossible

to measure experimentally, the two models (drying and volatiles burning) were combined to predict the time to maximum volume. The regression between predicted and measured time to maximum volume had an $r^2$ of 0.82. The rate of volatilization was accurately predicted by the model. The model fit the data over the entire oxygen range tested (0%-21%).

Char burning was modeled as limited by oxygen mass transfer to the char surface. The carbon consumption reactions considered were the carbon/sulfate, carbon/oxygen, and carbon/carbon dioxide reactions. The presence of the sulfate/sulfide cycle in char burning was established through tests with pure soda liquor and soda liquor loaded with sodium sulfate. The char burning model accurately predicted the time for char burn (from maximum volume to smelt coalescence) for both kraft and soda liquors.

TABLE OF CONTENTS

APPENDICES

# INTRODUCTION

Chemical recovery is an integral part of the kraft pulping process. During chemical recovery, the cooking chemicals are regenerated and steam, used millwide, is generated. The pulping process produces both pulp and a weak black liquor containing water, organics, and inorganics. The pulp continues on to the papermaking process. The weak black liquor is concentrated into strong black liquor, approximately 65% solids, which is burned in the recovery boiler. The black liquor is sprayed into the boiler, and the drops average 1 mm to 3 mm in diameter. The organic fraction is oxidized to produce energy for steam generation. The inorganic fraction is reduced in the char bed on the floor of the boiler to recover $Na_2S$, a pulping chemical, and $Na_2CO_3$, in the form of smelt. The smelt exits the boiler through smelt spouts, and dissolves in an aqueous stream to form green liquor, which is causticized, converting $Na_2CO_3$ into NaOH. The regenerated cooking chemicals, $Na_2S$ and NaOH, then return to the digester to be used again in pulping.

The recovery boiler is often the bottleneck in the pulp mill. Increments in pulp production eventually force the recovery boiler to operate at full capacity, often as much as 30% above the rated capacity.[1] Recovery boilers are very expensive and economies of scale favor the use of large, high capacity units rather than a number of small units.[2] Over the last 40 years, the trend in pulp mills has been to use a single large boiler. This ties pulp production closely to recovery boiler productivity. Because of this close tie, knowledge of how black liquor burns and the factors affecting burning are very important in effective boiler operation,

and ultimately pulp mill operation.

Black liquor drops burn through four distinct stages:[3,4] drying, volatiles burning, char burning, and inorganic reactions. Drying is the evaporation of water from black liquor as a result of heat transferred to the drop. During drying, the drop is continually swelling and releasing gas, or bursing. Volatiles burning consists of volatiles evolution and combustion. During volatiles burning, sustained swelling of the particle occurs. The removal of the volatiles converts the dried black liquor solids to a char containing inorganics and carbon. The char carbon is consumed during char burning. When the carbon content is sufficiently low, the char structure collapses and the inorganics, in the form of molten smelt, coalesce. Inorganic reactions occur after smelt coalescence, and consist of oxidation of the smelt, i.e. sulfide to sulfate. The stages overlap slightly, especially in the larger drops. Throughout this thesis, the term 'drop' refers to the wet liquor and the term 'particle' refers to the dry drop.

Single particle reactors have been used to study black liquor combustion.[3,5-9] Two types of single particle reactors were used for these studies, suspended and flowing. In the suspended type reactors, individual drops are held stationary throughout combustion on wires. Drops are sprayed into the flowing reactors, and burn while passing from one end of the reactor to the other. The advantage of studying captive single particles, as opposed to moving particles, is that changes in particle mass, temperature, and size can be observed throughout combustion for the same particle. The observations (drop mass, temperature, and size) can

then be correlated. Preliminary investigations using single particle reactors yielded information on the stages of combustion, and empirical correlations for each stage.

Based on the single drop studies, several models for black liquor combustion have been proposed.[10-13] These models are good preliminary models and give an estimate of combustion times and other key factors in combustion. The purpose of this thesis is to develop detailed models, based on engineering fundamentals, for each stage of black liquor single particle combustion, validated with data from the single particle reactor at The Institute of Paper Chemistry.

# LITERATURE REVIEW AND ANALYSIS

## BLACK LIQUOR

Studies of single particle combustion, that is the technique of studying the combustion behavior of a single particle of fuel and extrapolating the results to sprays of fuel, has been used in the conventional fuel industry for many years. This technique was first applied to the paper industry in 1963 by Monaghan and Siddall,[5] with the objective of determining the applicability of this method to the study of spent pulping liquors. They measured the ignition delay and the burning time for 2 mm diameter drops of sulfite liquor suspended on a silica wire in a non-convective furnace. The air temperature inside the furnace ranged from 550°C to 800°C. They concluded that combustion of single particles in a controlled atmosphere was an effective method of studying black liquor combustion, as both qualitative information in visualizing combustion and quantitative information in the burn times were available.

In 1985, Hupa et al.[3] reported findings on the burning behavior of single particles burned with a variety of initial conditions. The initial drop diameters ranged from 0.5 mm to 2.5 mm, and the air temperature inside the muffle furnace ranged from 600°C to 900°C. Films were taken of each test and four burning stages (drying, volatiles burning, char burning, and inorganic reactions) were defined from visual events.

Drying, the evaporation of water from the drop and the heating of the dried solids to pyrolysis temperatures, began when the drop was inserted into the hot furnace and ended at the appearance of the first

flame, or ignition. Volatiles burning, consisting of volatiles evolution and combustion, began at ignition and ended when the yellow flame surrounding the particle disappeared. This usually coincided with the particle reaching its maximum swollen volume. Either reference point, flame disappearance or maximum swollen volume, was used to mark the end of volatiles burning. The yellow flame only appeared when the furnace temperature was above 600°C. Char burning consumed the char carbon formed during volatiles burning and began at either the point of maximum swollen volume or the disappearance of the yellow flame, and ended at smelt coalescence, the collapse of the char matrix into a smelt bead. Inorganic reactions, the last stage of black liquor combustion, occurred after smelt coalescence and included all the oxidation reactions of the inorganics in the smelt, and fuming. Hupa et al. did not investigate the inorganic reactions stage. In this thesis, pyrolysis refers to volatiles evolution in a nitrogen environment.

Hupa et al. measured the time to complete each of the first three burning stages - drying, volatiles burning, and char burning. They reported that the initial drop diameter had a large influence, and the gas temperature had a smaller influence, on the total burning time. This is shown in Table 1. When the initial diameter of the drop was increased from 1.0 to 1.5 mm, the ratio of external surface area to drop mass decreased by 33%. If drying is driven by external heat transfer, then an increase in drop diameter should result in an increase in drying time, and an increase in gas temperature should result in a decrease in drying time. This agrees with Hupa's observations, suggesting that external heat transfer is important in drying. If all the heat transferred to the drop is assumed to

be through radiation from the muffle furnace walls, then a 300°C increase in gas temperature should result in a 300% increase in heat transferred through radiation, resulting in a drying time decrease. The measured drying time for a 1.5 mm drop decreased from 3 seconds at 600°C to 0.8 seconds at 900°C.

Table 1. Effect of initial diameter and gas temperature on drying, volatiles burning, and char burning times.[3]
+ denotes increase in time and - denotes decrease in time.

| | Drying | Volatiles Burning | Char Burning | Total |
|---|---|---|---|---|
| Increase diameter from 1.0 mm to 1.5 mm at 800°C | + 50% | + 87% | + 100% | + 71% |
| Increase gas temperature from 600°C to 900°C for 1.5 mm drops | - 73% | - 33% | - 44% | - 57% |

The influence of the diameter increase on the time was reported to be large for both volatiles burning and char burning. The physical meaning of this influence is difficult to quantify because of particle swelling. During volatiles burning, the particle surface area increased dramatically, but no relation was reported between the initial diameter and the swollen diameter. The surface area throughout volatiles burning and char burning was therefore impossible to calculate. The influence of furnace temperature on the volatiles burning and char burning stages was low. Hupa *et al.*[3] concluded that the particle temperature was determined by the heat generated in combustion. The furnace temperature only influenced the drying time, before the volatiles began to burn.

Swelling

Swelling of kraft black liquor during pyrolysis and combustion is well documented[3,14-16] but is not well understood. A certain unknown amount of swelling is desired for effective combustion in the recovery boiler.[17] The furnace and compositional conditions which influence swelling have been determined, although a predictive equation for swelling has not been developed. Hupa et al.[3] and Noopila et al.[16] measured the amount of swelling for liquors burned in air; Miller[14,15] measured the amount of pyrolysis swelling in nitrogen.

Miller[14] investigated the influence of physical factors (gas temperature, 300°C - 900°C; solids level, 65% - 100%; initial liquor mass, 2 mg - 100 mg; and heating rate, 18000 $W/m^2$ - 106000 $W/m^2$) on pyrolysis swelling in a convective environment. The two factors with the largest influence on the swollen volume, normalized on the initial dry mass, were the gas temperature and the liquor solids content. The maximum swollen volume vs. temperature relation went through a maximum at 500°C for all the liquors tested. The maximum swollen volume at 300°C was approximately 20 cc/g. dried solids for all liquors, and at 900°C it was approximately 30 cc/g. dried solids. At 500°C, the 65% solids liquor swelled to the largest volume, 210 cc/g. dried solids, while the 100% solids liquor swelled to 90 cc/g. dried solids, indicating that drop moisture had a large influence on the maximum swollen volume. When they performed pyrolysis tests in steam with dried liquor, the maximum swollen volume did not increase significantly over the volume obtained by pyrolysis in nitrogen. Apparently, to promote swelling moisture is needed in the original liquor

and is not absorbed from the surrounding gas. This indicates that drying influences the magnitude of the maximum swollen volume.

There was a great deal of scatter in the reported results.[14] At 700°C, 40 mg of 65% solids black liquor swelled in 13.0 ± 2.6 seconds to 68 ± 40 cc/g. dried solids. This variability could not be explained and casts doubts on their absolute results, although the general trends are valid. Miller[14,15] concluded that pyrolysis gases drove the swelling process, and that the physical properties of the particle controlled the degree of swelling. At temperatures above 500°C, the maximum swollen volume decreased because the char was formed faster, decreasing the plasticity of the surface. The pyrolysis gases then escaped through cracks in the char layer instead of pushing the whole surface out.

Swelling during combustion was studied by Hupa et al.[3] and Noopila et al.[16] Both studies compared the time for char burning to the degree of swelling the particle underwent, for single drops burned in a non-convective air environment at 800°C. Hupa et al. reported a volume expansion of 10-30 times the initial volume during volatiles burning for kraft liquors. They noted for a variety of mill kraft and sulfite liquors an inverse relation between the swollen volume and the char burning times. The data they reported showed this to be true on the average, although the highest swelling liquor had the longest char burn time. No explanation was given for this discrepancy.

The combined result of these four studies is that kraft black liquor particles swell to a greater extent in nitrogen than in air, and that there is a great deal of variability in the swollen volume. No

predictive equation for either the time to finish swelling or the maximum swollen volume has been developed. Oxygen in the gas influences swelling, although no work has been done with oxygen concentrations below 21% (air).

Drying

Drying of black liquor drops at boiler conditions is a complex process. The drop is subjected to variations in temperature and heat flux which can cause uneven drying and the formation of local hot spots. These hot spots will pyrolyze and possibly begin char burning before the remainder of the drop has dried. High temperatures cause the drops to dry rapidly, making them difficult to study. Because of the possibility of pyrolysis and the rapidity of moisture loss, drying at high temperatures has not been investigated in any detail. Low temperature drying of single drops of kraft black liquor was studied by Robinson and Clay.[9] The drops were formed with a microsyringe, on a thermocouple bead connected to a microbalance, and dried in a convective air flow at 167°C, below pyrolysis temperatures. The data collected were drop mass, drop temperature, and visual observations via videos, as functions of time.

Robinson and Clay[9] modeled drying with an energy balance, which included convection from the flowing gas, conduction through the thermocouple wire, and radiation from the reactor walls. The dominant mode of heat transfer was convection. They assumed the drop was isothermal, but because the measured temperature and mass did not satisfy the energy balance, they determined that a temperature gradient had to exist inside each drop. They included an assumed surface temperature profile and conduction within the drop to fit the model to their data. Based on the

calculated temperature gradients, they postulated that significant temperature gradients would occur in drops drying in the recovery boiler.

Volatiles Burning

Volatiles burning consists of volatiles evolution and combustion. Single particle studies of the volatiles burning stage have resulted in insight into the physical factors affecting the time for volatiles burning[3] and the rate of volatilization.[6,7,18] These studies resulted in one empirical equation for the rate of volatilization, normalized on the initial dried solids, as a function of initial drop size and gas composition.[7] The influence of swelling was not explicitly included.

Clay and Ragland[6] measured the rate of mass loss for black liquor pellets (90 mg - 275 mg, 80% - 100% solids) suspended from a microbalance in an upflow hot gas (700°C - 900°C, air or nitrogen). The rate of mass loss is the slope of the mass vs. time curve, which is linear with time. The liquor was spray dried before pelletizing. Water was added to the dry liquor to obtain the 80% solids liquor. The total reaction time, defined as the time between the start of the test and when the rate of mass loss reached zero, was also measured. In the case of the tests run in nitrogen, the total reaction time included drying and pyrolysis. In the air experiments, the total reaction time included drying, volatiles burning, and char burning. Thus, the reaction times and the rates of mass loss from the air experiments and the nitrogen experiments can not be compared.

Clay and Ragland[6] reported that the rate of mass loss was a function of gas composition, gas temperature, and particle size. The

effect of gas composition (air or nitrogen) is an artifact of the method of defining the rate of mass loss, and the actual effect of gas composition on black liquor combustion is unclear. Approximately twice as much mass was lost in the air experiments as in the nitrogen experiments, because the air experiments had an additional stage, char burning. The liquor solids content had a small influence on the rate of mass loss. Clay and Ragland postulated from their data that the particle temperature had a large influence on the rate of mass loss.

Variability was reported in the mass loss data.[6] For 2 mm diameter pellets of 80% solids liquor pyrolyzing at 700°C, the rate of mass loss normalized on the initial dried solids was 4.2 $sec^{-1}$ ± 1.0 $sec^{-1}$. This variability could be due to particle swelling. They did not report any of the maximum swollen volumes, although they did note that greater swelling was observed in nitrogen than in air. They made no attempt to interpret the data in terms of observed physical events.

Moreland and Clay[18] investigated the effect of initial drop moisture on kraft black liquor combustion. The solids content in the drops ranged from 68% to 100%, and combustion was in a 600°C downflowing air stream. The liquor for each test was contained in a bucket in an attempt to provide uniform drag for the mass measurements. They defined a variable called char reactivity as the maximum slope of the mass vs. time curve. It is not clear what char reactivity refers to in terms of physical events. The char reactivity appeared to decrease slightly with decreasing initial drop moisture, although with the scatter in the data it is unclear whether this is a statistically significant decrease. The scatter is not

explained, although it could result from the arbitrary method of determining the char reactivity.

A dewpoint hygrometer was used to determine the level of water vapor in the off-gas. Moreland and Clay[18] reported that they could not measure the amount of water evolved in a test, but they could determine when water evolution ended. For all the liquors tested, water evolution ended at the start of char oxidation. No attempt was made to quantify the effect of initial moisture on swelling.

An empirical equation for the rate of volatilization was developed by Kulas and Clay[7] for single particles burned in a downward flowing hot gas. The drops (4 mg - 41 mg) were suspended on a microbalance to measure the mass throughout combustion. The gas temperatures ranged from 660°C to 860°C and the gas composition ranged from 0% oxygen to 21% oxygen with the balance nitrogen. The rate of volatilization is the slope of the measured mass vs. time curve between the points of ignition and maximum volume, and was normalized on the initial dried drop mass. In all the tests this region was linear with time. The statistically derived equation is

$$dm'/dt = 1.634/d_i + 0.034\ C_{O2}/d_i - 0.0054\ C_{O2} - 0.316 \qquad (1)$$

where $dm'/dt$ = rate of mass loss normalized on initial dried solids, $sec^{-1}$

$d_i$ = initial drop diameter, mm

$C_{O2}$ = percent oxygen in gas stream

The $r^2$ for the regression was 0.85. The data indicate that the influence of oxygen on the normalized rate of volatilization is greater for the

smaller drops (10 mg or 2.4 mm diameter) than for the larger drops (40 mg or 3.8 mm diameter). The scatter in the data was attributed to the variation in the gas temperature. Equation (1) predicts the normalized rate. To convert to the actual rate of volatilization, both sides of Equation (1) need to be multiplied by the initial dried mass, which is a constant times the cube of the initial diameter (assuming constant density). The rate of volatilization is then a function of the initial surface area.

Equation (1) is in terms of the initial drop diameter. No attempt was made to include the effects of swelling or the actual surface area during volatiles burning in the analysis. Equation (1) predicts the rate of volatilization accurately within the bounds of the experimental conditions, but the terms included have statistical, and not physical, significance.

Char Burning

The release of volatiles from dried black liquor produces a char containing inorganics and fixed carbon. In a laboratory study of char burning,[19] 34.3% of the initial solids were lost during volatilization. Table 2 lists the composition of the original solids and the resulting char. The original composition was calculated from the char composition and the percent loss of each element. They used a flowing type reactor with the black liquor sprayed into the top and collected as char at the bottom in a char bed. This work gives an indication of the composition of char formed from pyrolysis of black liquor drops.

Table 2. Composition of black liquor solids and the resulting char before bed burning.[19]

| Component | Black Liquor Solids (%) | Char Bed (%) | Lost as Volatiles |
|---|---|---|---|
| Carbon | 34.2 | 24.9 | 53.3 % |
| Hydrogen | 3.0 | 0.6 | 87.9 % |
| Oxygen | 35.3 | 35.0 | 36.4 % |
| Sulfur | 4.8 | 4.2 | 44.4 % |
| Sodium | 18.7 | 29.2 | 0.0 % |

Milanova and Kubes[17] used simultaneous thermogravimetric and differential thermal analysis to measure kraft char combustion. A known amount (3 mg - 10 mg) of ground black liquor solids was placed in a plate crucible, pyrolyzed in an oxidative atmosphere at low temperature (200°C - 450°C), and then burned. The temperature at which the char ignited, or the start of char burning, and the time for char burning were measured. They varied the sample size, oxygen content in the gas atmosphere (stagnant air or 5% oxygen with carbon dioxide and nitrogen in flowing gas), and heating rate (20°C/min or 50°C/min). They also looked at the effects of swelling and NaCl addition to the original liquor.

The ignition temperature of the char ranged from 580°C to 780°C and was a function of the NaCl content. Addition of NaCl lowered the melting point of the kraft smelt. The char burn time was a function of the NaCl content and the degree of swelling. From this they concluded that the "presence of inorganics in a liquid or softened state may be beneficial for carbon burning".[17] They also noted a weight increase at the end of kraft char burning which was attributed to the oxidation of $Na_2S$.

Carbon is consumed through several competing reactions. Reactions (1), (2), and (5) have been studied individually to determine the reaction kinetics. Reactions (3) and (4) have not been studied with kraft char but have been investigated for coal char.[20] Reaction (6) will be neglected in this work because the water vapor has been swept away after drying and volatiles evolution and will not be a factor in char burning. Moreland and Clay[18] reported that no water vapor was detected at the beginning of char oxidation of single particles in a convective environment. Water vapor could play a role in char combustion in the recovery boiler char bed.

$$Na_2SO_4 + 4\ C \Rightarrow Na_2S + 4\ CO \qquad \text{(Rxn. 1)}$$

$$Na_2SO_4 + 2\ C \Rightarrow Na_2S + 2\ CO_2 \qquad \text{(Rxn. 2)}$$

$$2\ C + O_2 \Rightarrow 2\ CO \qquad \text{(Rxn. 3)}$$

$$C + O_2 \Rightarrow CO_2 \qquad \text{(Rxn. 4)}$$

$$C + CO_2 \Rightarrow 2\ CO \qquad \text{(Rxn. 5)}$$

$$C + H_2O \Rightarrow CO + H_2 \qquad \text{(Rxn. 6)}$$

$$Na_2S + 2\ O_2 \Rightarrow Na_2SO_4 \qquad \text{(Rxn. 7)}$$

Reactions (1) and (2), sodium sulfate reduction with carbon, have been studied by Thorman and Macur[21] and by Grace *et al.*[4,8,22] Thorman and Macur reacted activated carbon particles (0.41 mm - 0.47 mm diameter) in an agitated molten salt pool containing $Na_2SO_4$. The temperature of the smelt pool was varied between 644°C and 794°C. They monitored the CO and $CO_2$ concentrations in the off-gas to determine the extent of reaction. They developed an Arrhenius type expression for $Na_2SO_4$ consumption, Equation (2), which was pseudo zero order in $Na_2SO_4$ and 0.31 order in carbon.

$$- d[SO_4]/dt = A \exp(-Ea/RT)\ [SO_4]^0\ [C]^{0.31} \qquad (2)$$

where $[SO_4]$ = sulfate concentration

$[C]$ = carbon concentration

A = pre-exponential factor

Ea = activation energy

R = gas constant

T = temperature

The use of an agitator enabled them to use small carbon particles. Other investigations of this type used gas spargers to mix the carbon, salts, and gas. The activated carbon is light enough to easily entrain in the gas stream when a sparger is used. This is not a problem with a mechanically agitated system. When mechanical agitation was used,[21] the reaction rate was dependent on the speed of agitation until the agitator tip speed exceeded 0.33 m/sec. The reaction rate was limited by mass transfer at low agitation speeds and by kinetics at higher agitation speeds, where the rate was independent of tip speed. The data used in Equation (2) was from the kinetic limited region.

Grace et al.[4,8] also studied sodium sulfate reduction with carbon. They took the reaction sequence a step further by postulating that the sulfide formed by Reactions (1) and (2) is oxidized to form sulfate via Reaction (7), and the sulfate is then consumed through Reactions (1) and (2). This is the sulfate/sulfide cycle. The premise of this cycle is that the molten salts, $Na_2SO_4$ and $Na_2S$, act as a carrier to bring the oxygen into contact with the char carbon. The sulfate/sulfide cycle also "permits simultaneous sulfate reduction and carbon consumption in the presence of an

oxygen containing atmosphere, as long as the rate limiting step during char burning is oxygen mass transfer to the burning char".[8] Reaction (7) is much slower than Reactions (1) and (2), causing the smelt to be mainly composed of $Na_2S$. The sulfate/sulfide cycle was shown to operate in char pile combustion.[23]

The kinetics of Reactions (1), (2), and (7) were investigated with a smelt pool reactor in the temperature range of 870°C - 980°C.[24] Samples of kraft char, soda char or pulverized graphite rods were mixed with molten salts by a gas flow through a sparger. Sulfide oxidation, Reaction (7), was limited by mass transfer of oxygen as long as the reduction ratio (mol $Na_2S$/(mol $Na_2S$ + mol $Na_2SO_4$) was above 2 percent. In developing Equation (3) for the rate of sulfate consumption, it was assumed that the total amount of sodium and sulfate present in the char was constant throughout burning (no fuming).[22] The only gases monitored were $O_2$, CO, and $CO_2$.

$$- d[SO_4]/dt = K_1 \left( [SO_4]/(K_2 + [SO_4]) \right) [C] \exp(-Ea/RT) \qquad (3)$$

$K_1$, $K_2$, and Ea are kinetic constants which depend on the carbon source. Equations (2) and (3) are in the same general form. For large sulfate concentrations, $[SO_4]/(K_2 + [SO_4])$ is equivalent to $[SO_4]^0$. The biggest difference between the two equations is the magnitude of the carbon concentration effect. Thorman and Macur[21] found the order to be 0.31 on carbon while Grace et al.[8] found the order to be 1.0 on carbon. The difference could be from the different methods of mixing; agitation compared to bubbling gas. Thorman and Macur reported that the rate of reaction in their system was a function of degree of agitation. Thorman

and Macur were able to use a higher amount of carbon loading than Grace et al. The carbon concentration is more important at low concentrations, explaining why Grace's reaction order was higher (1.0 compared to 0.31). Another difference between the two is the source of carbon. Thorman and Macur burned activated carbon with a large specific surface area while Grace et al. burned kraft char, soda char, or pulverized graphite rods, all with lower specific surface areas. Because the carbon source Grace et al. used is more representative of single particle combustion, their kinetic expression will be used in this thesis.

Reactions (3) and (4), oxidation of carbon with oxygen, have not been investigated for black liquor char. The closest work was done with coal chars and is summarized in Smoot and Smith.[20] The kinetics are discussed in detail in the char burning section of this thesis.

Reaction (5), carbon oxidation with carbon dioxide, has been studied by Li and van Heiningen[25] and Goerg and Cameron.[26] Li and van Heiningen pyrolyzed ground black liquor solids inside their reactor, and introduced $CO_2$ into the gas stream to begin char burning. The carbon dioxide reacted directly with the char carbon, no molten salts were initially present. Goerg and Cameron bubbled $CO_2$ through a molten salt pool containing a small amount of ground kraft char. Both investigations yielded kinetic expressions of the same general type, Equation (4).

$$-\frac{d[C]}{dt} = \frac{K_1 \, p_{CO2} \, [C]}{1 + K_2 \, p_{CO2} + K_3 \, p_{CO}} \exp(-Ea/RT) \qquad (4)$$

$K_1$, $K_2$, and $K_3$ are kinetic constants, and $p_{CO2}$ and $p_{CO}$ are partial

pressures of $CO_2$ and CO respectively. In single particle combustion, the majority of the char carbon is exposed directly to the combustion gases. The system used by Li and van Heiningen[25] is more representative of single particle combustion, and their kinetic constants will be used in this thesis, as is described in the char burning section.

## MODELS FOR SINGLE PARTICLE COMBUSTION

The next step in analyzing black liquor combustion is to develop models from the available pool of knowledge. Several models have been proposed for recovery boiler combustion and include sections on single particle combustion.[10-12] One model has been developed for single particle combustion which is not in conjunction with a boiler model.[13]

The first single particle model for kraft black liquor was developed by Merriam[10] as part of a total computer model for the recovery furnace. Drying and volatiles burning occurred in the drops after they were fired into the furnace, and char burning occurred solely on the bed. Drying was modeled as a receding liquid front surrounded by a porous solid shell. The effects of swelling and deflation as the gases were released, or bursting, were not included. The drop was assumed to be dry when the radius of the liquid portion was zero. Pyrolysis was modeled as a system of first order reactions with a single rate constant. This method had been successfully used in pulverized coal pyrolysis. The particles were assumed to be isothermal to simplify the calculations, and the activation energies were determined from a Gaussian distribution. Volume expansion due to swelling was assumed to be linear with time, and the particle volume after drying and after pyrolysis were input parameters to the model. The model

was not compared to experimental data.

Shick[11] developed a model to simulate the recovery furnace processes by extending the Merriam[10] model. The simplifying assumptions he made were that the time for each stage of burning was based on the initial drop diameter, that the end of each stage was determined by the appropriate relative mass as compared to the initial dry mass, that swelling is linear with mass consumption up to a user input expansion value, that drying and pyrolysis were heat transfer controlled, and that no heat was conducted within the particle, i.e. isothermal particle. He also assumed that the rate of mass loss during drying was half of the rate of pyrolysis mass loss. He adjusted the parameters to make the model give partial agreement to data reported in the literature.[3]

Shick's model[11] was a two-dimensional model which demonstrated the effects that changes in firing and boiler conditions had on particle combustion. His model did not address the fundamental processes which occur in black liquor combustion.

Walsh[12] developed a single particle model which when combined with models by Sumnicht[27] and Jones[28] simulated a recovery boiler. Walsh's three-dimensional model combined single particle combustion with a trajectory analysis to predict the condition and the location of black liquor drops sprayed into the furnace. Sumnicht's model analyzed the char bed. Jones's model predicted the gas flows and tied the three models together.

Walsh[12] modeled drying as an external heat transfer limited process. The expansion during drying was an input parameter. At times less than 0.2 seconds the drop diameter was the initial diameter and at times greater than 0.2 seconds the drop diameter was the initial diameter times an expansion factor, usually set at 1.5. The temperature of the drop was assumed to remain constant throughout drying at the water boiling temperature in the liquor, 127°C, and the drop was assumed to be isothermal throughout drying. Drying ended when the drop reached a specified solids content.

Volatiles burning started when the particle reached the specified solids content. The model[12] calculated the mass of the particle at any time using Equation (1), developed by Kulas[7] and described earlier in this literature review. Particle expansion was calculated with an input expansion factor, and the maximum expansion was assumed to occur at the end of volatiles burning. The degree of expansion at any time was a function of the dried solids left to undergo volatiles burning. The temperature of the particle was also assumed to increase as a function of the dried solids. At the end of volatiles burning the particle was at the gas temperature. The particle model did not account for volatiles combustion.

Char burning started when volatiles burning was complete. The rate of mass loss was assumed to be a function of the oxygen mass transfer to the particle surface. The particle shrank as the 1/3 power of the char mass fraction remaining to react. The diameter of the smelt bead in relation to the initial drop diameter was another input parameter.

In Walsh's model[12] an attempt was made to model each stage from theoretical considerations. However, a great deal of empiricism entered the analysis in the temperature/time and diameter/time relationships. This was particularly true in the treatment of volatiles burning, which is completely based on an empirical equation.

The last model, by Frederick et al.,[13] is strictly a single particle combustion model with no ties to a boiler simulation. This model is very similar to the model by Walsh[12]. Drying was assumed to be limited by external heat transfer, and the heat transferred to the drop was used to evaporate the water and to heat the drop to the final temperature. Expansion during drying was held to a constant value, assumed to be the initial diameter times an expansion factor. The expansion factor was an input parameter usually set equal to 1.5. Drying was assumed to end at a specified solids content.

The only values calculated by Frederick et al.[13] were the times for each stage. The times for drying and volatiles burning were assumed to be functions of the total heat necessary to complete each stage, and the amount of heat used at any time. The time for char burning was a function of the total amount of oxygen needed to completely burn the assumed carbon content in the char, and the amount of oxygen which had reached the char surface at any time.

Particle expansion during volatiles burning was assumed to follow a power-law relation with the heat transferred to the drop divided by the total heat needed for volatiles burning. The expansion factor, the maximum diameter/initial diameter, was an input parameter. The surface temperature

of the drop was calculated from a similar expression with the final temperature set at the gas temperature. Particle shrinking during char burning was handled in a like manner, although the mass of oxygen reacting with the char carbon was used instead of the heat to volatilize the particle.

The model fit data reported by Hupa[3] reasonably well. The model was based on engineering fundamentals, although like Walsh's model,[12] it included many simplifying assumptions. The input parameters - expansion values for each stage, solids content at ignition, and temperature/time relationship for each stage - all point out the need for a better understanding of the stages of black liquor combustion.

OTHER FUELS

In the burning of liquid fuels, combustion does not begin until enough fuel vapor has evaporated to reach spontaneous ignition conditions. The burning stages do not parallel black liquor very closely. The importance of liquid fuel burning to the modeling of black liquor burning is that single drop studies were first done with liquid fuels, and theoretical models are most simple with liquid drops. During evaporation and combustion, the liquid fuel drops shrink uniformly, are nearly spherical, and upon completion of burning no ash is left.

The combustion of coal can be divided into two stages, volatiles burning and char burning. Swelling may occur during volatiles burning but not to the same degree as black liquor. Not all the original coal is consumed during burning, as ash is left at the end of char burning. Coal

slurries are suspensions of pulverized coal in a carrier fluid, usually oil or water. Most coal slurries behave like a Number 6 fuel oil. Coal-water slurries burn like black liquor, undergoing drying, volatiles burning, char burning, and ash extinction (instead of inorganic reactions).

A great deal of work has been done with coal, coal slurries, and liquid fuels. The majority of the work is based on the Nusselt relation that combustion time is proportional to the square of the initial particle diameter.[29] Nusselt derived the diameter squared law for a single particle of non-swelling coal dust burning in an infinite atmosphere. He assumed that if the burning rate was controlled by a diffusional boundary layer around the particle, then the burning time, $t_b$, is proportional to the square of the initial particle diameter, $d_i$, Equation (5). This was experimentally shown for liquid fuel[30] and extrapolated for coal-oil slurry,[31] Equation (6). The drop diameter at extinction, $d_o$, was added to the diameter squared law to account for the ash left after coal combustion. The diameter squared law is equivalent to the law of evaporation for fuel drops, and has been theoretically derived for liquid fuel.[30,32]

$$d_i^2 = k_b t_b \qquad (5)$$

$$k_b = (d_i^2 - d_o^2)/t_b \qquad (6)$$

Hayhurst et al.[33] rigorously derived $k_b$ for a liquid oil drop and calculated the temperature of the flame front surrounding the drop. The equations assumed that the drop surface area was shrinking at a constant rate. No provisions were made in the model for a surface area which does not decrease linearly with time. Black liquor swells as it burns. The

surface area of a black liquor particle increases during the time when it should decrease to follow the $d^2$ law. Therefore, black liquor combustion, especially volatiles burning, goes against a key assumption in Nusselt's development.[29] The diameter squared law which, was successful in predicting combustion times for non swelling fuel drops, does not apply to black liquor combustion.

Models for single particle coal combustion are varied.[34-39] Most of these models treat volatiles burning as limited by external heat transfer and char burning as limited by oxygen diffusion. Several of the models make an attempt to describe the volatiles combustion flame.[36,37]

Timothy et al.[34] burned single particles of coal in a downflow reactor. The particles were injected at the same velocity as the hot gas stream (1000°C - 1400°C). Data obtained as the particle passed by the viewport were the particle temperature, measured with an optical two-color pyrometer, and the surface area, estimated from the pyrometer output. The surface area was assumed to remain constant throughout volatiles burning and to decrease linearly with time during char burning. They developed a diffusion limited model to predict the burn times. The model successfully predicted the burn time for bituminous coal burned at 1000°C, but underpredicted the burn time by a factor of 2 for bituminous and lignite coal particles burned at 1400°C. The underprediction was rationalized as due to an ash layer surrounding the particle.

An analytical model of volatiles evolution and swelling for pulverized coal (0.01 mm - 0.1 mm diameter) was derived by Melia and Bowman.[35] Multiple first order reactions were allowed for volatilization

with the pre-exponential factor and volatile fraction assumed to be the same for each reaction. The activation energies were assumed to follow a Gaussian distribution. Swelling was modeled using three assumptions: the internally generated pyrolysis gas provided the driving force for swelling; the pores provided the escape path for the pyrolysis gas; and the increase in particle size was due to increased pore diameters which relieved the internal pressure. The predicted swelling matched with available data when an upper temperature limit was assumed. When the particle's temperature exceeded this temperature, no more swelling was allowed to occur. An assumed temperature for the start of swelling was an additional model parameter. These two temperatures were coal specific.

The two models which include the flame sheet surrounding the burning pulverized coal particle are by Jost et al.[36] and Gururajan et al.[37] Jost et al. visualized the burning particle as surrounded by an infinitely thin flame sheet which fed heat back to the particle via radiation and conduction. Five equations were used: mass transport of oxygen to the flame sheet; the energy balance of the flame sheet; the energy balance of the particle; the devolatilization rate of the particle; and the enthalpy of combustion on the flame sheet. All of the heat released by volatiles combustion was assumed to occur at the flame sheet. The flame sheet was located at the point where the mass flux of oxygen needed for stoichiometric combustion equaled the mass flux of volatiles. When the oxygen flux was greater than the volatiles flux, the flame boundary moved in towards the particle surface until eventually combustion occurred on the particle surface. When the volatiles flux was greater than the oxygen flux, the flame boundary moved away from the particle surface

until eventually the flame did not influence the particle heat transfer.

The flame sheet model predicted that for gas temperatures below 1200°C, combustion of volatiles had to first occur on the particle surface to raise the particle temperature above the gas temperature. Fast volatilization rates which would support a flame sheet only occurred when the particle temperature was high enough.[40] The model successfully predicted experimental volatiles evolution rates which were measured in a flow tube furnace. Swelling was not included in this model, which makes it difficult to apply to black liquor combustion. The model is complex, and particle diameters changing with time would greatly increase the complexity. The flame sheet model illustrates one method of partitioning the energy released in combustion, and needs to be considered in black liquor combustion models.

The flame sheet model by Jost et al.[36] was simplified into the Diffusion Limited Volatiles Combustion (DLVC) model by Gururanjan et al.[37] The rate of volatiles evolution was described by two competing reactions. Two energy balances around the particle were used, before and after flame liftoff. Flame liftoff occurs when the rate of volatiles evolution is high enough to support a stable flame around the particle. The model calculated the particle mass, the flame radius, the particle temperature, and the flame temperature at any time. The predictions of the model depended strongly on the assumed kinetics of volatiles evolution. The effects of the various parameters (heat of volatiles evolution, particle specific heat, and extent of volatiles combustion) were difficult to quantify due to the kinetic dependency.

Peck and Pollock[38,39] burned coal particles (1 mm - 6 mm diameter) in a levitation reactor. The coal was placed in a vertical jet which was at the appropriate velocity to hold the coal particle stationary. This technique only worked for non swelling coals as swelling disrupted the force balance around the particle. They visually observed the particles and measured the surface temperature with an infrared pyrometer. The combustion model consisted of mass and energy balances around the particle. The carbon consumption was assumed to follow the shrinking core model, and volatiles evolution was assumed to be a first order decomposition. The model accurately predicted the measured particle temperature during the burn. They concluded that the levitation reactor was an acceptable technique to study coal combustion.

Coal-water slurry combustion has been modeled by Murdoch et al.[41] They applied an energy balance to the surface of a single drop of slurry and predicted the drop mass and temperature as functions of time. The balance included the reaction kinetics and oxygen diffusion to the particle surface in the heat of combustion term. A temperature gradient inside the drop, between the assumed surface layer and the drop interior, was included in the model.

The model[41] accurately predicted the experimentally measured mass and temperature for a 1.3 mm diameter drop during the drying and volatiles burning stages. The model did not accurately describe char burning. The temperature predictions were compared to the measured internal temperature (using a thermocouple embedded inside the drop) and the measured surface temperature (using a two-color optical pyrometer). The model did not allow

the drop to swell or shrink, making it not directly applicable to black liquor combustion. The largest drawback to the model is the assumed surface layer. They did not report how they determined the thickness of this layer. The thickness was most likely the adjustable parameter used to fit the model to their data.

The importance of this model[41] to black liquor combustion is that an energy balance was successfully applied to the stages of drying and volatiles burning to predict the drop mass and temperature as functions of time. Coal-water slurries burn similarly to black liquor during those two stages. Therefore an energy balance applied to black liquor, for drying and volatiles burning, will most likely be successful.

SUMMARY

The models for kraft black liquor combustion are empirical in nature and as such are only valid within the bounds of the data they are based on. The modeling of black liquor combustion is evolving in a manner similar to the modeling of other fuels. As the degree of knowledge of the particular combustion phenomena grows, the models are more detailed and less dependent on empirical observations. The current state of knowledge of black liquor combustion is such to support a detailed model for single particle combustion, with additional experimental data.

Data and previous models for black liquor single particle combustion have suggested physical processes which are important for each stage of combustion. Drying has been successfully described by an energy balance around the entire drop at low temperatures, 167°C.[9] It is

possible that a similar balance will accurately describe drying at higher temperatures. Volatiles burning has been described by an empirical equation.[7] Data suggest that key factors in determining the rate and duration of volatilization are the initial particle size, the combustion gas composition, and the swelling, which determines the particle surface area.[3,6,7,14] From these factors, an approach similar to Murdoch et al.,[41] used for single drops of coal-water slurry, could work for black liquor combustion. An energy balance could be drawn around the entire drop, with kinetic and mass transfer considerations contained in the heat of combustion term. As swelling influences black liquor combustion, the model needs to account for the effect of particle swelling.

Data on char burning suggest several reactions which are important in the consumption of char carbon. The carbon reacts with sulfate as part of the sulfate/sulfide cycle,[8] with oxygen directly, or with carbon dioxide.[25] Carbon reactions with water vapor can be neglected in single particle combustion as no water vapor was detected at the start of char burning for a particle in a convective flow reactor.[18] The sulfate/sulfide cycle has been demonstrated to apply in char bed and char pellet burning,[8] and char pile burning,[23] but not in the char burn stage of the combustion of single particles of kraft black liquor. Whether or not the sulfate/sulfide cycle operates in single particles will have to be determined before the mechanism may be included in the char burning model.

The surface temperature of a burning drop has been a key part of several models.[34,38,39,41] The surface temperature has not yet been measured during combustion of black liquor drops. Black liquor models

reported in the literature contain assumed particle surface temperature profiles as functions of time. Experimentally determining the surface temperature will eliminate that uncertainty in this combustion model.

## THESIS OBJECTIVES

Black liquor combustion has not yet been modeled in any depth. Several single particle combustion models have been proposed which make questionable assumptions about the drop burning mechanisms due to a lack of experimental data.[10-13] The objective of this thesis was to propose a detailed model for single particle combustion of kraft black liquor based on engineering fundamentals, mass transfer, heat transfer, and reaction kinetics. Only the first three stages of combustion - drying, volatiles burning, and char burning - were to be modeled. Each stage was to be modeled and validated separately using data generated in the single particle reactor (SPR). The following secondary objectives needed to be accomplished to meet the primary objective:

1. The drying stage was to be modeled using an energy balance coupling the drop mass and temperature.

2. The volatiles burning stage was to be modeled using mass and energy balances drawn around the drop.

3. The char burning stage was to be modeled using all the major carbon consumption reactions. The sulfate/sulfide cycle, $C/O_2$, and $C/CO_2$ reactions were to be considered. Carbon reacting with water vapor would not be considered due to the small amount of water vapor present in the experimental apparatus.

4. A two-color pyrometer was to be constructed to measure the drop surface temperature.

## EXPERIMENTAL APPROACH

The objective for drying was to develop a model which would predict the drop mass and temperature as functions of time. Validation of the model would then be through comparing the predicted and measured drop mass and temperature. The apparatus used in this thesis is discussed in the next section. Since drying occurs rapidly at high temperatures (>700°C), the experiments were run at relatively low temperatures, 550°C and 650°C, with no gas flow. The drop temperature was measured with a thermocouple embedded inside the black liquor drop. The initial size was calculated from the projected area trace from the test video. The mass data was not used because the balance had been failing slowly throughout the thesis experimental work, and was not operational during this stage of the thesis. The mass data was not needed to validate the drying model.

The objective for volatiles burning was to develop a model which would predict the particle mass, temperature, and diameter as functions of time. Validation was then through comparing the measured and predicted rate of volatilization, and the time to finish volatiles burning. The mass measurement data was collected while the balance was operational. The two-color pyrometer does not measure the drop surface temperature, because volatiles combustion between the pyrometer and the drop surface interferes with the measurement. The maximum swollen volume needed to be measured for black liquor combustion under a wide range of conditions to incorporate into the model. The time to finish volatiles burning included both drying and volatiles burning times, as the break point between the two stages is diffcult to measure experimentally.

The objective for char burning was to develop a model which predicted the particle mass, reduction ratio (mol $Na_2S$/mol ($Na_2S$ + $Na_2SO_4$)), and ratio of CO to $CO_2$ as functions of time. The role of the sulfate/sulfide cycle needed to be determined for char combustion of black liquor drops. The effect of sulfur in char burning was determined by loading soda liquor with several levels of $Na_2SO_4$. The data obtained were the char surface temperature (with the two-color pyrometer) as a function of time and test videos. The mass data was not used because the balance was not operational during this stage of the thesis. The model was validated with the time to complete char burning.

## APPARATUS

The apparatus, a convective downflow single particle reactor, used for this work is shown in Figure 1. The gas was heated in an electrical furnace, traveled through an insulated pipe, passed through a flow straightener, and then across the particle. The flowrate of the gas was adjustable up to 100 std. lpm. A damper was used to divert the gas flow while the sample was suspended on a wire connected to the electronic microbalance. The microbalance and the gas analyzers (not used in this work) were connected to an Apple II+ microcomputer with an analog/digital interface. Heat transfer to the sample was through two modes, convection from the flowing gas and radiation from the surrounding heater. A radiant heater was installed inside the reactor to supply a constant amount of radiant heat to the particle. This was especially important in the cases where there was no gas flow. A video was taken of each burn through the optical trench. The times for each stage of the burn were obtained from the videos.

On either side of the optical trench were holes for light pipes to illuminate the particle. The left light pipe was removed to insert the two-color pyrometer fiber optic probe. The two-color pyrometer measures the temperature by ratioing the intensity of light it detects at two wavelengths. It is described in detail in Appendix I.

At the start of each burn the kraft black liquor was weighed and wrapped around the wire (or thermocouple bead) in the approximate shape of a sphere. The black liquor preparation is discussed in Appendix II. A wire coil and screen, the basket, surrounded the sample to provide minimal

drag variations throughout the burning as the drop swelled. The basket/wire arrangement can be seen in Figure 2. Once the drop had been formed the reactor was opened by lowering the lower section. The damper was closed to divert the hot gas so the sample in the basket could be hooked onto the microbalance wire. The reactor was closed and the video camera and the data acquisition system were started. The computer opened the damper, allowing the hot gas to reach the sample at a defined time zero.

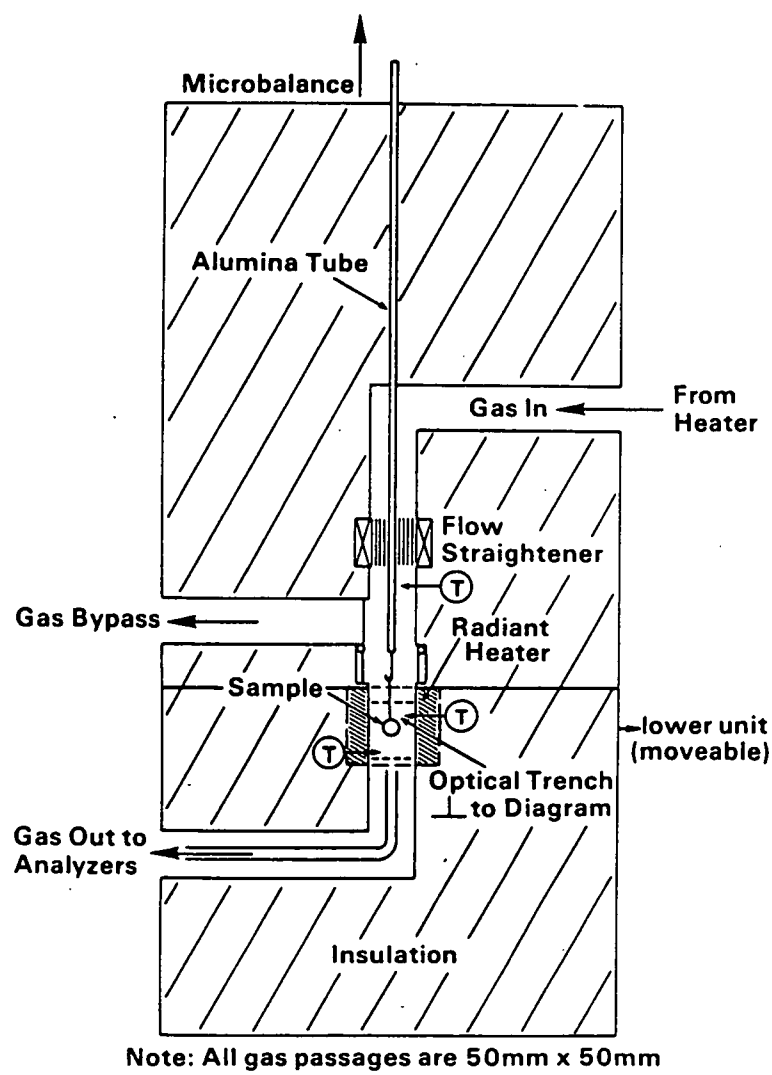


Figure 1. Single Particle Reactor

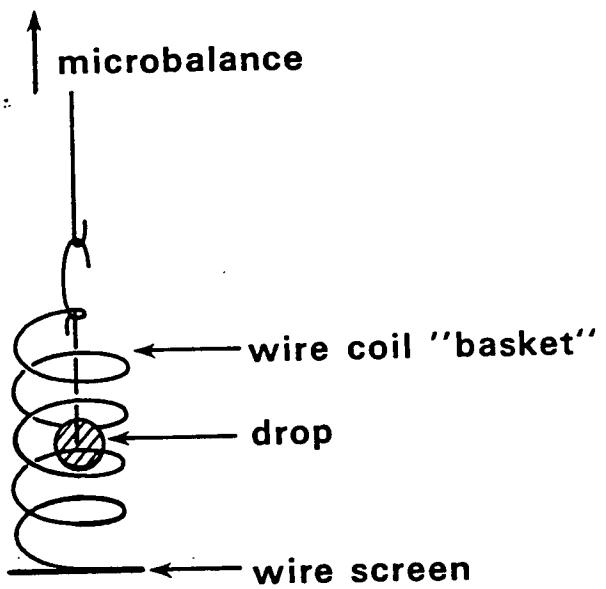


Figure 2. Basket/Wire Arrangement

## DRYING

In the recovery boiler the black liquor drops are sprayed directly into a hot convective environment. Heat is transferred to the drop through convection and radiation from the gas, and radiation from the boiler walls and the surrounding combusting particles. In the single particle reactor (SPR) heat is transferred to a single drop of liquor through convection from the gas and through radiation from the reactor walls. There are no particle interactions in the SPR. The drying model presented here does not include interparticle interactions as it was developed for drops drying in the SPR.

Drying at high temperatures is driven by external heat transfer. The heat transferred to the drop evaporates the water and raises the temperature of the drop. Once the black liquor solids are at pyrolysis temperature, volatiles evolution starts. The drop ignites when the mixture of volatiles and oxygen is at the required concentration and temperature for spontaneous ignition. This required concentration of volatiles and oxygen is not known for black liquor, because the composition of the first volatiles to evolve is not yet known. Ignition is not an automatic response to the loss of water.

Hupa et al.[3] defined the end of drying as the first evidence of ignition. This does not necessarily mean that the drop is dry, or that the drop has just finished drying, at ignition. Ignition is a convenient visual observation which occurs in the first few seconds of the burn, when intuitively drying should be completed. The exact point of the end of

drying water loss is impossible to measure experimentally as water is a pyrolysis product. Mass changes were not measured in Hupa's system, so the drying time could not be measured via mass loss. In the SPR, drying is masked by the balance adjusting to the gas flow and the reactor closing.

Measurement of the amount of water evaporated could be used to indicate the end of drying. Unfortunately, the water vapor measured includes the water vapor originally in the combustion air, the water vapor released during drying, and the water vapor formed during volatiles evolution and combustion. Moreland[18] used a dewpoint hygrometer to measure the water vapor in the off-gas for black liquor combustion in the SPR. At a gas temperature of 600°C, water vapor was detected until char combustion started. Therefore, water vapor measurement is not an accurate method to indicate when the drop is dry.

The drying model developed as part of this thesis predicts both the moisture and the temperature of the drop as functions of time. The model is validated by comparing predicted and observed temperature profiles.

MODEL

A sketch of the drop can be seen in Figure 3. In the sketch, $T_g$ is the gas temperature, $T_w$ is the wall temperature, and $T_d$ is the drop temperature. $Q_{conv}$ is the heat transferred through convection, cal/sec and $Q_{rad}$ is the heat transferred through radiation, cal/sec.

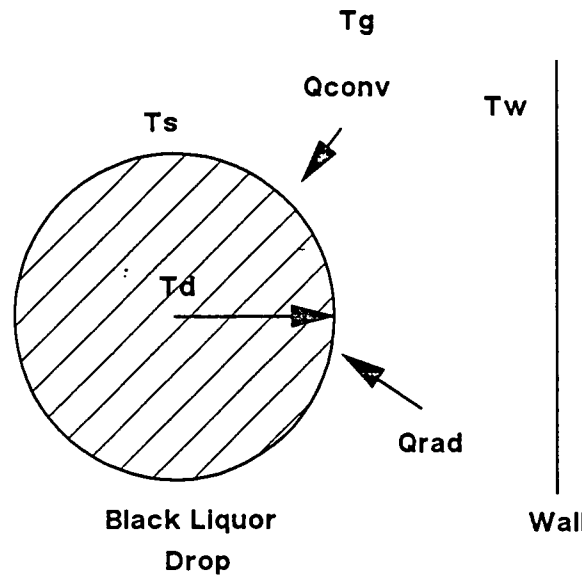


Figure 3. Sketch of the Drying Drop

Equations

The energy balance for drying is

$$Q_{conv} + Q_{rad} - L_w \, dm_{evap}/dt = Cp_d \, m_d \, dT_d/dt \qquad (7)$$

with $$Q_{conv} = h \cdot A \, (T_g - T_d) \qquad (8)$$

and $$Q_{rad} = \sigma \, F_{wd} \, A \, (T_w^4 - T_d^4) \qquad (9)$$

where $L_w$ = Latent heat of water, cal/g $H_2O$

$dm_{evap}/dt$ = amount of water evaporated, g/sec

$Cp_d$ = heat capacity of the drop, cal/g °C

$m_d$ = mass of drop, g

$T_d$ = drop temperature, K

$T_g$ = gas temperature, K

$T_w$ = wall temperature, K

h = convective heat transfer coefficient, $cal/m^2$-s-°C

A = drop surface area, $m^2$

$\sigma$ = Stefan-Boltzmann constant, $1.355x10^{-12}$ $cal/s-cm^2-K^4$

$F_{wd}$ = combination of the view factor between walls and drop, and the particle emissivity

The convective heat transfer coefficient, h, is determined by the Ranz and Marshall correlation for flow past a sphere,[42]

$$Nu = h\ d/k = 2 + 0.6 * Re^{1/2} * Pr^{1/3} \qquad (10)$$

where Nu = Nusselt number

d = drop diameter, cm

k = thermal conductivity of gas, cal/sec-m-K

Re = Reynolds number = D v/$\nu$

v = gas velocity past particle, cm/sec

$\nu$ = kinematic viscosity, $cm^2/sec$

Pr = Prandtl number = Cp $\mu$/k

The cumulative amount of water evaporated, $m_{evap}$, equals $m_{wo}$ - $m_w$, where $m_{wo}$ is the amount of water initially present and $m_w$ is the amount of water in the drop at time t. Differentiating both sides with respect to time, $dm_{evap}/dt = - dm_w/dt$. The heat stored in the drop can be partitioned between the solid and the liquid fractions as $Cp_d\ m_d = Cp_o\ m_o + Cp_w\ m_w$,

where $Cp_o$ is the heat capacity of the black liquor solids, 0.4 cal/g °C, and $Cp_w$ is the heat capacity of the water in the drop, 1.0 cal/g °C. The mass of the black liquor solids in the drop, $m_o$, is assumed to be constant. Substituting into Equation (8),

$$L_w \, dm_w/dt = hA(T_g - T_d) + \sigma A F_{wd}(T_w^4 - T_d^4) - (Cp_o m_o + Cp_w m_w) dT_d/dt \qquad (11)$$

Equation (11) has two variables changing with time, $m_w$ and $T_d$. A second equation relating $m_w$ and $T_d$ is needed to have two equations and two unknowns. The boiling point rise equation,[43] Equation (12), empirically relates $m_w$ and $T_d$ for a single high solids (85%-98%) liquor.

$$\text{Moisture, \%} = 54.678 \exp(-0.046 (T_d - 100)) \qquad (12)$$

$T_d$ is the drop temperature, °C. Since moisture is just $m_w/(m_w+m_o)$, Equation (12) can be restated as

$$\frac{100 * m_w}{m_o + m_w} = 54.678 \exp(-0.046 (T_d - 100)) \qquad (13)$$

differentiating both sides with respect to time,

$$\frac{(m_o + m_w)\, dm_w - m_w\, d(m_o + m_w)}{(m_o + m_w)^2 \qquad dt} = \qquad (14)$$

$$0.54678 (-0.046) \exp[-0.046 T_d + 4.6] \, dT_d/dt$$

simplifying,

$$\frac{(m_o + m_w - m_w)\, dm_w}{(m_o + m_w)^2\, dt} = -0.02515 \exp [4.6 - 0.046\, T_d]\, dT_d/dt \quad (15)$$

and solving for $dT_d/dt$,

$$\frac{dT_d}{dt} = - \frac{39.758\, m_o}{(m_o + m_w)^2 \exp (-0.046\, T_d + 4.6)} \frac{dm_w}{dt} \quad (16)$$

Substituting Equation (16) into Equation (11) and rearranging yields,

$$\frac{dm_w}{dt} = - \frac{h\, A\, (T_g - T_d) + \sigma\, A\, F_{wd}\, (T_w^4 - T_d^4)}{L_w + \left[ \frac{39.758\, m_o\, (Cp_o\, m_o + Cp_w\, m_w)}{(m_o + m_w)^2 \exp (-0.046\, T_d + 4.6)} \right]} \quad (17)$$

Equation (17) has two unknowns, $m_w$ and $T_d$. Equations (13) and (17) relate $m_w$ to $T_d$. These equations were solved numerically using the fourth order Runge-Kutta method. At each timestep, $m_w$ was calculated from Equation (17) using the old $m_w$ and $T_d$. The new $m_w$ was substituted into Equation (13) to calculate a new $T_d$. The new $T_d$ and $m_w$ were then used in the next timestep. This continued until the mass fraction of water equaled 0.1 percent. At that point the drop was considered to be dry and the program stopped. When $m_w$ equals zero Equation (12) is no longer valid. The computer code is contained in Appendix III.

Assumptions

The assumptions for the model are:

1. The drop is spherical.

2. The drop is well mixed, due to rapid boiling. This implies that no heat is conducted through the drop and that $T_d = T_{thermo}$, measured by a thermocouple inside the drop.
3. Energy balance is around the entire drop.
4. Drying is external heat transfer limited.
5. A swelling factor is used to account for surface expansion. While this neglects the dynamic effects of swelling and bursting, it accounts for an average amount of swelling.
6. The only mass lost is water.
7. Radiant heat transfer is independent of the water vapor formed during drying.
8. Radiant heat transfer from the gas is neglected.
9. The heat capacity is independent of temperature and is divided up into water and solids

Discussion of Assumptions

Assumption 1: The drop is spherical. Projected area traces of a drying drop can be analyzed to determine the shape factor, a measure of deviation from circular. The projected area was traced from the test video, and the area within the shape was measured using a Sigma Scan Graphics Tablet. As part of the area measurement, the perimeter of the shape is measured, and the shape factor is determined from how much the measured area differs from the calculated area, if the shape was circular with the measured perimeter. A shape factor of one means the drawn shape is circular. Figure 4 is a plot of the shape factor for a drop dried in air at a gas temperature of 550°C in a non-convective atmosphere. The shape factor during drying averages between 0.85 and 0.9. The shape of the drop during drying is approximately spherical.

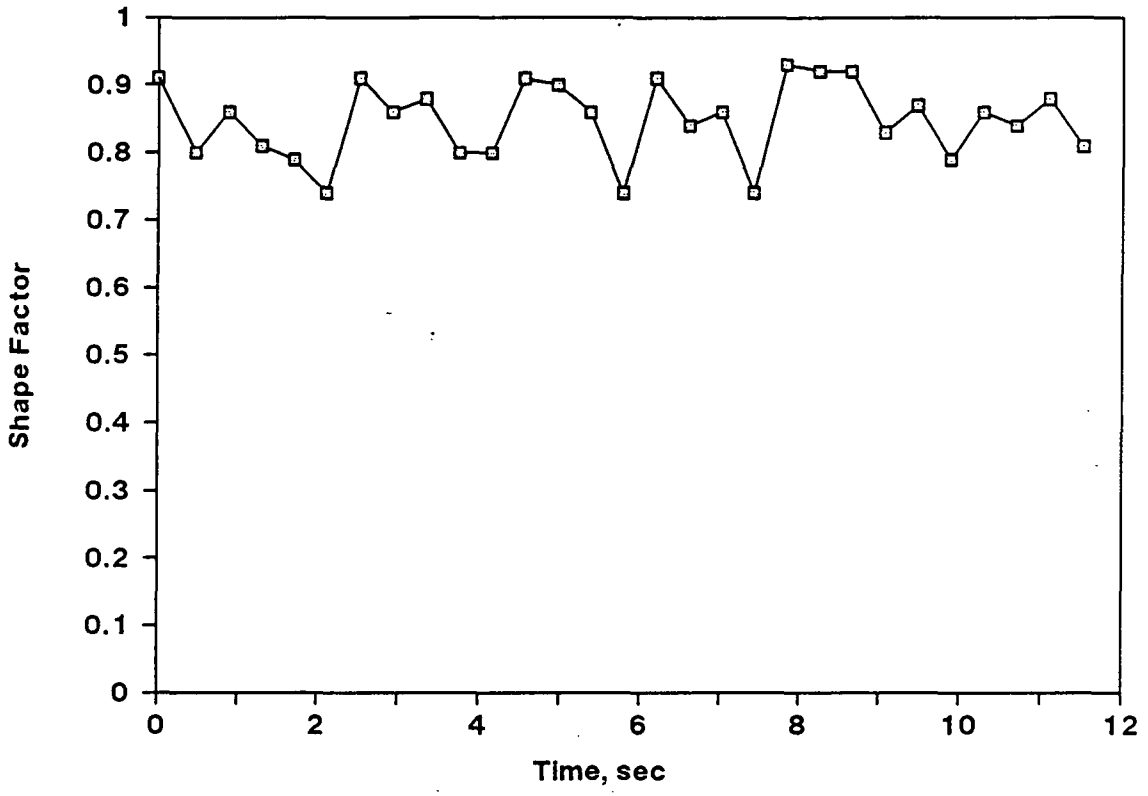


**Figure 4. Shape factor, the measure of deviation from circular vs. time for a 2.77 mm drop during drying. Tg = 550 C, Tw = 600 C, v = 0 m/sec**

Assumption 2: The drop is well mixed. This assumption is valid for the duration of rapid boiling, because the entire drop is fluid. Once rapid boiling ceases, the surface of the drop dries before the interior, and the water vapor needs to pass through a dried solid layer to escape. The temperature of the surface will rise more rapidly than the interior. Robinson[9] calculated that the surface temperature of a drop of black liquor drying at a gas temperature of 167°C was not equal to the internal temperature measured with a thermocouple for 50% solids liquor. He assumed a heat transfer model to fit his drying data. The data fit the model only

after he assumed a surface temperature profile linear with time between 110°C and 118°C. At those temperatures eight degrees make a large difference in the amount of convective heat transferred. Assuming the heat transfer coefficient remains constant, the increase in convective heat transferred when the surface temperature was lowered from 118°C to 110°C is 16% for a gas temperature of 167°C and 2% for a gas temperature of 550°C. A small difference in surface temperature is significant at lower temperatures, i.e. 167°C, but is insignificant at higher reactor temperatures.

The surface temperature during drying has not been measured. The two-color pyrometer is not useful during the drying stage since it does not measure temperatures below 500°C. In order to calculate the surface temperature from the thermocouple temperature, questionable assumptions about the amount and the physical properties of both the dried fraction and the wet fraction of the drop need to be made. The assumption that the drop is well mixed is also implicit in the moisture relation (Equation (12)) used as the tie between water content and drop temperature.

Assumption 3: The energy balance is around the entire drop. This ties in with the first assumption, that the drop is well mixed. The drop is treated like a black box. Energy comes in by heat transfer, water evaporates and leaves, and the remainder of the energy heats up the black liquor solids to pyrolysis temperatures.

Assumption 4: Drying is external heat transfer limited. This is consistent with Robinson's high temperature drying conclusions.[9]

Assumption 5: Use of a swelling factor. The surface area changes during the rapid boiling period and should be accounted for in the model. The swelling factor is a measure of the expanded drop diameter. It is defined as $d_{avg}/d_i$, where $d_{avg}$ is the average diameter during drying and $d_i$ is the initial diameter. It is assumed to be constant throughout drying. The validity of this assumption is shown later, when the model predictions using several swelling factors are compared to the model predictions using the actual surface area for one set of reactor conditions. Use of the swelling factor avoids the necessity of knowing how the drop diameter changes with time during drying. This is shown in Figure 5, a plot of the surface area as a function of time for a 2.77 mm diameter drop in a 550°C environment with no gas flow. The particle surface area is calculated from the area measurement of the projected area traces. The determination of the projected area traces also yields the shape factors discussed in Assumption 1. The same drying test is shown in Figures 4 and 5. The three horizontal lines correspond to the calculated surface areas for diameter swelling factors of 1.0, 1.25, and 1.5. The swelling factor simplifies the model, and is a user input parameter. The average value for $d_{ign}/d_i$ is 1.5, the ratio of the diameter at ignition to the initial diameter. The swelling factor for drying therefore falls between 1.0, the value for no swelling, and 1.5, the value at ignition.

Assumption 6: Only mass lost is water. This simplifies the model by neglecting any volatilization of the drop. It is appropriate due to Assumption 2, that the drop is well mixed. Volatilization could occur during drying if local hot spots are present, causing the temperature to rise. The model does not take local hot spots into consideration.

Assumption 7: Radiant heat transfer is not influenced by the water vapor released during drying. The effects of the water vapor are assumed to be negligible in the SPR since the volume of water vapor is several orders of magnitude lower than the volume of air.

Assumption 8: Neglect radiant heat transfer from the gas. The only radiant heat transfer considered is that from the walls. The gas supplies convective heat transfer. This assumption is specific to the experimental apparatus used to validate the model. To apply the model to drying in a recovery boiler, radiation from the gas has to be added to the energy balance.

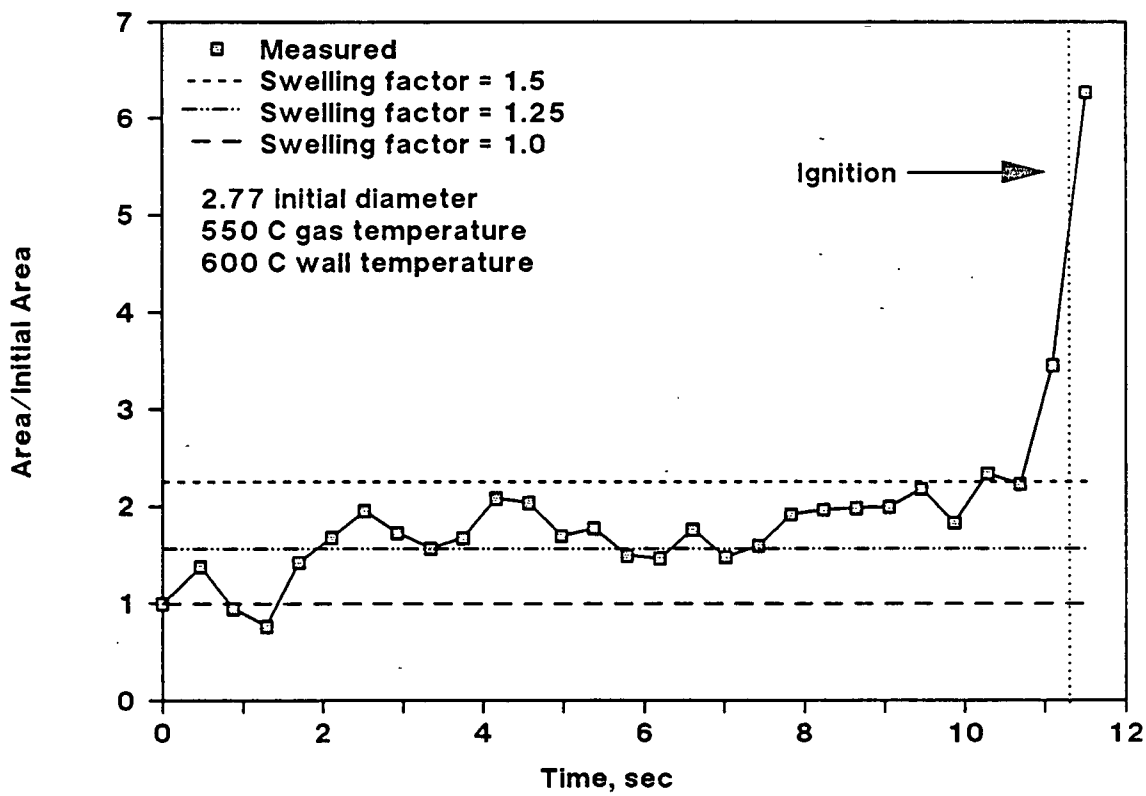


Figure 5. Surface area vs. time, 2.77 mm drop, Tg = 550 C, Tw = 650 C, v = 0 m/sec

Assumption 9: The heat capacity is independent of temperature, and is divided up into water and solids fraction. A 50% increase in gas temperature (100°C - 150°C) results in a 5% increase in the heat capacity of the water and a 10% increase in the heat capacity of the black liquor solids.[1]

Parameters

Several adjustable parameters were used in the drying model. The density of the black liquor, used to convert between the initial mass and diameter of the drop, was set at 1.4 $g/cm^3$. $F_{wd}$, the combination of the view factor and the drop emissivity, was set at 0.65. The drop emissivity was assumed to be 0.9. A sensitivity analysis of the drying model to $F_{wd}$, h, and SF, is done in the Conclusions section of this thesis.

DRYING MODEL RESULTS

The drying model predicts both the temperature and the moisture of a drying drop. Figure 6 shows the measured and the predicted temperature vs. time profile for drying a 2.77 mm drop at a gas temperature of 550°C with no gas flow using the measured surface area. The drop temperature was measured with a thermocouple embedded inside the drop. The predicted temperature is within 8°C (6%) of the measured temperature after 2 seconds. In the first two seconds, the drop is heating to the liquor boiling point. The model assumes that the liquor is initially at the boiling point. This difference in starting points has a very minor effect on the drying time. The drying model using the measured surface area accurately predicts the temperature of the drop. The drop ignited at

11.3 seconds and is calculated to be dry at 7.4 seconds.

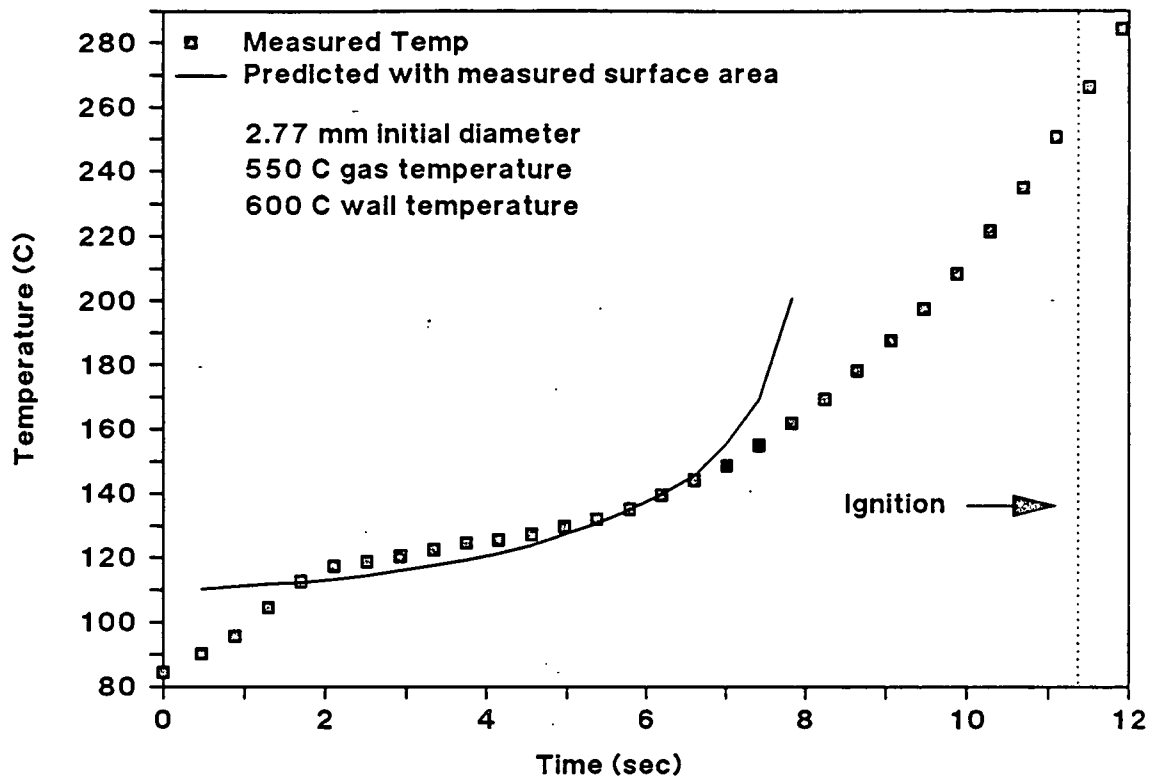


**Figure 6. Predicted/measured temperature vs. time for 2.77 mm drop. Tg = 550 C Tw = 600 C, v = 0 m/sec, using measured surface area.**

Assumption 5 concerned the use of a swelling factor to avoid the necessity of knowing the measured surface area during drying. The model was run using three swelling factors, 1.5, 1.25, and 1.0. The 1.0 case refers to no swelling, the drop remained at the inital diameter throughout drying. Figure 7 shows the predicted temperature for a 2.77 mm diameter drop drying in a 550°C gas with the walls at 600°C, using all three swelling factors. The curve for the swelling factor of 1.25 most closely predicts the measured temperature profile. The swelling factor of 1.25 best predicted the temperature for three drop sizes (2.77 mm, 3.12 mm, and 3.33 mm) dried at two gas temperatures (550°C and 600°C).

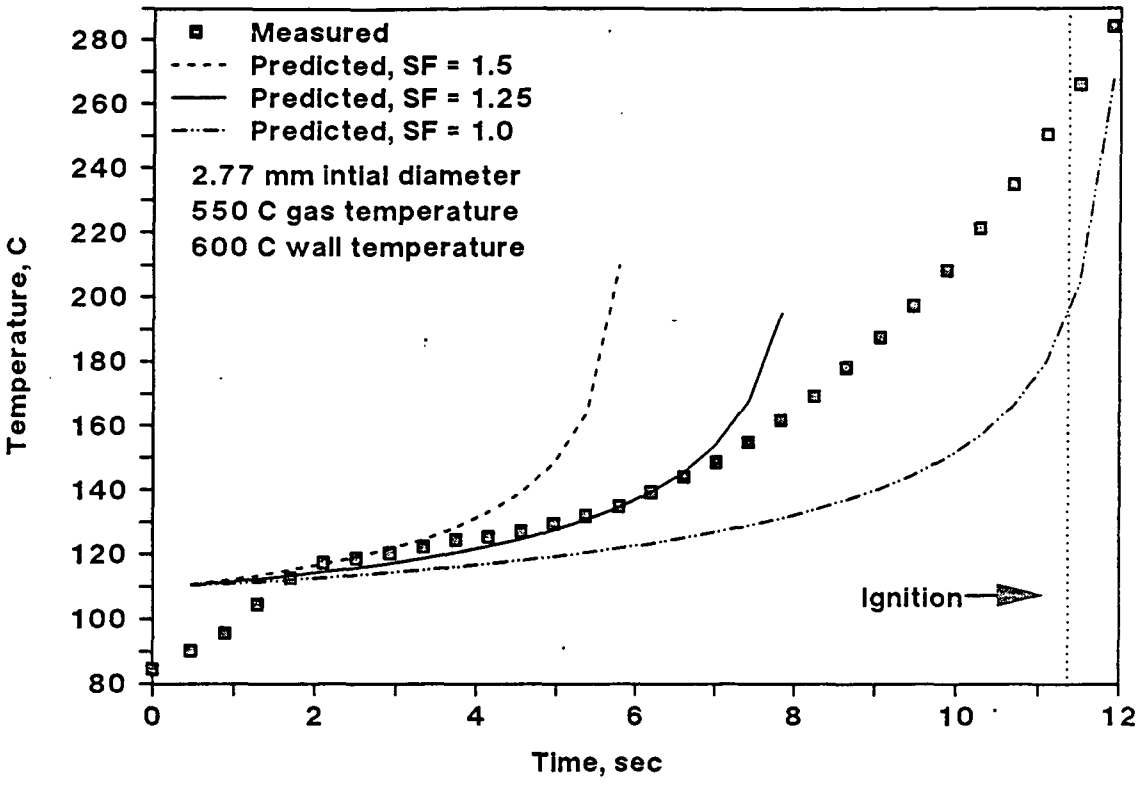


**Figure 7. Predicted temperature using three swelling factors, 2.77 mm drop Tg = 550 C, Tw = 600 C, v = 0 m/sec, swelling factors - 1.5, 1.25, 1.0**

The predicted moisture of the drop during drying is shown in Figure 8. The moisture is the mass of the water divided by the total mass of the drop. The graph shows the profiles using three swelling factors, 1.5, 1.25, and 1, and the measured surface area. The moisture predictions are approximately the same for the case with the swelling factor of 1.25 and for the case with the measured surface area. This is especially apparent in the later stages of drying. Since the drying model will be used to predict the drying time and the amount of moisture at a given time, a swelling factor of 1.25 is a good approximation for the measured surface area. Using a swelling factor of 1.25, the drop was predicted to be dry at

7.8 seconds, which is considerably before the observed ignition at 11.3 seconds. The ignition delay is due to the need to generate sufficient quantities of volatiles before spontaneous ignition. At a gas temperature of 550°C, the rate of volatiles generation is slow, causing a sizable ignition delay.

At a gas temperature of 650°C with no gas flow, the temperature and moisture profiles follow the same trends. The swelling factor of 1.25 most closely approximates the measured temperature profile, as shown in Figure 9. Figure 10 shows the predicted moistures for all three swelling factors, 1.5, 1.25, and 1.0. This is for a 3.33 mm diameter drop drying at 650°C with no gas flow and the wall heaters set at 700°C. This drop ignited at 7.6 seconds, and the drop was predicted to be dry at 6.6 seconds. This corresponds to a 1.0 second ignition delay. A 20% increase in gas temperature shortened the ignition delay by 70 percent.

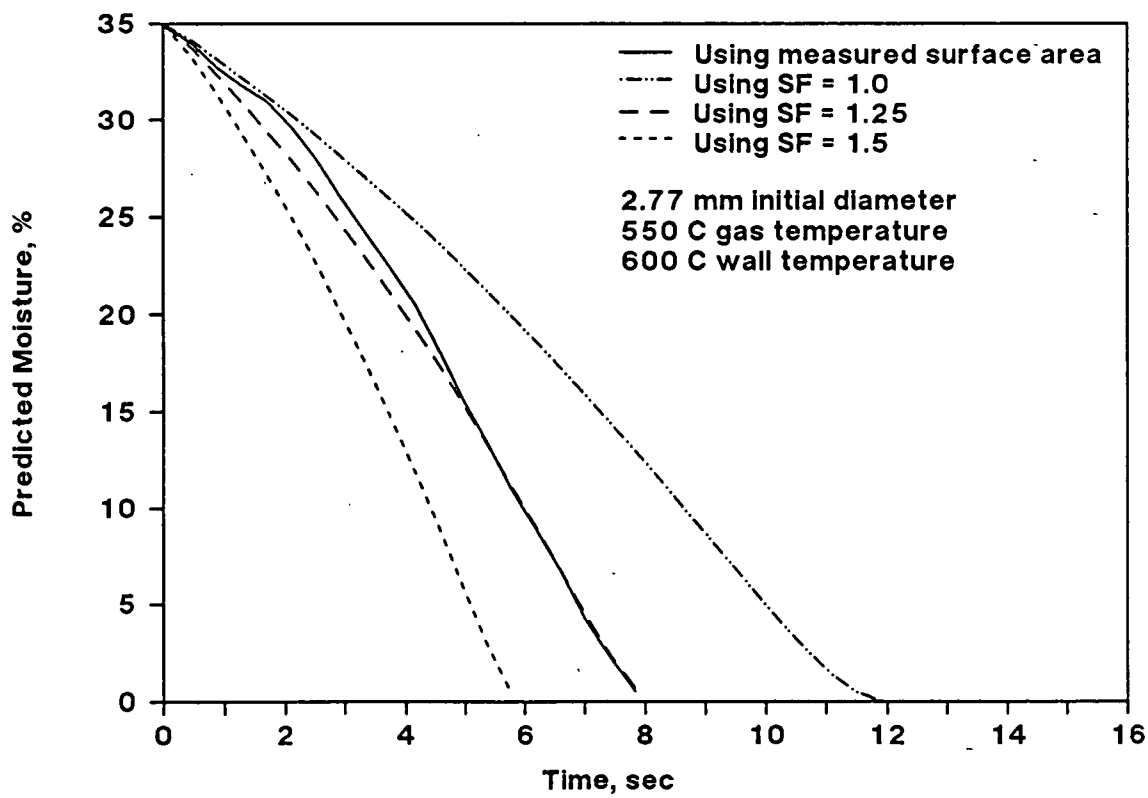


Figure 8. Predicted moisture for swelling factors - 1.5, 1.25, and 1.0 for 2.77 mm drop, Tg = 550 C, Tw = 600 C, v = 0 m/sec

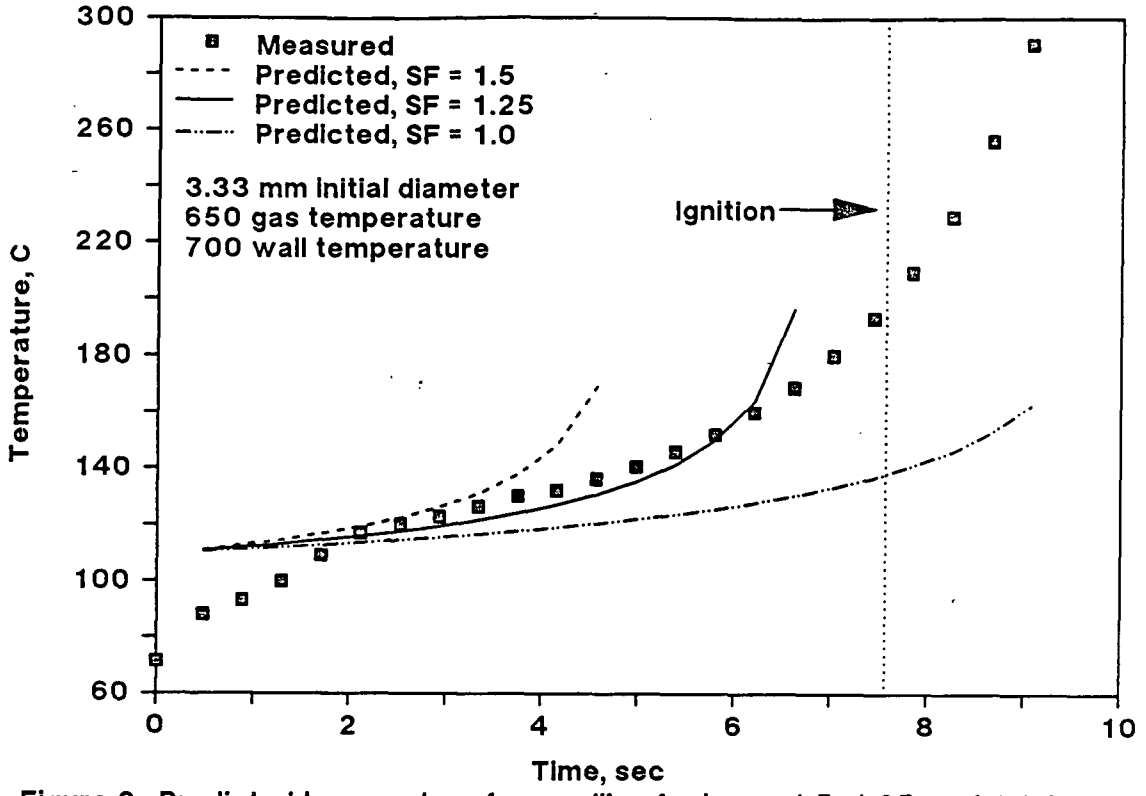


Figure 9. Predicted temperature for swelling factors - 1.5, 1.25, and 1.0 for a 3.33 mm drop, Tg = 650 C, Tw = 700 C, v = 0 m/sec

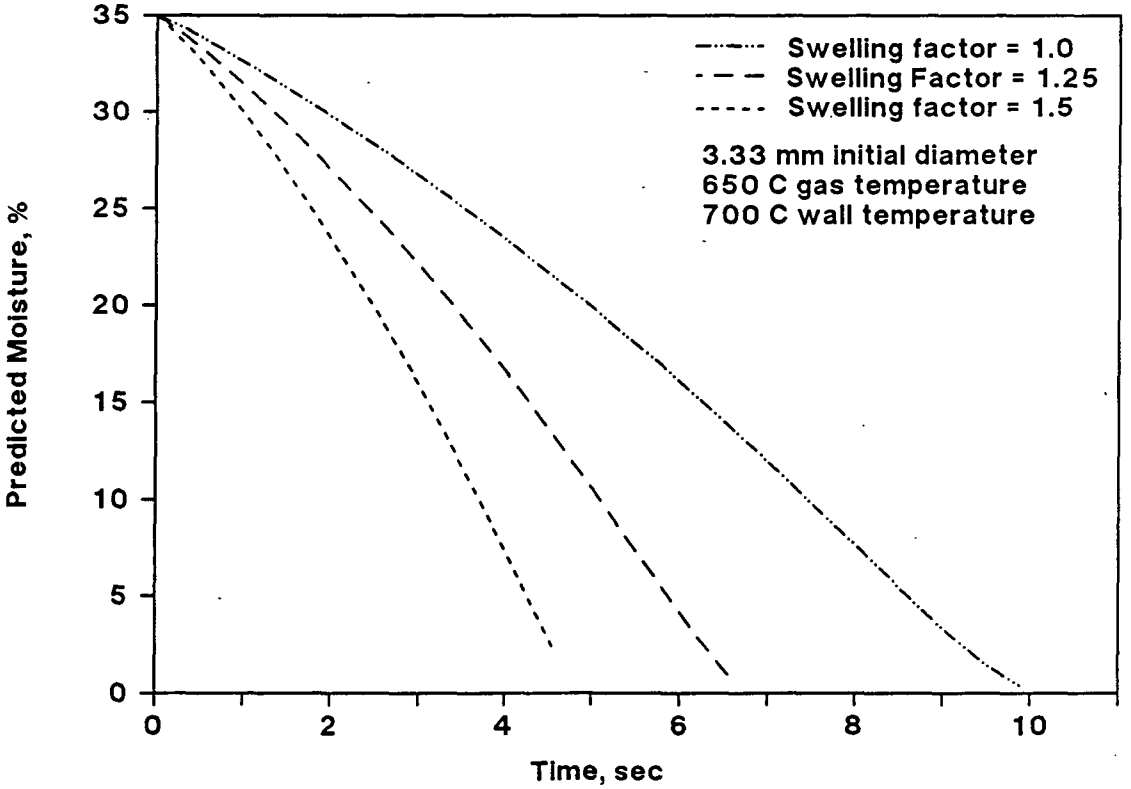


Figure 10. Predicted moisture for swelling factors 1.5, 1.25, 1.0 for a 3.33 mm drop, Tg = 650 C, Tw = 700 C, v = 0 m/sec

The gas temperature influences the drying rate because drying is limited by external heat transfer. Figures 11 and 12 show the influence of gas temperature. Figure 11 shows the predicted temperature profiles for two 3.33 mm diameter drops. One drop was dried at 550°C and the other at 650°C. The measured temperature profiles are shown for comparision with the predicted profiles. Figure 12 shows the predicted moisture profiles. As could be expected, the drop drying at the higher temperature is predicted to dry faster than at the lower temperature.

Comparision with Hupa et al.[3] reported drying times

Hupa[3] measured the drying times for drops burning in air at 800°C in a radiant environment. Drying began when the drop entered the reactor and ended at the first sign of ignition. Predicted drying, using the present model, ended when 0.1% moisture remained in the drop. Table 3 contains the measured drying times[3] and the predicted drying times using a swelling factor of 1.25.

Figure 13 shows the comparision between the measured times and times predicted with the present model. The drying model predicted the drying time accurately for the entire range of initial drop diameters. The $r^2$ for the model is 0.90. The scatter is due in part to the uncertainty of the amount of water present in the drop at ignition. Ignition makes a good visual end to drying, easy to note from either videos or movies of the burns. Ignition is not an integral part of the drying process; it does not automatically occur at a specific moisture. Ignition occurs when volatiles and oxygen are sufficiently mixed at the appropriate temperature and composition to ignite spontaneously. The volatiles are generated when the

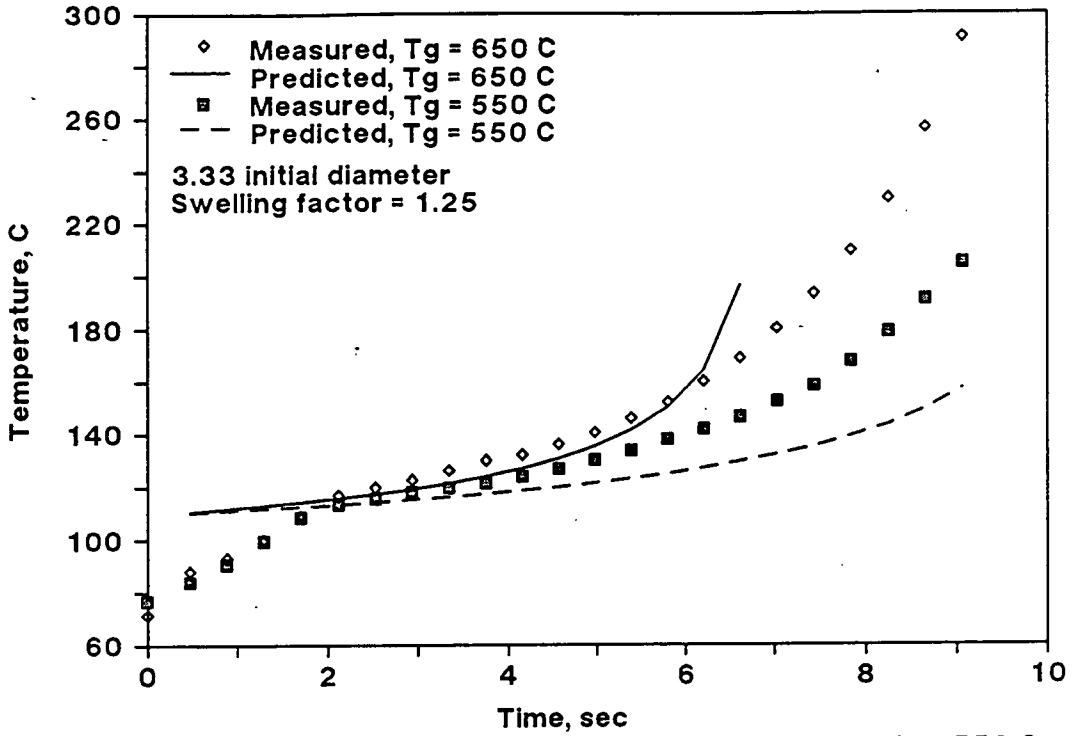


Figure 11. Predicted temperature for two reactor conditions, Tg = 550 C and Tg = 650 C for 3.33 mm diameter drops

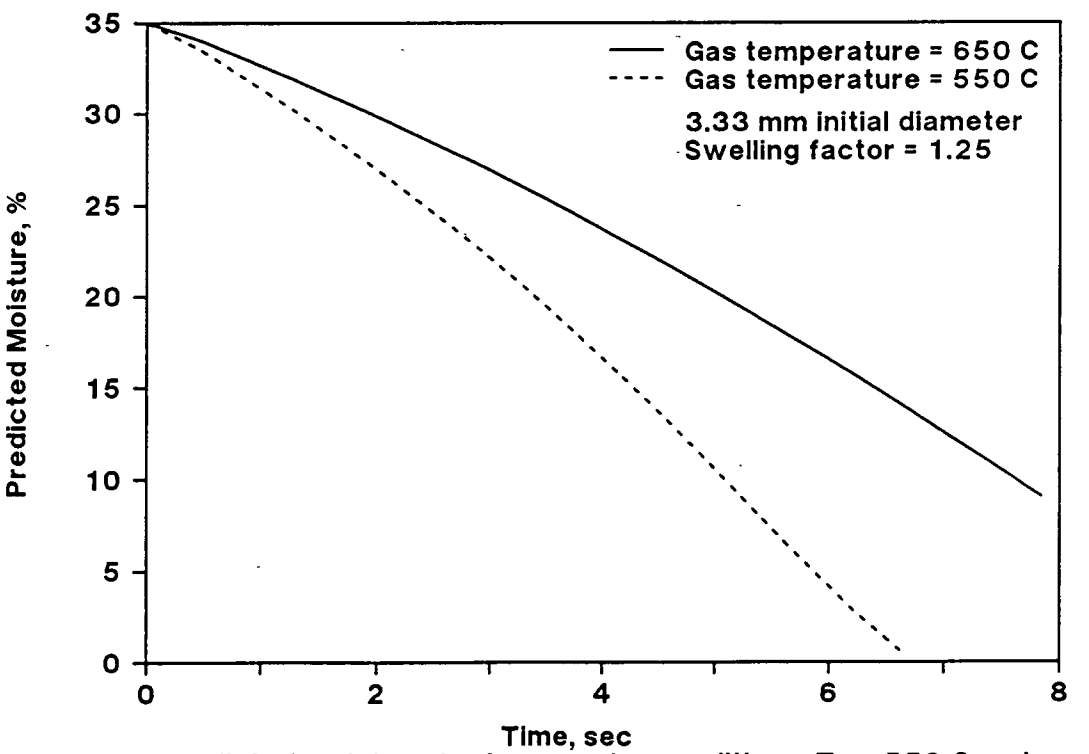


Figure 12. Predicted moisture for two reactor conditions, Tg = 550 C and Tg = 650 C for 3.33 mm drops

drop reaches a certain temperature, which can happen in local hotspots before the majority of the drop is dry. This occurs in larger drops, with a low surface area/mass ratio.

Table 3. Measured[3] and Predicted Drying Times at 800°C.

| Initial Diameter (mm) | Measured Dry Time (sec) | Predicted Dry time SF = 1.25 (sec) |
|---|---|---|
| 0.0802 | 0.821 | 0.61 |
| 1.066 | 0.923 | 0.95 |
| 1.136 | 1.064 | 1.05 |
| 1.136 | 1.346 | 1.05 |
| 1.365 | 1.295 | 1.37 |
| 1.341 | 1.436 | 1.34 |
| 1.570 | 1.654 | 1.68 |
| 1.728 | 1.885 | 1.92 |
| 1.863 | 1.756 | 2.03 |

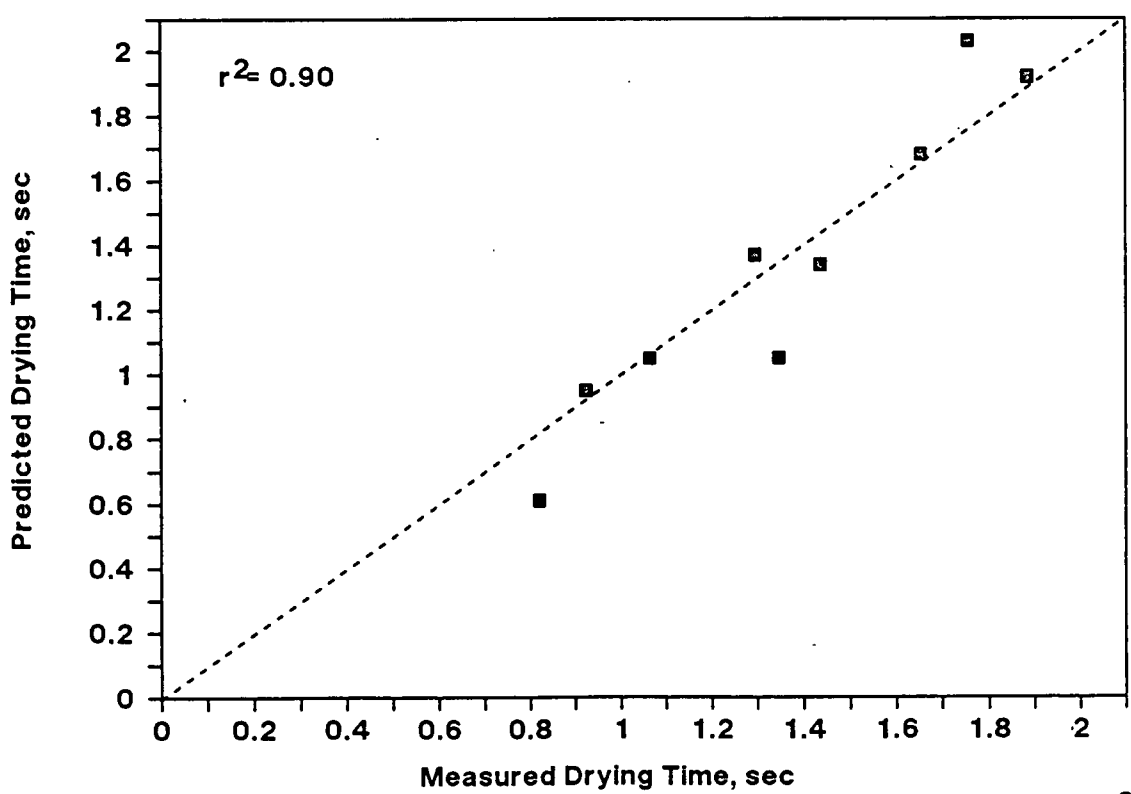


Figure 13. Predicted vs. measured drying time, measured time from Hupa et al.[3]

CONCLUSIONS

1. A drying model based on external heat transfer will adequately predict black liquor drop drying times. The drying model predicts the temperature and moisture profiles for drops during drying as was shown in Figures 6, 7, and 9. The predicted temperature is within 10% of the temperature measured with a thermocouple. The dynamic surface area during drying can be approximated by an average value.

2. The predicted moisture profile for drops dried in a non-convective 550°C gas environment indicates that the drop is dry before ignition. This can be attributed to the necessity to generate sufficient volatiles before ignition. Drops dried in a non-convective 650°C gas are predicted to have a smaller ignition delay.

3. Using the measured dynamic surface area in the drying model, the temperature was correctly predicted, as seen in Figures 5 and 6.

4. At 800°C, experimental results obtained by Hupa et al.[3] were correctly predicted from the drying model using a swelling factor of 1.25. This means that the drop ignites when the moisture is gone, further implying that portions of the drop had volatilized sufficiently to produce enough volatiles to ignite prior to the last water being evaporated.

## VOLATILES BURNING

Volatiles burning, the second stage of black liquor combustion, consists of volatiles evolution and combustion. Volatiles evolution occurs when black liquor solids reach pyrolysis temperatures. Volatiles combustion does not begin until the concentration of volatiles and oxygen reach the flammibility limit. This limit is determined by the composition of the volatiles and the resulting oxygen requirement, at the specific temperature, and is not known for black liquor.

Volatiles combustion can occur in one of three locations - near the particle surface or in the surface pores, in a flame around the particle, or in the gas stream some distance from the particle. The location for volatiles combustion depends on the ambient conditions, the temperature and composition of the gas, and the gas flow rate. From tests in the SPR with a gas temperature range of 660°C to 910°C and gas compositions from 0% to 21% oxygen in nitrogen, the intensity of the flame surrounding the particle was observed to depend on the experimental conditions.

If the oxygen concentration was less than 5%, a flame was not observed surrounding the particle. Volatiles combustion was not intense enough at any location to produce visible light. The only evidence of combustion on the particle surface was a slight reddening of the particle. From visual observations, it is not clear whether this reddening is due to volatiles combustion within the surface pores or from the onset of char combustion.

As the concentration of oxygen in the gas increased, the amount of visible volatiles combustion increased. When the oxygen concentration was above 16%, flame liftoff, the formation of a stable flame surrounding the particle, always occurred. The stable flame will be referred to as the flame sheet. The flame was intense, often making it impossible to observe the particle behind it. Flame liftoff occurred rapidly after local ignition. The flame sheet remained stable until the particle swelled to its maximum volume, indicating the end of volatiles evolution. Flame observations for the intermediate oxygen levels are tabulated in Table 4.

Table 4. Flame observations for single particles of black liquor burning with several gas temperatures (660°C - 910°C) and gas compositions (2% - 21% oxygen in nitrogen). Gas velocity = 1.7 m/sec.

| Gas | Oxygen Concentration | | | | | | |
|---|---|---|---|---|---|---|---|
| Temperature | 2% | 4.3% | 5% | 8% | 10.5% | 16.7% | 21% |
| 666 | none | none | — | — | | | intense |
| 763 | none | none | --- | — | flame | flame | intense |
| 800 | none | none | puff | puff | — | — | intense |
| 870 | none | none | puff | weak | flame | flame | intense |
| 910 | none | none | puff | weak | flame | flame | intense |

none = no flame
puff = puff of flame, like candle flame, associated with volatiles released by rapid extension of an "arm" or protrusion, usually occurs at maximum volume
weak = like a candle flame, not stable in gas flow
flame = stable flame surrounding particle
intense = stable flame surrounding particle, intense enough to mask particle, only occurs in air (21% oxygen)

The flame sheet for particle combustion is located at the point where the stoichiometric mass flux of oxygen into the particle surface equals the mass flux of volatiles away from the particle surface.[44] When the volatiles flux increases for a constant oxygen flux, the flame radius will increase until eventually the flame becomes unstable and blows away.

When the volatiles flux decreases, the flame radius will decrease until eventually the flame is located on the particle surface or inside the surface pores.

In the recovery boiler, the particle will be exposed to less than 10% oxygen except near the airports. Oxygen measurements on gas samples obtained immediately below the liquor guns in several operating recovery boilers indicate an average oxygen concentration of 7% (dry volume).[45] Walsh[12] predicted the location for volatiles release in the boiler to be at the liquor gun level. Based on predictions for the location of volatile release[12] and gas composition measurements at that location,[45] the flame sheet will not influence single particle black liquor combustion in the boiler. The flame sheet is an important factor for combustion under conditions of high oxygen concentration, as is found in the SPR and in the furnace used by Hupa.[3]

The volatiles burning model developed as part of this thesis predicts particle mass, temperature, and diameter as functions of time. An energy balance is drawn around the particle, and temperature dependent pyrolysis kinetics are used to model the rate of volatilization. A flame sheet surrounding the particle is not included in this model. The maximum swollen diameter is empirically predicted from the test conditions. The model is validated by comparing predicted and measured rates of volatilization, and the time to reach maximum volume. The predicted time to reach maximum volume is obtained by adding the predicted drying and volatiles burning times together.

MODEL

A sketch of a black liquor particle during volatiles burning, with a flame sheet surrounding it, is shown in Figure 14. $T_g$ is the gas temperature, Tp is the particle temperature, and $T_w$ is the wall temperature. $Q_{cond}$ is the heat transferred through conduction to the surrounding gas and particle from the flame sheet, and $Q_{rad}$ is the heat transferred through radiation to the walls and the particle from the flame sheet. The heat of combustion is only released at the flame surface and the flame is located at $r_f$, where the stoichiometric oxygen flux equals the volatiles flux. The present model does not include the flame sheet, so $r_f = r_p$, and $Q_{cond} = Q_{conv}$ = the heat transferred through convection between the hot gas and the particle, and $Q_{rad}$ is the heat transferred through radiation between the walls and the particle. The radiation from the gases is neglected for the present apparatus, although when the model is applied to combustion in a recovery boiler, radiation from the gases must be included.

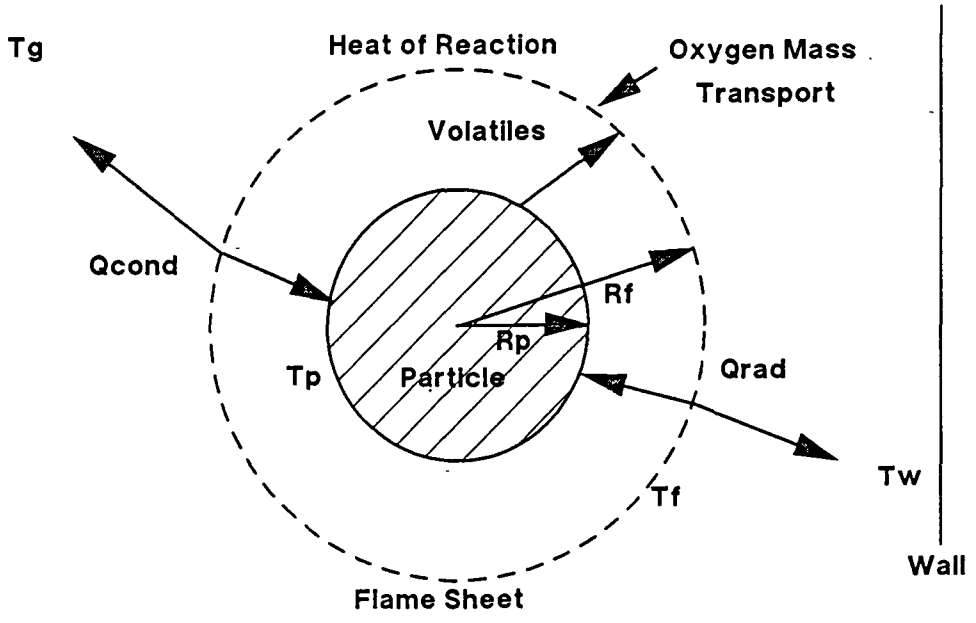


Figure 14. Sketch of black liquor particle during volatiles burning

Energy Balance

The energy balance for volatiles burning is

$$Q_{conv} + Q_{rad} + Q_{comb} - dm_p/dt * H_p = m_d\ Cp_d\ dT_d/dt \qquad (18)$$

where $Q_{conv}$ = heat transferred to particle by convection from the gas

$= h\ A\ (T_g - T_d)$ , cal/sec

$Q_{rad}$ = heat transferred to particle by radiation from the walls

$= \sigma\ F_{wd}\ A\ (T_w^4 - T_d^4)$ , cal/sec

$Q_{comb}$ = heat transferred to particle by volatiles combustion on the surface, cal/sec

$= dm_v/dt * H_{comb}$

h = convective heat transfer coefficient, cal/cm$^2$-K-sec

A = surface area of drop, cm$^2$

$T_g$ = gas temperature, K

$T_w$ = wall temperature, K

$T_d$ = particle temperature, K

$\sigma$ = Stefan-Boltzman constant, $1.355 \times 10^{-12}$ cal/cm$^2$-K$^4$-sec

$F_{wd}$ = combination of the view factor between wall and particle and the particle emissivity

$dm_v/dt$ = mass of volatiles which combust on the surface, g/sec

$H_{comb}$ = heat of combustion, cal/g

$dm_p/dt$ = volatiles evolution rate, g/sec

$H_p$ = heat of pyrolysis, cal/g

$m_d$ = mass of particle, g

$Cp_d$ = heat capacity of particle, cal/g-K

The convective heat transfer coefficient, h, is determined by the Ranz and Marshall correlation for flow past a sphere,[42]

$$Nu = h\ d/k = 2 + 0.6\ Re^{1/2}\ Pr^{1/3} \qquad (10)$$

Combustion

Combustion will occur on or near the particle surface during volatiles burning in low concentrations of oxygen (<10%). The rate of combustion depends on the rate of oxygen reaching the surface and the rate of volatilization. The stoichiometric limit, $\Omega$, of oxygen needed to burn one gram of volatiles can be calculated from the composition of the evolved volatiles. Bhattacharya et al.[46] pyrolyzed crushed black liquor solids in nitrogen. They analyzed the gases evolved as a function of time and reactor temperature. The average gas composition, and the oxygen requirements for complete combustion, are listed in Table 5.

Table 5. Pyrolysis gas composition and oxygen requirement for complete combustion[46]

| Compound | Volume % | g/mol gas | mol $O_2$/mol gas |
|---|---|---|---|
| Methane | 5 | 0.8 | 0.1 |
| Hydrogen Sulfide | 15 | 5.1 | 0.225 |
| Carbon Monoxide | 30 | 8.4 | 0.15 |
| Carbon Dioxide | 30 | 13.2 | 0.0 |
| Hydrogen | 10 | 0.2 | 0.05 |
| Water and other | 10 | 1.8 | 0.0 |
| Total | 100 | 29.5 | 0.525 |

$\Omega$ = 0.0178 mol $O_2$/g volatiles

The rate of oxygen reaching the particle surface can be calculated from mass transfer considerations.

$$n_{O2} = Kox\ C_{O2}\ A \qquad (19)$$

where $n_{O2}$ = oxygen reaching particle surface, mol/sec

$C_{O2}$ = oxygen concentration in gas stream, $mol/cm^3$

Kox = mass transfer coefficient, cm/sec

The Kox can be calculated from the Ranz and Marshall correlation for heat transfer from flow past a sphere by inserting mass transfer dimensionless groups in place of the heat transfer groups.

$$Sh = Kox\ d/D_{O2} = 2 + 0.6\ Re^{1/2}\ Sc^{1/3} \qquad (20)$$

where Sh = Sherwood number, analogous to Nusselt number for heat transfer

$D_{O2}$ = diffusivity of oxygen through air, $cm^2/sec$

Sc = Schmidt number, $\nu/D_{O2}$

The mass of volatiles actually combusted on the surface, $dm_v/dt$ is set equal to the mass of volatiles evolved, $dm_p/dt$, until $\Omega * dm_p/dt$ is greater than $n_{O2}$. At this point, more volatiles have been evolved than can be completely combusted by the rate of oxygen transfer, and $dm_v/dt = n_{O2}/\Omega$.

Rate of Volatiles Evolution

The rate of volatiles evolution is assumed to follow a first order Arrhenius expression. The use of global constants, $A_v$ and $E_v$, is a common simplification of a system of reactions used in coal pyrolysis.[47]

$$dm_p/dt = A_v\ m_b\ \exp\ (-E_v/RT_d) \qquad (21)$$

where $A_v$ = frequency factor for volatiles evolution, $sec^{-1}$

$E_v$ = activation energy for volatiles evolution, J/mol

$m_b$ = mass of unreacted black liquor solids, g

R = gas constant, 8.314 J/mol-K

The mass of unreacted black liquor solids, $m_b$, can be determined from the mass of volatiles and the mass of the particle. Assuming 35% volatile yield,[48] $m_p = 0.35\ m_o$ after volatilization is complete, where $m_o$ is the initial dry mass of the particle and $m_p$ is the mass of volatiles produced. For each gram of liquor solids, 0.35 g ends up as volatiles and 0.65 g ends up as char. Since $m_o = 2.857 * m_p$, then $m_c = 0.65 * (2.857 * m_p) = 1.857 * m_p$, with $m_c$ = mass of the char.

At any time, $$m_b = m_o - m_p - m_c \qquad (22)$$

and $$m_b = m_o - 2.857\ m_p \qquad (23)$$

There are no values for the kinetic constants $A_v$ and $E_v$ reported in the literature for volatiles evolution of black liquor particles. Bhattacharya et al.[46] reported kinetic constants for pyrolysis of crushed black liquor solids. Black liquor solids were heated in a ceramic boat and the mass fractions of pyrolysis gas, tar, and char were collected. They interpreted their results as a system of three parallel reactions,

$$\text{Black liquor Solids} \xrightarrow{K_1} \text{Volatiles}$$
$$\xrightarrow{K_2} \text{Tar}$$
$$\xrightarrow{K_3} \text{Char}$$

$$dm_b/dt = -(K_1 + K_2 + K_3)\ m_b \qquad (24)$$

$$dm_p/dt = K_1 m_b \ , \ K_1 = A_1 \exp(-E_1/RT_d) \qquad (25)$$

They determined values of A and E for $K_1$, $K_2$, $K_3$. Adapting Bhattacharya's sequence to single particle pyrolysis, the kinetic constants $A_1 = 3.42\ min^{-1}$ and $E_1 = 34600$ J/mol did not predict observed rates of volatilization. The rate of volatilization was underpredicted by several orders of magnitude. Crushed black liquor solid pyrolysis kinetic constants reported by Bhattacharya[46] do not apply to single black liquor particle pyrolysis. $A_v$ and $E_v$ were estimated from several single particle tests in the SPR. Details of the calculation are in Appendix IV. The values used in the model were $A_v = 10.07\ sec^{-1}$ and $E_v/R = 2628\ K^{-1}$.

Swelling

During volatiles evolution the particle swells to roughly 3 times its initial diameter.[3] Previous work on swelling did not result in a predictive equation relating the swollen diameter to the initial conditions.[3,14-16] Data from the SPR for one liquor suggested that the swollen diameter was a linear function of the initial dry mass of the drop, Equation (26). The gas temperature (800°C - 910°C), gas composition (2% - 8% oxygen in nitrogen), and the initial liquor mass (7 mg - 53 mg, 2.1 mm - 4.1 mm) were varied.

$$d_{max} = 0.0221 * m_o + 0.72 \qquad (26)$$

Figure 15 shows the comparision between predicted and measured maximum diameter. The $r^2$ for the regression is 0.83. Gas temperature and composition did not statistically influence the swollen diameter, for this liquor. The maximum swollen diameter is predictable for black liquor

particles burning in low concentrations of oxygen (2% - 8%). Previous work on swelling in nitrogen[14] and in air[3,16] indicated that swelling was not predictable from test conditions. Apparantly, low levels of oxygen in the gas control the amount of swelling which occurs.

Swelling as a function of time is not predictable with the information currently available. Equation. (27), was assumed to estimate the particle diameter as a function of particle mass. Frederick et al.[13] treated swelling in a similar manner. The difference is that Frederick et al.[13] used the fraction of cumulative heat transferred to the particle to determine the extent of swelling while Equation (27) used the fraction of volatiles evolved. Both methods assume that volatiles evolution is complete when the particle has finished swelling.

$$d = d_i + (d_{max} - d_i) * \Sigma m_p / m_{po} \qquad (27)$$

where d = particle diameter at time t, cm

$d_i$ = initial dried diameter, cm

$d_{max}$ = maximum diameter, cm

$\Sigma m_p$ = cumulative mass of volatiles evolved at time t, g

$m_{po}$ = total mass of volatiles to evolve, g

Figure 16 compares the predicted and measured diameter as a function of time for a 21 mg drop combusting in 10.5% oxygen at 763°C. The measured diameter is calculated from the projected area traces drawn from the test video. The predicted diameter is held constant throughout drying at 1.25 * $d_i$ and is calculated from Equation (27) throughout volatiles burning. The predicted diameter remains constant at $d_{max}$ throughout char burning because Equation (27) does not handle char burning. The particle began swelling

before the drop was predicted to be dry, causing the predicted diameter to be less than the measured diameter in the first part of volatiles burning. Burning in 10.5% $O_2$ allows volatiles ignition to occur early, at approximately 2 seconds. Localized volatiles evolution occurred before the drop was completely dry, causing early swelling. The point of maximum diameter is reached at approximately the same time.

The two differential equations solved by the volatiles burning model are Equations (18) and (21) and the two unknowns are $T_d$ and $m_d$. The program uses a fourth order Runge-Kutta method to solve the two equations simultaneously. The program code is contained in Appendix V. Volatiles burning was considered complete when $d = 0.975\ d_{max}$, which was when the drop was predicted to finish rapid swelling.

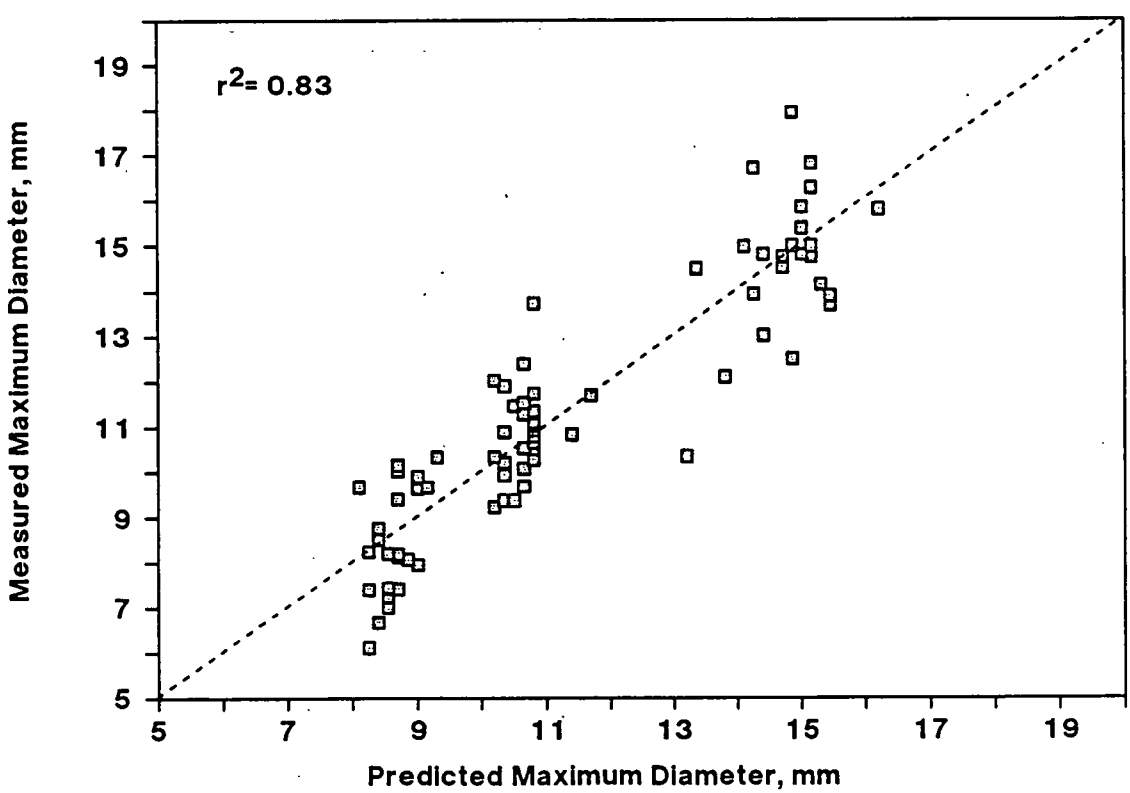


Figure 15. Predicted vs. measured maximum diameter, Tg = 800 C - 910 C, 2% - 8% oxygen in nitrogen, 10 mg - 50 mg initial liquor mass, v = 1.7 m/sec

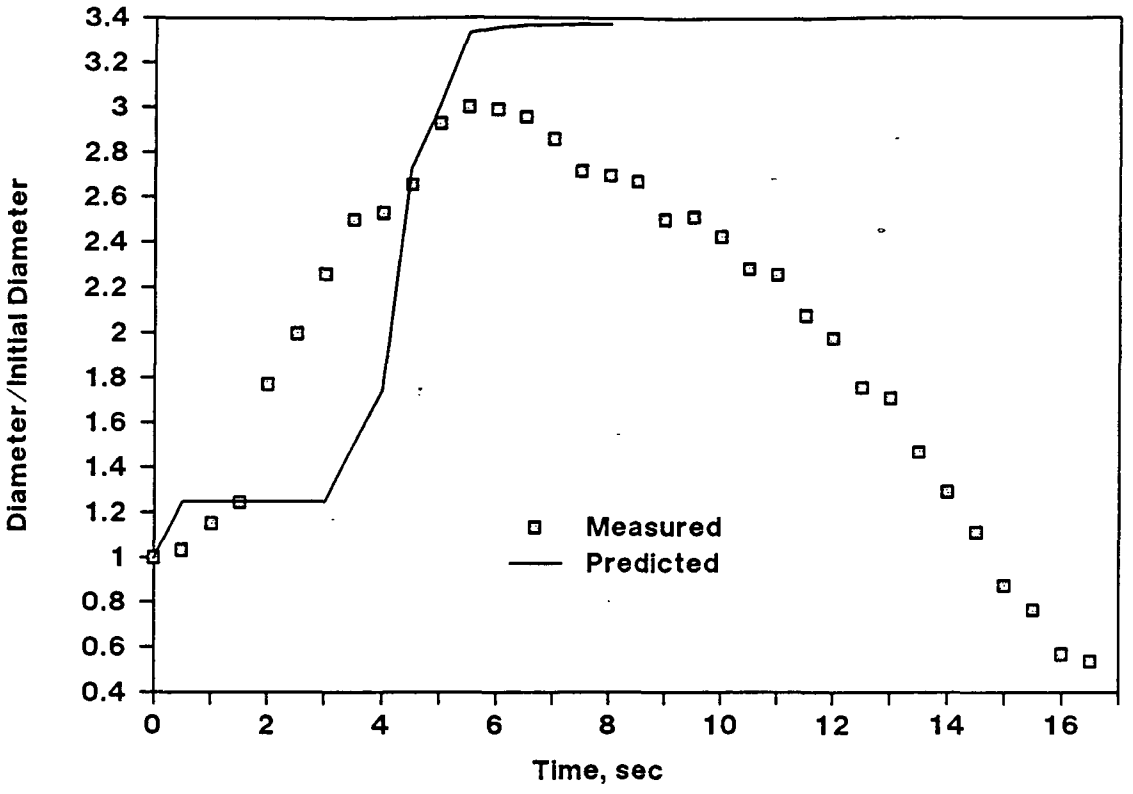


**Figure 16. Predicted and measured diameter as function of time for a 21 mg drop Tg = 763 C, 10.5% oxygen in gas with balance nitrogen, v = 1.7 m/sec**

Assumptions

1. Spherical geometry, with uniform swelling
2. No flame sheet surrounding particle
3. Combustion on surface is limited by oxygen mass transfer to the surface
4. Oxygen requirement for volatiles combustion is constant throughout volatilization
5. Volatile evolution is external heat transfer limited
6. The particle is isothermal
7. Heat of combustion, heat of pyrolysis, and particle heat capacity are constant throughout volatiles burning
8. Ideal gas
9. Only mass lost is volatiles

10. Pyrolysis kinetics are first order in mass of unreacted black liquor solids

11. Maximum swollen volume occurs when volatilization is complete

Discussion of Assumptions

Assumption 1: Spherical geometry with uniform swelling. This is a simplifying assumption and is reasonably accurate. Visual observations indicate that the particle is spherical at ignition (the end of drying) and initially swells uniformly. As the particle approaches maximum volume, the swelling tends to make the particle cylindrical. Particles obtained after pyrolysis in the Department of Energy Flow Reactor (DOE reactor) at the Institute of Paper Chemistry (IPC) are spherical. The tendency for the particles pyrolyzed in the SPR to become cylindrical is an artifact of constraining them to expose them to one direction of gas flow. This causes the drop to expand preferentially in the direction of the gas flow. Particles in the recovery boiler are free to rotate and will expand uniformly in all directions, similar to particles pyrolyzing in the IPC DOE reactor. A measure of the deviation from circular is the shape factor, with a circle having a shape factor of 1.0. Figure 17 shows the shape factor during combustion.

Assumption 2: No flame sheet surrounding particle. This is based on Walsh's predictions[12] on the location for volatiles release (liquor gun level) and the oxygen concentration at that location (7% on dry volume).[45] In the SPR, the flame sheet did not stabilize unless the oxygen concentration in nitrogen was above 16 percent.

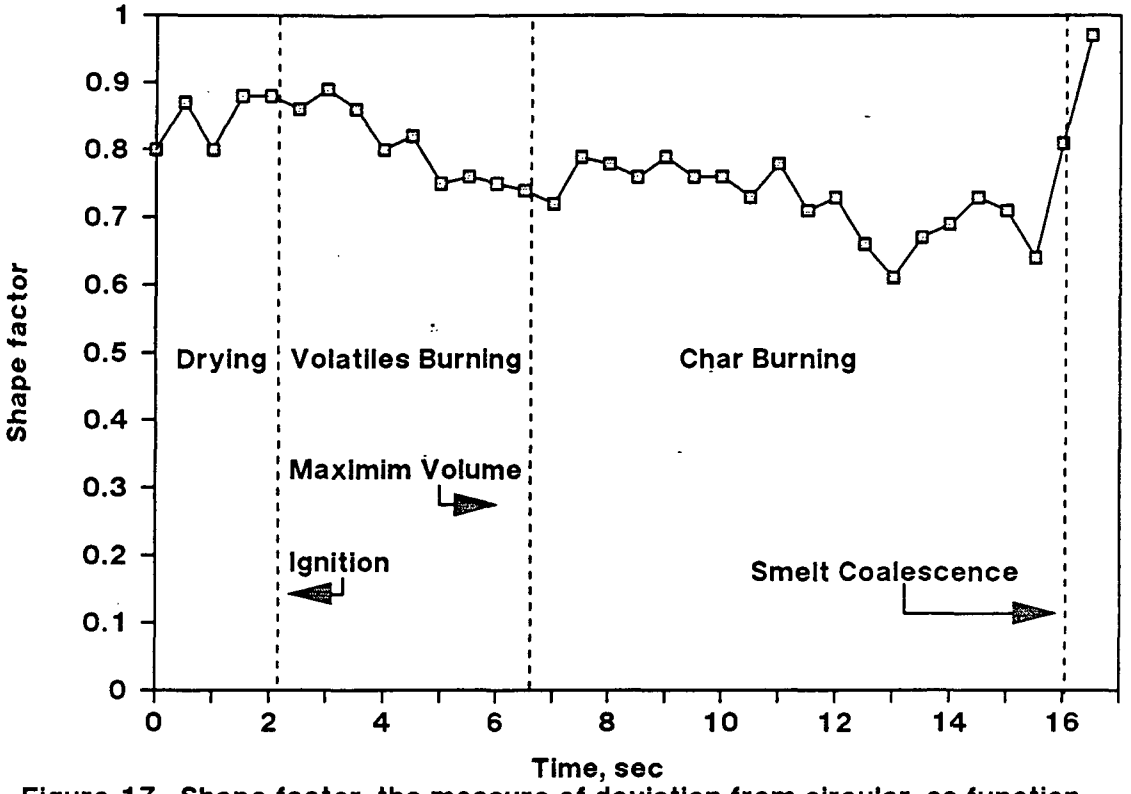


**Figure 17. Shape factor, the measure of deviation from circular, as function of time, Tg = 763 C, 10.5% oxygen in nitrogen, 21 mg liquor**

Assumption 3: Combustion on the particle surface is limited by the mass transfer of oxygen to the surface. This is valid until the rate of oxygen reaching the surface exceeds the rate required to stoichiometrically burn the volatiles evolved. When this occurs the combustion at the surface is limited by the rate of volatiles evolution.

Assumption 4: The oxygen requirement for combustion of one mole of volatiles is constant throughout volatilization. This assumption implies that the composition of the volatiles remain constant throughout volatilization. Bhattacharya et al.[46] reported gas composition as a function of pyrolysis time. At a gas temperature of 740°C, the concentration of $CO_2$ decreased 9.7% from start to end of pyrolysis, CO

increased 29%, $H_2$ increased 55.9%, $CH_4$ decreased 10%, and $H_2S$ decreased 15.8%. While the gas composition changed considerably, the oxygen requirement increased only 0.9% from 0.492 mol $O_2$/mol volatiles to 0.4965 mol $O_2$/mol volatiles. Thus the assumption that the oxygen requirement for combustion of one mole of volatiles remains constant throughout volatilization is valid.

Assumption 5: Volatile evolution is external heat transfer limited. This is consistent with Frederick's model,[13] and is generally accepted for pyrolysis of black liquor.

Assumption 6: The particle is isothermal. This is a simplifying assumption to neglect heat conduction through the particle and thus avoid the necessity of making major assumptions about the surface layer thickness, particle conductivity, particle porosity, and the pyrolysis reaction profile across the particle radius. Because of the swelling and the high heat flux to the particle, the assumption of an isothermal particle is not very good.

Assumption 7: Heat of combustion, $H_{comb}$, heat of pyrolysis, $H_p$, and the heat capacity, $Cp_d$, are constant throughout volatiles burning. This again is a simplifying assumption. $H_{comb}$ was taken to be 1530 cal/g volatiles. Bhattacharya et al.[46] reported this to be the average gas heating value for all their pyrolysis experiments. As they did not report how it varied with time, it is assumed to remain constant. $H_p$ was taken to be one tenth of the gas heating value, 150 cal/g volatiles. No values for the heat of pyrolysis are reported in the literature, and most pyrolysis models for coal and black liquor set $H_p$ equal to zero. The heat capacity, $Cp_d$, of

the solids is assumed not to change with temperature or solid composition. A 50% increase in particle temperature increases $Cp_d$ by 10%.[1]

Assumption 8: Ideal gas. Most gases and mixtures of gases do not deviate from PV = nRT until very high pressures and low temperatures are reached. Combustion gas can be considered ideal, since it is at atmospheric pressure and high temperatures.

Assumption 9: The only mass lost is volatiles. The particle is assumed to be completely dry at the start of volatiles burning, and no carbon is consumed through char burning reactions until all the volatiles evolution is complete. No mass is lost through sparking or fuming. Sparking occurs during char burning, and usually occurs close to the time for smelt coalescence. Fuming occurs throughout char burning, but most of the visible fume in the SPR was released after smelt coalescence.

Assumption 10: Pyrolysis kinetics are first order in the mass of unreacted black liquor solids. This is a common method of expressing a system of first order reactions, often used successfully in modeling coal pyrolysis.

Assumption 11: The maximum swollen volume occurs when volatiles evolution is complete. This has been experimentally shown in Figure 16, which compared the actual diameter to the predicted diameter during volatiles burning. Both curves reached the maximum swollen diameter simultaneously.

Parameters

Several adjustable parameters were used in the volatiles burning model. The density of the black liquor, used to calculate the initial

diameter of the wet drop, was set at 1.4 g/cm$^3$. The initial diameter for volatiles burning was set at 1.5 times the initial wet diameter. This is based on experimental observations in the SPR and is in agreement with results reported by Hupa.[3] The combination view factor and particle emissivity was set at 0.54. The particle emissivity was assumed to equal 0.75. The total amount of volatiles evolved was assumed to be 35% of the original dried mass. This is consistent with the volatilization yields reported in the literature.[19,46,48]

RESULTS

Inputs to the volatiles burning model were the initial wet mass, the gas temperature, the wall temperature, the particle temperature after drying was complete, the liquor solids, the drying time, and the gas stream oxygen concentration. The particle temperature and the drying time were obtained from the results of the drying model. Outputs of the model, at each time step, were the mass of the particle, the temperature of the particle, the diameter of the particle, and the percentage of volatiles left to evolve.

The time to finish volatiles burning is defined as the time between the end of drying and the end of particle swelling. As discussed in the drying section of this thesis, the end of drying is impossible to determine experimentally. To avoid the necessity of measuring the end of drying, the two stages can be combined. The time to complete drying and volatiles burning is experimentally the time between insertion of the drop into the hot environment and the end of particle swelling. Figure 18 is a plot of the predicted and measured combined drying and volatiles burning

times. The initial solids for the liquor, a mill kraft, was 68 percent. The data were measured for the gas temperature range of 800°C to 910°C, gas composition between 2% and 8% oxygen in nitrogen, and 10 mg to 50 mg initial liquor mass. The $r^2$ for the prediction is 0.82.

Experimental curves of the particle mass profile with time show a region of rapid mass loss which is linear with time. This is shown for a 21 mg drop burning in 10.5% oxygen at 763°C in Figure 19. This is the same test as was used for Figures 16 and 17. Figure 19 shows the apparant mass of the particle, not the absolute mass. The initial rise in the curve results from the balance adjustment to the introduction of the gas past the particle. The model predicts this same region. The slope of this line, the rate of volatilization, can be measured from the curves and a comparision between the predicted and the experimentally obtained curves can be made. Figure 20 shows the comparision between the predicted and the observed rates of volatilization for combustion tests of a 71.8% solids mill kraft black liquor (660°C - 860°C, 0% - 21% $O_2$ in $N_2$, 4 mg - 40 mg initial liquor mass).

Figure 20 shows oxygen concentration in the gas stream as a variable parameter. The model predicts equally well for the entire range of gas compositions tested. The model, without including a flame sheet, predicts satisfactorily for tests burned in greater than 16% oxygen. The $r^2$ for the model is 0.72. While the $r^2$ is low, statistics done using the F-test to calculate the lack of fit of the model show that there is no significant lack of fit in the model. The low $r^2$ is due to experimental error and not model error. For the model, F = 1.603 and the tabulated

value for F is 4.68. Since 1.603 < 4.68, there is no significant lack of fit in the model for predicting the rate of volatilization.

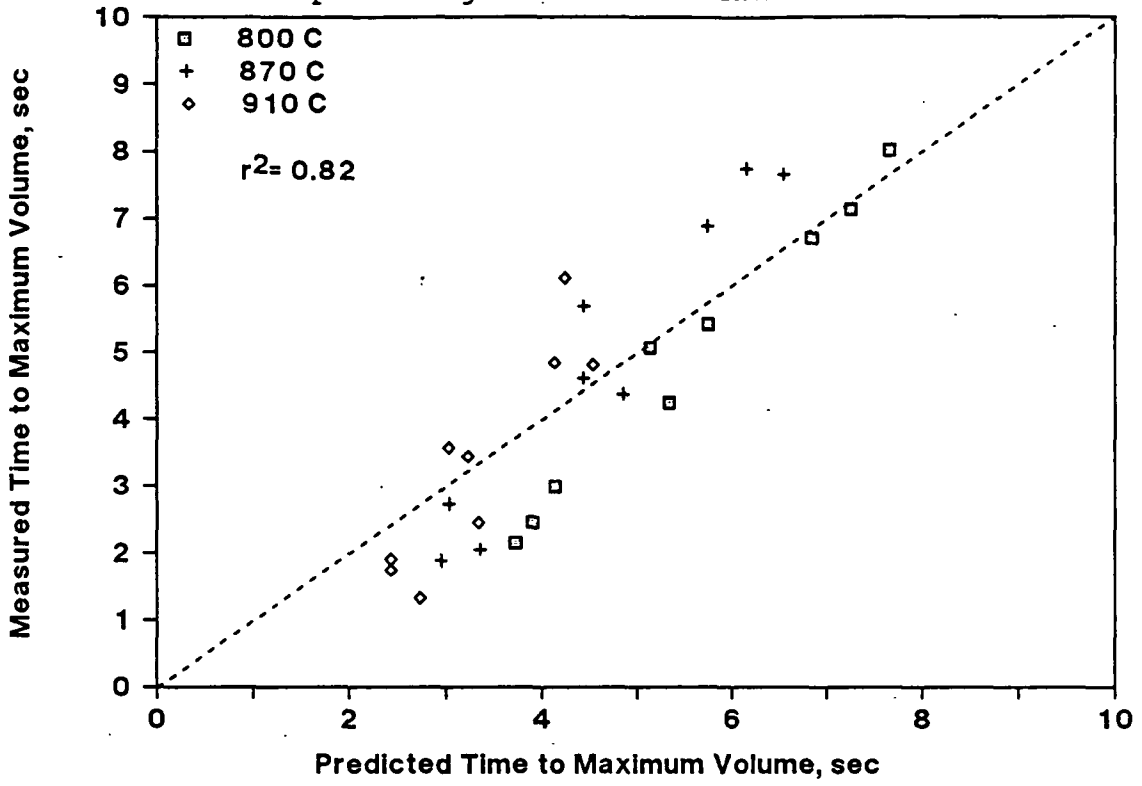


Figure 18. Predicted vs. measured combined drying and volatiles burning times. Tg = 800 C - 910 C, 2% - 8% oxygen in nitrogen, 10 - 20 mg initial liquor mass

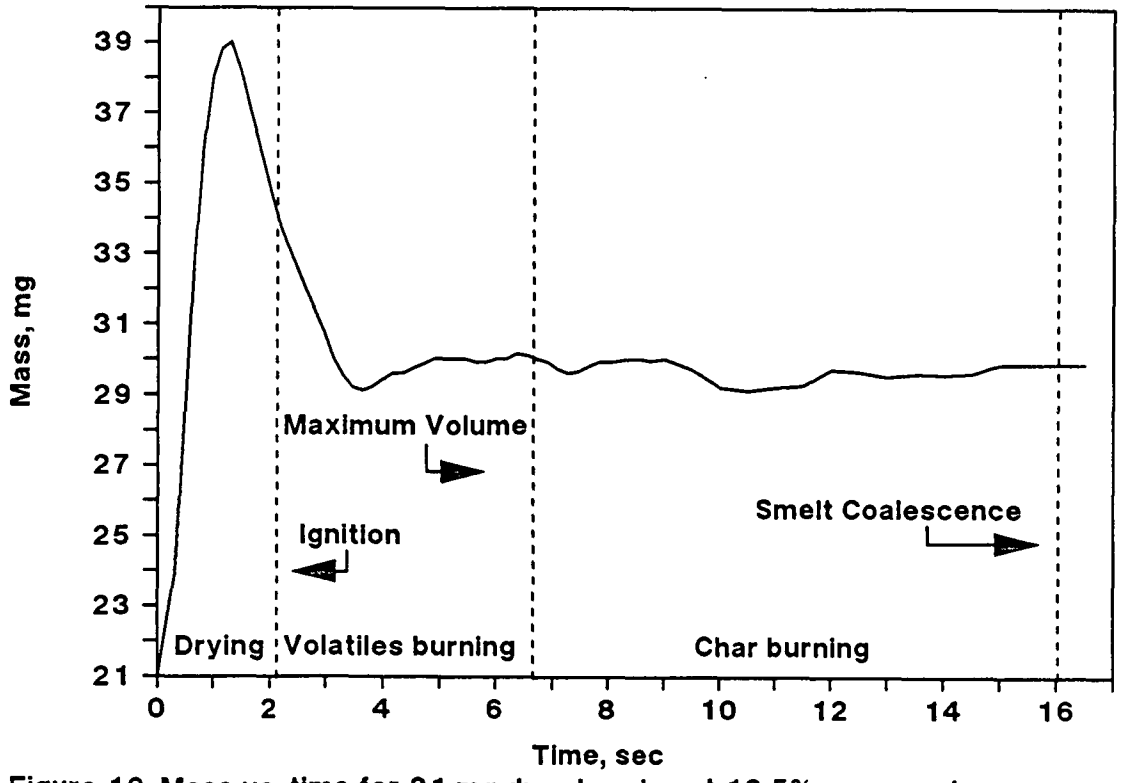


Figure 19. Mass vs. time for 21 mg drop burning at 10.5% oxygen at 763 C. Gas velocity = 1.7 m/sec

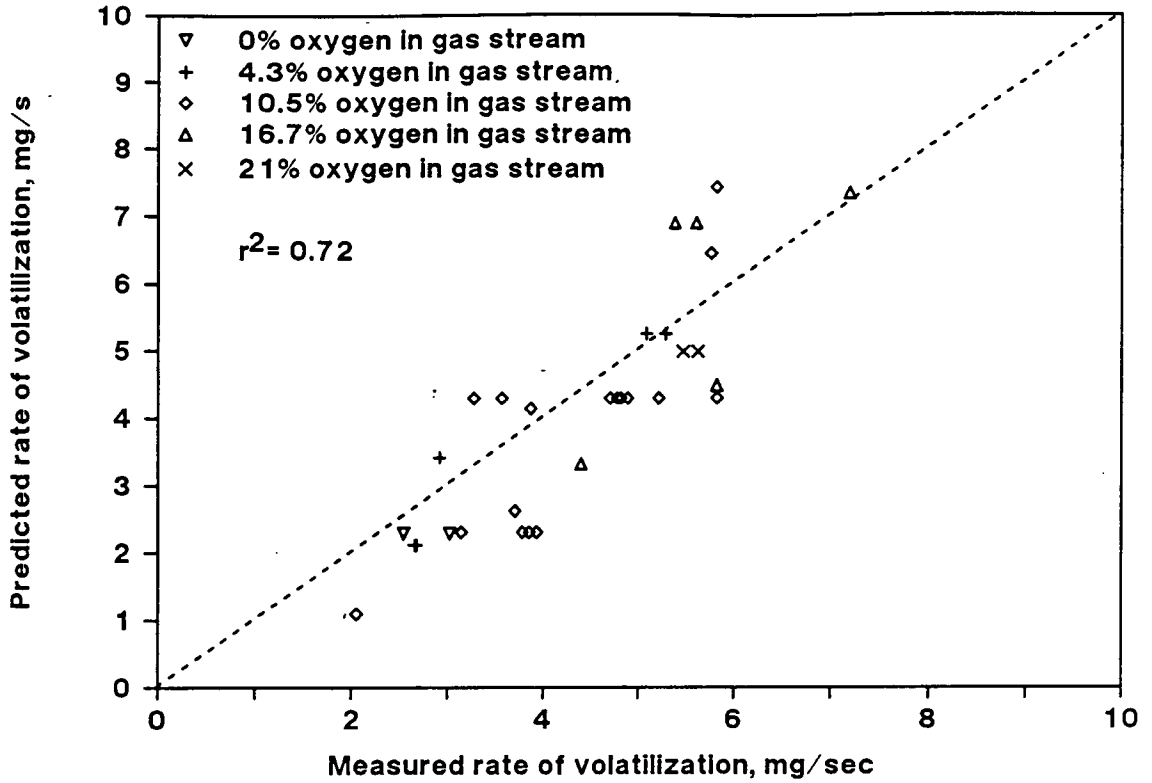


Figure 20. Predicted vs. measured rate of volatilization, Tg = 660 C - 860 C, 0% - 21% oxygen in nitrogen, 4 mg - 40 mg initial liquor mass, v = 1.7 m/sec

CONCLUSIONS

1. The maximum swollen diameter of a burning kraft black liquor drop can be predicted for one liquor from the initial drop mass. The gas temperature (800°C - 910°C) and the gas oxygen concentration (2% - 8%) did not statistically influence the maximum swollen diameter.

2. Volatiles burning in less than 10% $O_2$ is without a distinctive flame sheet surrounding the particle.

3. The combination of drying and volatilization models successfully predicts the time to reach maximum volume.

4. The volatiles burning model successfully predicts the rate of volatilization for a wide range of experimental conditions.

## CHAR BURNING

Char is composed of fixed carbon and inorganics. The fixed carbon, approximately 25-30% of the char by weight, is consumed through several reactions.

$$Na_2SO_4 + 4\ C \Rightarrow Na_2S + 4\ CO \qquad \text{(Rxn. 1)}$$

$$Na_2SO_4 + 2\ C \Rightarrow Na_2S + 2\ CO_2 \qquad \text{(Rxn. 2)}$$

$$2\ C + O_2 \Rightarrow 2\ CO \qquad \text{(Rxn. 3)}$$

$$C + O_2 \Rightarrow CO_2 \qquad \text{(Rxn. 4)}$$

$$C + CO_2 \Rightarrow 2\ CO \qquad \text{(Rxn. 5)}$$

$$C + H_2O \Rightarrow CO + H_2 \qquad \text{(Rxn. 6)}$$

Reactions (1) and (2) make up half of the sulfate/sulfide cycle proposed by Grace *et al.*[8] for char bed burning. Reactions (3-6) are carbon gasification reactions. This model will neglect the water/carbon reaction, Reaction (6), as the amount of water vapor in the present system is negligible.[18] The gas stream sweeps the water vapor formed during drying and volatiles burning away from the char particle.

The sulfate/sulfide cycle consists of Reactions (1), (2), and (7).

$$Na_2S + 2\ O_2 \Rightarrow Na_2SO_4 \qquad \text{(Rxn. 7)}$$

Reactions (1) and (2) describe carbon consumption by reaction with $Na_2SO_4$ to form $Na_2S$ and either CO (Reaction (1)) or $CO_2$ (Reaction (2)). Reaction (7) describes the oxidation of sulfide to sulfate. Grace *et al.*[8] concluded

that the rate of carbon consumption was controlled by the rate of sulfide oxidation. This was the only way they could explain high reduction ratios, the molar ratio of $Na_2S$ to $Na_2S$ and $Na_2SO_4$, while burning in air. They measured the mass of fairly large (110 mg) pellets of dried black liquor during combustion. The pellets were pyrolyzed in nitrogen and the remaining char was immediately burned in air. At the end of the tests with kraft liquor char they observed weight gain which was attributed to the oxidation of sulfide to sulfate. The weight gain was not seen with soda chars. Milanova and Kubes[17] also reported a weight gain at the end of kraft char burning which was attributed to the oxidation of $Na_2S$ to $Na_2SO_4$.

The sulfate/sulfide cycle has not been shown to apply directly to black liquor single particle combustion, although it was shown to fit a few observations of dried pellet combustion.[8] The role of sulfur in char burning can be studied by the effect it has on combustion of soda liquor. Soda liquor contains no significant amounts of sulfur. If the sulfate/sulfide cycle plays a role in char burning, then soda liquor loaded with sulfur will burn faster than pure soda liquor. If sulfur plays no role in char burning, then the loaded and the pure soda liquor will have similar burn times.

A lab cook soda liquor was loaded with four levels of sulfur, as shown in Table 6. The method by which this was done is described in Appendix II. The sulfur was added in the form of $Na_2SO_4$, the most stable form of sulfur in black liquor. The heating value of the liquor decreased as the amount of sulfur loading increased, because the amount of deadload increased. The solids content of these liquors varied over a wide range

because the viscosity of the liquor decreased with sulfur loading, making it easier to evaporate the higher sulfur liquors.

Table 6. Soda Liquors

| Liquor | % Sulfur | % Solids | HHV, Btu/lb |
|---|---|---|---|
| SDA | 0.03 | 59.2 | 6990 |
| SDC | 4.03 | 61.7 | 5630 |
| SDD | 6.88 | 65.4 | 4910 |
| SDE | 7.35 | 73.0 | 4031 |
| SDF | 8.55 | 70.0 | 3580 |

Single drops of these liquors were combusted in the SPR. The drops (50 mg - 150 mg) were dried and pyrolyzed under nitrogen at 800°C before the gas flow was switched to air. The reactor was equipped with a set of switches upstream of the particle to allow the gas change without affecting the total gas flow past the char particle. The char surface temperature and the char burn time were measured for each test. Unfortunately, the microbalance was not operational during these tests so mass data from these burns is not available. Figure 21 shows the results of this set of tests. The char burn time is plotted as a function of initial dry mass. The char burn time is the time between the oxygen reaching the particle, detected by a glow, and smelt coalescence, the collapse of the char structure into a smelt bead. In the case of liquor SDA, the pure soda liquor, there was no smelt coalescence. Char burning ended when the visible flame around the particle faded away. Immediately after the flame disappeared the glowing char started cooling evidenced by the char color changing from orange to black.

Each sulfur level is plotted separately in Figure 21. Sulfur makes a difference in the time for char burn and thus in the carbon

consumption mechanism. The sulfate/sulfide cycle has been shown to apply to char beds, char pile combustion,[23] and dried black liquor pellet combustion.[8] It seems reasonable to conclude from the observed influence of sulfur on the soda char burn time, that the sulfate/sulfide cycle applies to black liquor particle combustion. As the char burn time is reproducible over the range of the drop sizes tested, validation of the char burn model will be with the predicted and measured char burn times.

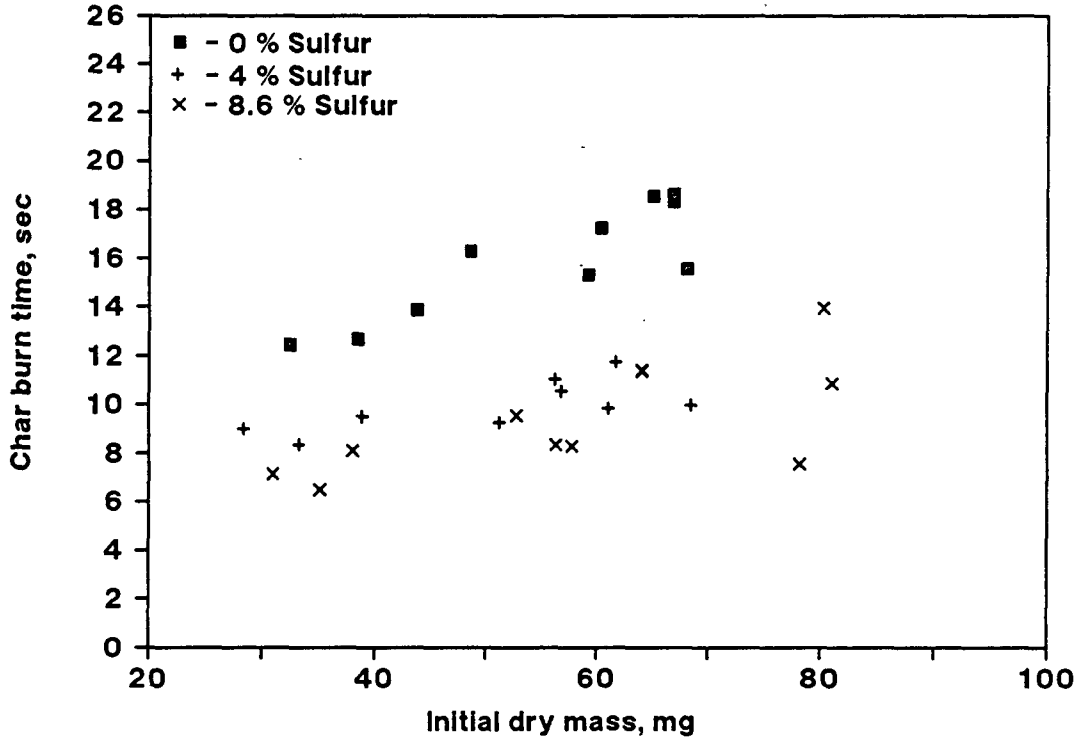


**Figure 19. Char burn time vs. initial dry mass, liquor was dried and pyrolyzed in nitrogen at 800 C before burning in air. Soda liquors loaded with 0% - 8.6% sulfur as sodium sulfate.**

MODEL

A sketch of the black liquor particle during char combustion is shown in Figure 22. The cross hatched area is (1-P), the fraction of the char surface which is inorganic. $T_d$ is the char temperature, $T_g$ is the gas temperature, and $r_d$ is the char radius. Oxygen is transferred to the char surface from the surrounding gas.

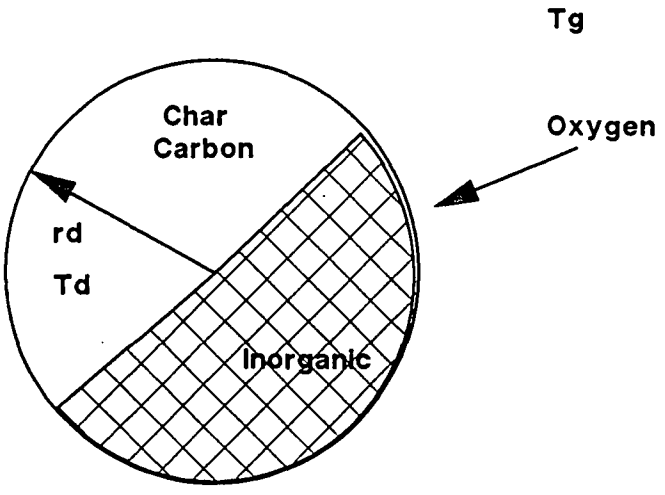


Figure 22. Sketch of the black liquor particle during char burning

Carbon consumption, through Reactions (1-5), can be expressed by Equation (28),[49]

$$-\frac{d[C]}{dt} = \frac{4}{2 - f_{cs}} RCS + \frac{2}{2 - f_{ox}} ROX + RCO_2 \qquad (28)$$

where [C] = mol C/mol $Na_2$

$f_{cs}$ = mol CO/(mol CO + mol $CO_2$), CO is produced by Reaction (1) and $CO_2$ is produced by Reaction (2)

RCS = C/$Na_2SO_4$ reaction rate, mol $Na_2SO_4$/mol $Na_2S$ - sec

$f_{ox}$ = mol CO/(mol CO + mol $CO_2$), CO is produced by Reaction (3) and $CO_2$ is produced by Reaction (4)

ROX = C/$O_2$ reaction rate, mol $O_2$/mol $Na_2$ - sec

$RCO_2$ = C/$CO_2$ reaction rate, mol C/mol $Na_2$ - sec

Carbon/Sulfate Reaction

Grace et al.[8] determined an expression, Eqn. (29) for RCS using a small quantity of ground char in a smelt pool reactor. Kinetic constants were developed for both kraft and soda chars.

$$RCS = - K_1 \frac{[SO_4]}{K_2 + [SO_4]} [C] \, EXP \, (-E_1/RT_d) \qquad (29)$$

where $K_1$ = 1310 $sec^{-1}$, for kraft char

$K_1$ = 3.04E+05 $sec^{-1}$, for soda char

$K_2$ = 0.0011 mol $SO_4$/mol $Na_2$, for kraft char

$K_2$ = 0.00055 mol $SO_4$/mol $Na_2$, for soda char

$[SO_4]$ = the sulfate concentration, = (1-r) s

r = reduction ratio, mol $Na_2S$/(mol $Na_2S$ + mol $Na_2SO_4$)

s = sulfidity, mol S/mol $Na_2$

$E_1$ = 29200 cal/mol, for kraft char

$E_1$ = 39850 cal/mol, for soda char

R = gas constant, 1.987 cal/mol-K

$T_d$ = char temperature, K

Carbon/Oxygen Reaction

An expression for ROX, the rate of carbon oxidation with oxygen was obtained from the coal literature.[20] This is for bituminous coal char, with an irreversible heterogenous reaction which is first order in oxygen concentration. The kinetic rate constant, Kr, is

$$Kr = Kp\ T_g\ R/M_{O2} \tag{30}$$

and

$$Kp = 92\ \exp\ (-E_2/RT_d) \tag{31}$$

substituting in,

$$Kr = 236\ T_g\ \exp\ (-E_2/RT_d) \tag{32}$$

where Kr = kinetic rate constant, cm/sec

Kp = reaction rate coefficient, $g/cm^2$-sec-atm $O_2$

$E_2/R$ = 11022, $K^{-1}$

$M_{O2}$ = molecular weight of oxygen, 32 g/mol

The validity of Equation (32) can be shown as follows. If all of the carbon consumption is assumed to be through the carbon/oxygen pathway of Reaction (4), and it is assumed that char combustion is kinetically limited, then

$$-\ d[C]/dt = ROX = Kr\ C_{O2}\ A_p \tag{33}$$

where $C_{O2}$ = oxygen concentration in the bulk gas, $mol/cm^3$

$A_p$ = particle external surface area, $cm^2$

Now, [C] = $m_c$ * 12 and $m_d = m_c + m_s$, with $m_c$ as the mass of carbon in the particle, g/mol $Na_2$, $m_d$ as the mass of the particle, g/mol $Na_2$, and $m_s$ as the mass of the inorganic salts in the particle, g/mol $Na_2$. Differentiating with respect to time, $dm_d/dt = dm_c/dt$. Substituting into Equation (33),

$$- dm_d/dt = -7.248\ A_p \exp(-11022/T_d) \qquad (34)$$

Assuming $A_p$ is constant at the initial particle external surface area and $T_d = T_g$, the initial value for $dm_d/dt$ can be calculated. For a pure soda liquor combusted at 800°C, $dm_d/dt$ was calculated using Equation (34) to be -7.325 mg/sec and was measured to be -7.071 mg/sec. Therefore, Equation (34) accurately predicts $dm_d/dt$ for a pure soda liquor and the kinetics of Equation (32) are valid for black liquor char oxidation with oxygen.

The overall rate constant for the carbon/oxygen reaction, Kcox, cm/sec, is a combination of kinetics and mass transfer of oxygen to the char surface.

$$Kcox = \frac{1}{1/K_{O2} + 1/Kr} \qquad (35)$$

The mass transfer rate constant, $K_{O2}$, is determined by replacing the Nusselt and Prandtl numbers by the Sherwood and Schmidt numbers in the Ranz and Marshall correlation for heat transfer from a sphere in one dimensional flow.[50]

$$Sh = K_{O2}\ d/D_{O2} = 2 + 0.6\ Re^{1/2}\ Sc^{1/3} \qquad (20)$$

Finally, the rate of the carbon/oxygen reaction is

$$ROX = Kcox\ C_{O2}\ A\ P \tag{36}$$

where A = surface area, $cm^2/mol\ Na_2$

P = fraction of surface which is carbon

The method proposed by Sumnicht et al.[49] to determine P is as follows. P is defined as

$$P = \frac{A_C}{A_C + A_S} \tag{37}$$

where $A_C$ = surface area which is carbon

$A_S$ = surface area which is inorganic

Assuming the char particle is spherical, A is proportional to $V^{2/3}$, and the volume is related to the mass by the density, $V = m/\rho$, P is now

$$P = \frac{(m_C/\rho_C)^{2/3}}{(m_C/\rho_C)^{2/3} + (m_S/\rho_S)^{2/3}} \tag{38}$$

Substituting $m_C = [C] * m_{CO}/[C]_O$ and dividing by $(m_{CO}/\rho_C)^{2/3}$, P becomes

$$P = \frac{([C]/[C]_O)^{2/3}}{([C]/[C]_O)^{2/3} + (\rho_C\ m_S/(\rho_S\ m_{CO}))^{2/3}} \tag{39}$$

where $m_{CO}$ = initial mass of carbon, $g/mol\ Na_2$

$\rho_C$ = density of char[22], 0.2 $g/cm^3$

$\rho_S$ = density of inorganic salts, 2.0 $g/cm^3$

$m_S$ = mass of the inorganics, $g/mol\ Na_2$

Grace et al.[22] analyzed several kraft chars and concluded that the char composition could be simplified to a few species, shown in Table 7.

Table 7. Simplified kraft char composition[22]

| | mol/mol $Na_2$ | g/mol $Na_2$ |
|---|---|---|
| Carbon | 3.50 | 42.0 |
| $Na_2S$ | 0.06 | 4.68 |
| $Na_2SO_4$ | 0.06 | 8.52 |
| $Na_2CO_3$ | 0.88 | 93.28 |

The initial value of $m_c/m_s$ is 42/106.48 = 0.394. Substituting in, $(\rho_c/\rho_s * m_s/m_{co})^{2/3} = 0.4$. Sumnicht et al.[49] assumed that $m_s$ remained constant throughout char burning. The mass of inorganics, $m_s$, can remain constant only if the reduction ratio remains constant, or if there is no fuming or sparking from the particle. If there is no sparking or fuming, the total moles of inorganic do remain constant throughout char burning. P will be a function of the mass of the inorganics in the char burning model.

Char Diameter

The diameter of the particle changes during combustion. If the particle is assumed to remain spherical throughout combustion, then $d = (6\ V/\pi)^{1/3}$. V, the volume of the particle, can be calculated from the mass and density of the particle. The mass, $m_d$, is known at each timestep. The density, $\rho_d$, can be calculated by making several assumptions. If the particle is assumed to consist of char carbon, inorganic salts, and void space, then

$$\rho_d = \frac{m_c + m_s}{V_c + V_s + V_{void}} \qquad (40)$$

Sumnicht et al.[49] postulated that the strength of the carbon matrix enables the char particle to maintain its low density. If this is valid, then densification of the particle would occur when the carbon matrix loses strength due to carbon loss. The void volume and the mass of carbon can then be related by the following assumed expression,[49]

$$V_{void}/m_c = V_{void,o}/m_{co} \tag{41}$$

Substituting Equation (41) and $V = m/\rho$ into Equation (40) results in Equation (42),

$$\rho_d = \frac{m_c + m_s}{m_c/\rho_c + m_s/\rho_s + V_{void,o}\, m_c/m_{co}} \tag{42}$$

Separating out $m_c$, the denominator becomes $m_c*(1/\rho_c + V_{void,o}/m_{co}) + m_s/\rho_s$. Lumping together the terms in the paranthesis as the "apparant" carbon density, $\rho_{ca}$, Equation (42) can be rewritten as

$$\rho_d = \frac{m_c + m_s}{m_c/\rho_{ca} + m_s/\rho_s} \tag{43}$$

The particle volume is now

$$V = \frac{m_c + m_s}{\rho_p} = \frac{m_c}{\rho_{ca}} + \frac{m_s}{\rho_s} \tag{44}$$

At smelt coalescence, which is defined as the end of the char burn, the particle volume, $V_\infty$, is $m_s/\rho_s$ because the carbon has burned away. The

ratio of $V_\infty$ to the initial volume, $V_o$, is

$$V_\infty/V_o = x_s \rho_c/\rho_s \tag{45}$$

where $x_s$ is the mass fraction of inorganics in the char. Dividing Equation (44) by $V_o$, and rearranging, yields

$$\frac{V}{V_o} = \left(1 - \frac{V_\infty}{V_o}\right) \frac{[C]}{[C]_o} + \frac{V_\infty}{V_o} \tag{46}$$

and finally d is expressed as

$$d = d_{max} \left[ \left(1 - \frac{V_\infty}{V_o}\right) \frac{[C]}{[C]_o} + \frac{V_\infty}{V_o} \right]^{1/3} \tag{47}$$

Carbon/Carbon Dioxide

$RCO_2$, the rate of carbon consumption with $CO_2$, can be expressed as,[25,26]

$$RCO_2 = \frac{- K_3 p_{CO2} [C]}{1 + K_4 p_{CO2} + K_5 p_{CO}} \exp(-E_3/RT_d) \tag{48}$$

where $K_3$, $K_4$, $K_5$, and $E_3$ are kinetic constants

$p_{CO2}$ = partial pressure of $CO_2$, atm

$p_{CO}$ = partial pressure of CO, atm

This reaction was studied in two different systems. Goerg[26] bubbled $CO_2$ through a molten salt pool containing a small amount of char, and Li[25] exposed char directly to $CO_2$. In single particle combustion, the $CO_2$

reacts directly with the exposed char carbon, similar to Li's system. Li's kinetic constants will be used in this model, as his system was more representative of single particle combustion.

$K_3$ = 9.53E+07 $atm^{-1}$-$sec^{-1}$

$K_4$ = 10.8 $atm^{-1}$

$K_5$ = 6.3 $atm^{-1}$

$E_3$ = 18700 J/mol

Sulfide Oxidation

The rate of sulfide oxidation by Reaction (7) can be expressed by Equation (49),[8]

$$\frac{d[Na_2S]}{dt} = s\frac{dr}{dt} = RCS - RSO \qquad (49)$$

where RSO = rate of sulfide oxidation, mol $Na_2S$/mol $Na_2$-sec,

$$RSO = Kso\ C_{O2}\ [S]\ A\ (1-P) \qquad (50)$$

and,
$$Kso = \frac{1}{1/K_{O2} + 1/Krso} \qquad (51)$$

where Kso = overall rate constant for sulfide oxidation, cm/sec

$K_{O2}$ = mass transfer rate constant, cm/sec

Krso = kinetic rate constant, cm/sec

[S] = sulfide concentration, mol $Na_2S$/mol $Na_2$, = r * s

Grace et al.[22] concluded that sulfide oxidation is controlled by oxygen

mass transfer to the sulfide as long as the reduction ratio, r, in the smelt remains above 2 percent. This implies that Krso >> $K_{O2}$, leading to Kso = $K_{O2}$. $K_{O2}$ is determined by Equation (20). However, the present model predicts a reduction ratio of zero throughout the entire char burn when Kso = $K_{O2}$.

The particles used in this work were pyrolyzed from black liquor drops, and had very large surface area to mass ratios during char burning. They were small drops which swelled extensively during volatiles burning. The pellets of dried liquor used by Grace et al.[8] did not swell as much during pyrolysis, and had low surface area to mass ratios during char burning. This low ratio caused the particles to oxidize more slowly, making Krso >> $K_{O2}$ and the assumption that sulfide oxidation is mass transfer limited valid. In char produced from pyrolysis of black liquor particles, the sulfide was predicted to oxidize to sulfate instantaneously when the reaction was controlled by mass transfer of oxygen to the sulfide. The reaction kinetics become more important as r decreases, and dominate the reaction rate when r falls below 2%. The observed effect of moisture on black liquor swelling agrees with reported results in the literature.[14]

The sulfide oxidation data was summarized by Grace et al.[22] in a figure of RSO plotted against [S], the concentration of sulfide in the melt. The reaction rates for all of the temperatures they studied, 790°C - 870°C, fell on the same curve. Krso was determined from their data,

$$Krso = \frac{2250}{r\ s\ A\ (1-P)} \qquad (52)$$

Including Krso in Equation (50) causes the predicted reduction ratio to not fall to zero as fast as when the sulfide oxidation kinetics are not included. This will be discussed in more detail in the kraft results section.

Substituting Equations (29), (36), and (48) into Equation (28), and Equations (29) and (50) into Equation (49) yields two Equations, (53) and (54), and four unknowns, [C], r, $p_{CO2}$, and $p_{CO}$.

$$-\frac{d[C]}{dt} = 2K_1 \frac{(1-r)\ s}{K_2 + (1-r)\ s}\ [C]\ \exp\ (-E_1/RT_d) + Kcox\ C_{O2}\ A\ P + \frac{K_3\ p_{CO2}}{1 + K_4\ p_{CO2} + K_5\ p_{CO}}\ [C]\ \exp\ (-E_3/RT_d) \qquad (53)$$

$$\frac{dr}{dt} = \frac{K_1}{s}\ \frac{(1-r)\ s}{K_2 + (1-r)\ s}\ [C]\ \exp\ (-E_1/RT_d) - Krso\ C_{O2}\ r\ A\ (1-P)/2 \qquad (54)$$

Two more equations are needed to calculate $p_{CO2}$ and $p_{CO}$.

Assuming a boundary layer around the char particle, the boundary layer thickness, $\delta$, cm, can be approximated by an expression for flow near the leading edge of a flat plate.[51]

$$\delta = 5\ (\nu\ d/v)^{1/2} \qquad (55)$$

The volume of the boundary layer, $V_{BL}$

$$V_{BL} = \frac{\pi}{6}\ (d + 2\ \delta)^3 - d^3 \qquad (56)$$

The partial pressure of $CO_2$ and of CO in the boundary layer, assuming ideality, is

$$p_{CO2} = \frac{R\ T\ m_{CO2}}{M_{CO2}\ V_{BL}} \tag{57}$$

$$p_{CO} = \frac{R\ T\ m_{CO}}{M_{CO}\ V_{BL}} \tag{58}$$

where $m_{CO2}$ = mass of $CO_2$ in the boundary layer, g

$m_{CO}$ = mass of CO in the boundary layer, g

$V_{BL}$ = volume of boundary layer, $cm^3$

$M_{CO2}$ = molecular weight of $CO_2$, 44 g/mol

$M_{CO}$ = molecular weight of CO, 28 g/mol

A mass balance on $CO_2$ in the boundary layer is shown in Equation (59). A similar balance for CO is shown in Equation (60).

$$\frac{dm_{CO2}}{dt} = \left[\frac{2(1-f_{ox})}{2-f_{ox}}\ ROX + \frac{4(1-f_{cs})}{2-f_{cs}}\ RCS - RCO_2 - F_{CO2}\right] M_{CO2}\ n_{Na2} \tag{59}$$

$$\frac{dm_{CO}}{dt} = \left[\frac{2\ f_{ox}}{2-f_{ox}}\ ROX + \frac{4\ f_{cs}}{2-f_{cs}}\ RCS + 2\ RCO_2 - F_{CO}\right] M_{CO}\ n_{Na2} \tag{60}$$

where $F_{CO2}$ = mass transport of $CO_2$ away from boundary layer,

mol $CO_2$/mol $Na_2$-sec

$F_{CO}$ = mass transport of CO away from boundary layer,

mol CO/mol $Na_2$-sec

$n_{Na2}$ = moles of $Na_2$

$F_{CO2}$ and $F_{CO}$ can be expressed in terms of the mass transfer coefficient, similar to Equation (20).

$$K_{CO2} = \frac{D_{CO2}}{(d + 2\,\delta)} \left[2 + 0.6\ Re^{1/2}\ Sc^{1/3}\right] \tag{61}$$

$$K_{CO} = \frac{D_{CO}}{(d + 2\,\delta)} \left[2 + 0.6\ Re^{1/2}\ Sc^{1/3}\right] \tag{62}$$

where $K_{CO2}$ = $CO_2$ mass transfer coefficient, cm/sec

$K_{CO}$ = CO mass transfer coefficient, cm/sec

$D_{CO2}$ = diffusivity of $CO_2$ in air, $cm^2$/sec

$D_{CO}$ = diffisivity of CO in air, $cm^2$/sec

The four differential equations solved by the char burning model are Equations (53), (54), (59), and (60). The program uses a fourth order Runge-Kutta method to solve this system of equations. The program code is contained in Appendix VI. Char burning was considered complete when 1% carbon by weight remained in the particle.

Assumptions

The assumptions for this model are

1. Spherical geometry
2. Char combustion occurs on the char surface
3. Grace et al.[8] kinetics for sulfate/sulfide cycle
4. Carbon oxidation by oxygen is irreversible, heterogeneous, and first order in oxygen concentration. The kinetics are from coal combustion.[28]
5. Li et al.[25] kinetics for $C/CO_2$ reaction

6. A well mixed finite boundary layer around the char

7. Fraction of surface available, (1-P), for the sulfate/sulfide cycle is a function of char composition, carbon density, and inorganic density

8. The void fraction divided by the amount of carbon present in the char is constant throughout char burning

9. Fuming does not influence the char burn time

10. Ideal gas

11. Oxygen concentration, velocity, and temperature of the bulk gas is constant

12. Diffusivity of $O_2$, $CO_2$, and CO in air are independent of temperature

13. Sulfidity and the amount of sodium present in the char are constant

14. A time-temperature profile linear in time is assumed to approximate the char temperature for the tests with no surface temperature data

Discussion of Assumptions

Assumption 1: Spherical geometry. This is a simplifying assumption and is reasonably accurate. Visual observations indicate that the char is consumed from all sides at the same rate. Visual observations also indicate that initially the shape of the char particle is a mix between cylindrical and spherical. Figure 17 showed a plot of the shape factor, a measure of the deviation from circular, during char burning. A circle has a shape factor of one.

Assumption 2: Char combustion occurs on the surface. This assumption is based on visual observations indicating that the reaction front proceeds from the surface in towards the char center. The reaction front observed was a layer of smelt.

Assumption 3: Grace et al.[8] kinetic values are used for the carbon/sulfate reaction and for sulfide oxidation. This includes the kinetic values for both kraft and soda chars. Their experiments were done in a smelt pool reactor, with small quantities of char in a large pool of molten salts. Mixing of the smelt and char was accomplished by bubbling an oxygen containing gas through the smelt. Although this system is not representative of single particle combustion, the results do apply to single particle combustion. The sulfate/sulfide cycle operates when the molten smelt is in contact with the char carbon. This is the same situation as in the smelt pool reactor, with molten smelt in contact with char carbon. Thorman and Macur[21] also determined kinetic constants for the carbon/sulfate reaction. However, since they used graphite instead of kraft or soda char, Grace's kinetic constants are used in this model.

Sulfide oxidation is dependent on both mass transfer and kinetics. Char particles obtained by drying and pyrolyzing black liquor drops in nitrogen at a high reactor temperature, 800°C, have high surface area to mass ratios. This causes the limiting step of sulfide oxidation to shift towards chemical kinetics rather than mass transfer of oxygen to the char. Sulfide oxidation kinetics from Grace et al.[22] are used in the model to account for this shift.

Assumption 4: Carbon/oxygen reaction is irreversible, heterogeneous, and first order in oxygen concentration. The kinetics are from coal combustion.[20] The particular coal used was bituminous, and the swelling characteristics were not listed. Carbon/oxygen kinetics for black liquor char combustion have not been reported in the literature.

Assumption 5: Li and van Heiningen[25] kinetics for $C/CO_2$ reaction. Li's kinetics were better suited to single particle combustion than Goerg's[26] due to differences in reactor conditions. Li exposed large quantities of carbon, 1.2 - 5.8 mol C/mol $Na_2$, directly to $CO_2$ gas while Goerg exposed small quantities of carbon, 0.015 - 0.062 mol C/mol $Na_2$, to smelt. The $CO_2$ gas was bubbled through the smelt, and forced to diffuse through the molten salts to the carbon surface. In single particles, only part of the surface is molten and $CO_2$ has direct access to the surface char carbon. Another difference between the two systems was the reactor temperature. Goerg's data were taken in the temperature range of 927°C - 1010°C while Li's data were in the temperature range of 700°C - 775°C. Although Goerg's[26] data were obtained at temperatures closely approximating char combustion, the higher carbon concentration and mode of $CO_2$ access to the char carbon in Li's[25] system make his data more applicable to single particle char combustion.

Assumption 6: There is a well mixed finite boundary layer around the char, which is described by incompressible flow past the leading edge of a flat plate. Although flow past the leading edge of a flat plate is not the same as flow past a sphere, boundary layer calculations increase in complexity as the geometry described grows more complex. Once the char particle's shape approaches cylindrical, the approximation of flow past the leading edge of a flat plate becomes more applicable.

Assumption 7: The fraction of surface available, (1-P), for the sulfate/sulfide cycle is a function of char composition, carbon density, and inorganic density. P is calculated from Equation (39). Implicit in

this assumption is that $\rho_s$ and $\rho_c$ remain constant with temperature and composition.

Assumption 8: The void fraction divided by the amount of carbon present in the char is constant. This directly influences the amount the diameter reduces with carbon consumption, as was shown in Equations (42) - (47).

Assumption 9: Fuming does not influence the time for completion of the char burn. This is a good assumption because, based on visual observations, the majority of the fuming occurs after smelt coalescence. Spitting or sparking, the ejection of small projectiles from the main body of char, does occur during the char burn. These projectiles are assumed to have the same chemical composition as the main body of char. The model calculates the time needed to reach a specified weight fraction of carbon, not the time needed to reach a specified weight of carbon. Losing projectiles of identical composition to the main body of char will affect the weight of carbon, but will not affect the weight fraction of carbon, and hence will not affect the char burn time.

Assumption 10: The gas is ideal. Most gases and mixtures of gases do not deviate from PV = nRT until very high pressures and low temperatures are reached. Combustion gas can be considered ideal since it is at atmospheric pressure and high temperatures.

Assumption 11: Oxygen concentration, velocity, and temperature of the bulk gas is constant.

Assumption 12: Diffusivity of $O_2$, $CO_2$, and CO in air are independent of temperature. The range of char temperature, and of gas temperature near

the char surface, is 800°C - 1200°C, as measured by the two-color pyrometer. A 50% increase in gas temperature increases the diffusivity by 70 percent. An average value for each diffusivity was used in the model.

Parameters

Several parameters were used to fit the char burn model. The f ratio, molar $CO/(CO+CO_2)$, was used to determine the extent of Reactions (1-4). The relative contributions of Reactions (1) and (2) to the carbon/sulfate reaction was set by $f_{cs}$, and $f_{ox}$ determined the contributions of Reactions (3) and (4) to the carbon/oxygen reaction. For tests in air, $f_{cs}$ and $f_{ox}$ were set at 0 (no CO produced via Reaction (1) and (3)). For the kraft tests in less than 8% oxygen, $f_{cs}$ and $f_{ox}$ were set at 0.9. The initial reduction ratio was set at 0.5 for the kraft tests, 0.35 for the soda/sulfate tests, and 0.0 for the pure soda tests.

A time vs. temperature relation was assumed for the tests with no surface temperature data. The char was assumed to initially be at the gas temperature, and then the char temperature increased linearly with time to a maximum temperature, occurring at smelt coalescence. Observations with the two-color pyrometer indicate that the peak temperature occurs at smelt coalescence. The peak temperature, $T_{max}$, is a function of the oxygen concentration in the gas stream. Brown et al.[19] measured the temperature of the active layer of a burning laboratory char bed, Table 8. The gas temperature was 800°C. The peak temperature in single particle combustion is assumed to be approximately the same as the temperature measured for the active layer in the lab char bed. The data suggest a linear char temperature vs. gas composition relation, as a 7% increase in oxygen

concentration increased the char temperature by 100°C. Equation (63) is the assumed relation using the data in Table 8 to predict $T_{max}$ from the gas temperature and oxygen concentration. In Eqn. (63), $C_{O2}$ is the oxygen concentration expressed as a fraction.

$$T_{max} = T_g + 1430\ C_{O2} \qquad (63)$$

Table 8. Char bed temperature at different gas compositions[19]

| Oxygen concentration in gas (%) | Char bed temperature (°C) |
|---|---|
| 0 | 800 |
| 7 | 900 |
| 14 | 1000 |
| 21 | 1100 |

RESULTS

The model was tested with three liquors, kraft, soda, and soda loaded with sulfate. Table 9 contains the char elemental compositions for kraft, soda, and soda/$Na_2SO_4$ chars. These were calculated from the analysis of the original liquor using experimental volatile loss determinations by Brown et al.[19] The soda loading is described in Appendix II. The initial mass was calculated from the dried solids by assuming 35% volatile yield.[19] The initial char diameter was taken as the maximum swollen diameter, which marked the end of volatiles burning. The computer code had to be changed slightly in the case of pure soda to adjust for zero sulfidity. Equation (54), which solved for the reduction ratio, involved division by the sulfidity, and was set equal to zero for pure soda. The remainder of the program was identical for soda and kraft.

Soda Liquor

The soda liquor tested was a lab cook concentrated to 59.2% solids for the pure soda, and 61.2% solids for the loaded soda. The drops were dried and pyrolyzed at 800°C in the SPR under nitrogen prior to char burning. The gas was switched to air when pyrolysis was complete. The total flow of gas past the particle did not vary. The surface temperature was measured during char burning with a two-color pyrometer. Char burn started when the particle first glowed visibly. The time delay between switching to air and the first glow was approximately 3.5 seconds. For the pure soda liquor, the measured char burn time extended from the first evidence of the glow to when the visible flame surrounding the particle disappeared. For the soda loaded with sulfate, char burning ended when the particle coalesced into a smelt bead. The predicted end of char burning occurred when 1% carbon by weight remained in the char.

Table 9. Calculated char compositions from liquor analysis, based on volatile loss measurements on laboratory char,[19] weight percent.

| | Kraft | Soda | Soda/$Na_2SO_4$ |
|---|---|---|---|
| Carbon | 27.4 | 35.0 | 25.5 |
| Hydrogen | 0 | 0 | 0 |
| Sulfur | 4.3 | 0 | 6.2 |
| Sodium | 30.9 | 32.1 | 35.4 |
| Oxygen | 37.4 | 32.9 | 30.8 |

Figure 23 shows the comparision between measured and predicted char burn times. Included are both the pure soda and the loaded sulfur tests. The $r^2$ for the pure soda correlation is 0.8, and for the loaded sulfur, 0.3. There is insufficient data at any level of initial char mass

to perform a lack of fit test for the model. The slope of the pure soda regression line is 0.98 which approaches, though slightly offset, the x = y line. The model used the measured surface temperature as the char temperature at each time step.

The tests with the pure soda liquor show that the char burning model, using only the gasification reactions (Rxn. 3 - 5), accurately predicts the char burn times. The kinetics chosen for Reactions (3 - 5), the carbon/oxygen and carbon/carbon dioxide reactions, accurately describe soda char carbon burning behavior. These kinetics are then appropriate to use in Reactions (3 - 5) for kraft char burning.

The tests with the soda liquor loaded with sodium sulfate did not fit the model predictions according to the $r^2$ criteria. Figure 23 compares the results of the char burn model, with and without the sulfate/sulfide cycle. Except for three tests, the data all lie on the same line. These three points lowered the $r^2$ from 0.8 to 0.3 for the soda/sulfate liquor. In the tests in which the times were overpredicted, the measured peak temperature was 810°C, significantly lower than the average measured value of 960°C. The reason for the low measured temperature is that the char particle turned away from the pyrometer optics. The peak temperature in the test that greatly underpredicted the measured char burn times was 960°C. However, the temperature increased rapidly in the early stages of the char burn, causing the model to predict fast char carbon burnup rates early in char burning. Possibly in this test volatiles were still present when the air was introduced, producing a flame in front of the pyrometer optics.

The results of this set of tests show two things. The first is that the char burn model accurately predicts char burn times for soda liquor with and without sulfur present. The second is that using the measured surface temperature introduces uncertainties in the accuracy of the char temperature, resulting from the particle moving out of the pyrometer line of sight.

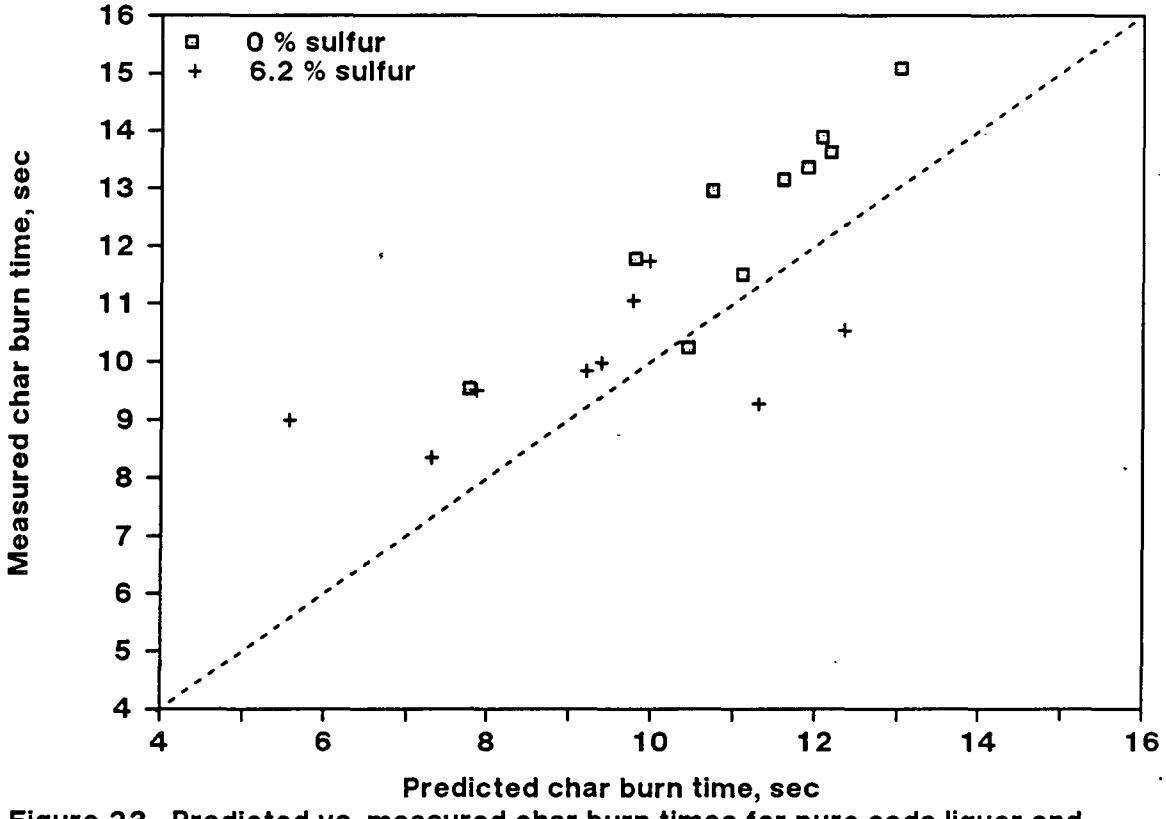


Figure 23. Predicted vs. measured char burn times for pure soda liquor and liquor loaded with sulfate. Tg = 800 C, 21% O2, initial char mass (20 - 40 mg)

Kraft Liquor

The kraft liquor studied was a mill liquor from Weyerhaeuser Paper Co. concentrated to 68% solids. Combustion conditions in the SPR were 2% - 8% oxygen in the gas stream and 800°C - 910°C gas temperature. The radiant heater was only used at the 910°C condition because it was not installed when the 870°C and 800°C tests were run. The range of initial wet liquor mass was 7 mg - 53 mg. The char burn was part of a combustion run, the particles were not initially dried and pyrolyzed in nitrogen.

This set of experiments was completed prior to the construction of the two-color pyrometer, and the char temperature profile is not known. The temperature profile is assumed to start at the gas temperature and ramp linearly with time to the maximum temperature at smelt coalescence as discussed in the Parameters section. The measured char burn time was an input to the model, and was used to estimate the temperature time profile. The predicted end of char burn occurred when 1% carbon by weight remained in the particle. Figure 24 shows the comparision between the predicted and the observed char burn time. The $r^2$ for the correlation is 0.98. The ratio of mol $CO/(CO+CO_2)$ depended on the assumed values for $f_{ox}$ and $f_{cs}$ used in fixing the extent of CO and $CO_2$ production through Reactions (1 - 4).

There is a strong dependency on oxygen in the char burn times. The tests in 2% oxygen took longer than those in 5% or 8% oxygen. The initial char mass and gas temperature influenced the char burn time, but not as significantly. At 8% oxygen, the influence of the initial char mass and the gas temperature is not as great as at 2% oxygen. These results are

consistent with a mass transfer limited process.

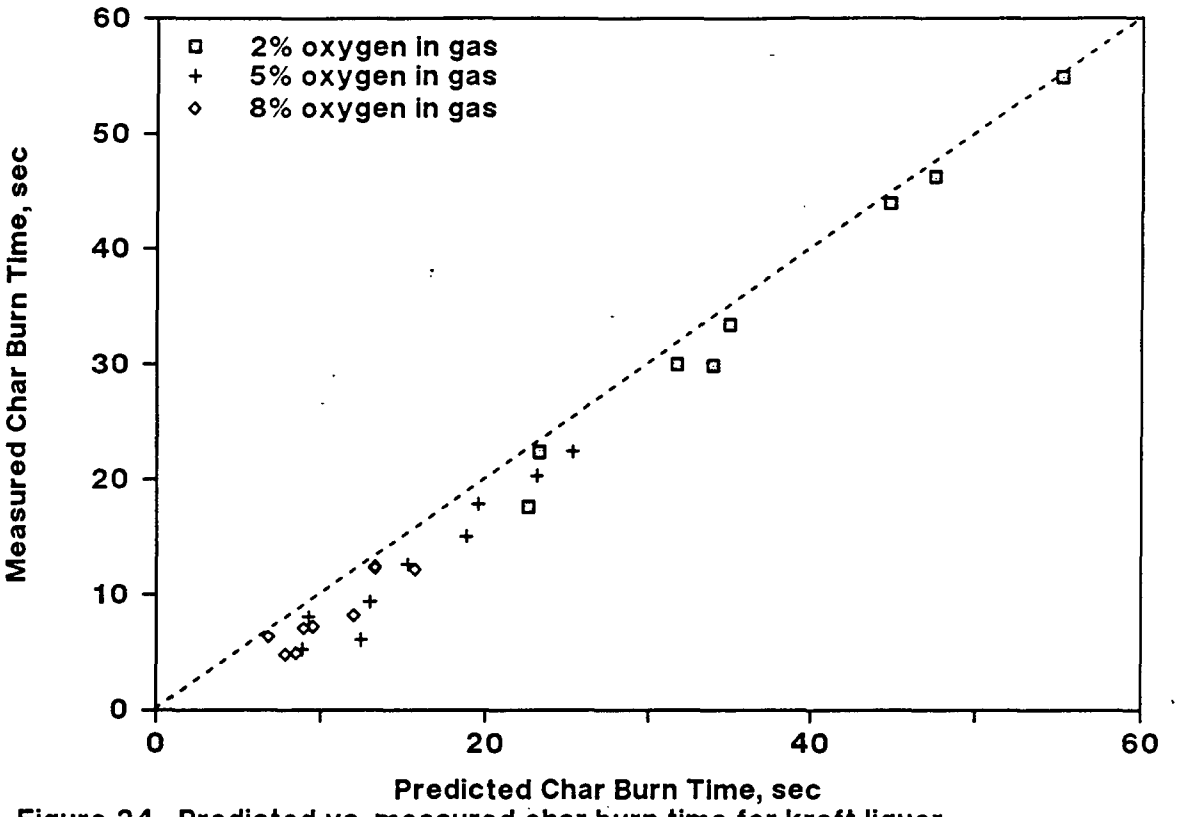


Figure 24. Predicted vs. measured char burn time for kraft liquor.
Tg = 800 C - 910 C, 2% - 8% oxygen in nitrogen, 10 mg - 50 mg initial liquor

The reduction ratio was predicted to be zero throughout char combustion. Experimental evidence indicates that the reduction ratio is not zero (all sulfur in sulfate form) until after smelt coalescence, when the inorganic reactions are complete.[8,17] The reduction ratio was predicted to be zero because the rate of sulfide oxidation was much greater than the rate of the carbon/sulfate reaction. The difference in the rates could be due to the high surface area/mass ratio in char formed by pyrolyzing black liquor drops, or due to slow carbon/sulfate reaction kinetics.

Figure 25 compares the average relative rates of the carbon consumption reactions for two cases with different surface area/mass ratios. The conditions for both cases were 8% $O_2$ and 870°C. The first case, A, is for char pyrolyzed from black liquor, 10.6 mg of char with $d_{max}$ = 1.112 cm. The second case, B, is for char pyrolyzed from pellets of dried black liquor, 110 mg of char with $d_{max}$ = 1.0 cm.[24] For approximately the same surface area, the char particle in case A is one tenth of the mass of char in case B. The carbon/sulfate reaction consumed only 9.7% of the total char carbon in case A, while in case B, the carbon/sulfate reaction accounted for 45.4% of the total char carbon consumed. Decreasing the surface area/mass ratio by an order of magnitude increased the relative rate of the carbon/sulfate reaction by a factor of 4.5. The reduction ratio in case B was predicted to be near 1.0 for most of the char burn.

The reduction ratio could have been predicted to be zero because the carbon/sulfate kinetics were too slow. The kinetic expression used in the model was from experiments with a small amount of kraft char in a smelt pool.[24] Since the carbon concentration was initially low, the effect of the carbon concentration on the rate kinetics was significant. Thorman and Macur[21] used a large amount of graphite carbon to obtain their carbon/sulfate reaction kinetics, and found the carbon concentration to have less of an effect on the reaction rate. Grace et al.[24] obtained a reaction order of 1.0 while Thorman and Macur[21] obtained a reaction order of 0.31 on carbon. Grace et al.[22] reported that kraft char was 13 times more reactive than graphite. When the Thorman and Macur[21] kinetic expression was adapted for kraft char and included in the char burn model, much different carbon/sulfate reaction rates were predicted. Table 10 compares the

average relative rates of the carbon consumption reactions for cases A and B using both carbon/sulfate kinetic expressions.

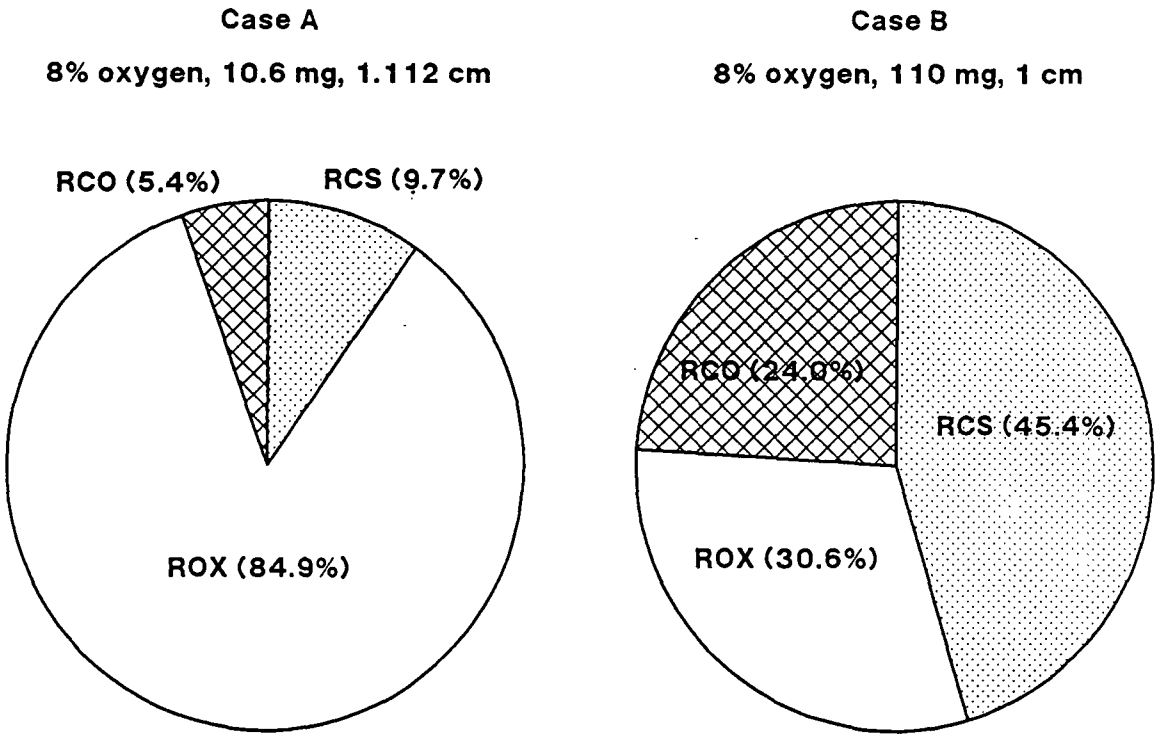


**Figure 25. Average relative rates of carbon consumption reactions**

Table 10. Average relative rate of char carbon consumption reactions using two carbon/sulfate kinetic expressions[24,21] for Case A, 10.6 mg char, $d_{max}$ = 1.112 cm, and Case B, 110 mg char, $d_{max}$ = 1.0 cm[24] $T_g$ = 870°C and $C_{O2}$ = 8%.

| | Case A | | Case B | |
|---|---|---|---|---|
| | Grace[24] | T&M[21] | Grace[24] | T&M[21] |
| C/Sulfate | 9.7 | 48.3 | 45.4 | 85.5 |
| C/Oxygen | 84.9 | 49.8 | 30.6 | 8.5 |
| $C/CO_2$ | 5.4 | 1.9 | 24.0 | 6.0 |

The use of Thorman and Macur[21] kinetics increased the rate of the carbon/sulfate reaction by a factor of 4.5 in case A, and doubled the

reaction rate in case B. The reduction ratio was predicted to be close to 1.0 for both cases. These results show that the carbon/sulfate kinetics determined by Grace et al.[8] are not fast enough for the char burning stage of black liquor combustion. The kinetics determined by Thorman and Macur are not directly applicable to black liquor char burning because they did not use black liquor char carbon in their experiments.

## CONCLUSIONS

1. The char burn model accurately predicts the time for char burning for pure soda liquor. The kinetics for the carbon/oxygen reaction and the carbon/carbon dioxide reaction apply to single particle combustion.

2. Sulfur influences the char burning time. This was evident when the measured times for pure soda char and for soda/sulfate char were compared. Therefore, the sulfate/sulfide cycle operates during single particle char burning as long as sulfur is present.

3. The char burn model including the sulfate/sulfide cycle accurately predicts the time for char burning for kraft liquor. Oxygen in the range of 2% - 8% in nitrogen had a large influence on the char burn time. The influence of the initial char mass and the gas temperature decreased as the percent oxygen increased. This is consistant with an oxygen mass transfer limited process.

4. The reduction ratio was calculated to be zero throughout most of the char burn. The model included sulfide oxidation kinetics to correspond to the published result that sulfide oxidation was mass transfer limited until the reduction ratio was below 2%.[8] The low predicted

reduction ratio is due to the large surface area that a small particle has, and to slow carbon/sulfate kinetics. The larger the swollen volume, the larger the surface area is at the start of char burning. This indicates that swelling during volatiles burning influences the relative rates of the carbon burnup reactions during char burning. Grace et al.[8] based their conclusion of a high reduction ratio during char burning on an observed weight gain after smelt coalescence for their single particle (dried liquor pellet) tests. This weight gain was not observed during tests with small liquor drops. The surface area to mass ratio was the only difference between the two sets of experiments.

## CONCLUSIONS

Three models have been proposed for the first three stages of the combustion of a single particle of kraft black liquor. Two of the models, drying and volatiles burning, combine mass and energy balances around the drop to predict the mass and temperature of the particle at any time during the stage, and to predict the completion time of the stage. The third model, char burning, predicts the completion time from the kinetics of the competing carbon burnup reactions and the rate of oxygen mass transfer to the char surface. The models were validated with experimental data generated using the SPR. The conclusions are as follows:

1. The model of the drying stage of single particle combustion is based on external heat transfer and predicts the drop moisture and temperature as functions of time. The predicted temperature was within 10% of the measured temperature for drops drying in air at temperatures between 550°C and 650°C, in a non-convective environment. The low temperatures were used to slow down drying, and are not indicative of actual boiler temperatures. The predicted drying time was compared with data reported by Hupa et al.[3] for small drops (.7 - 1.1 mm initial diameter) drying in air at 800°C, in a non-convective environment. A regression between the predicted and measured times had an $r^2$ of 0.9.

2. The model of the volatiles burning stage of single particle combustion predicts the particle mass, temperature, and diameter as functions of time. An empirical correlation was developed for one liquor to predict the maximum swollen diameter as a function of the initial drop mass. Gas conditions, temperature (800°C - 910°C) and oxygen

concentration (2% - 8%), did not influence the maximum swollen diameter. Volatilization was assumed to be complete when the particle reached its maximum swollen diameter. Volatiles burning in less than 10% oxygen is without a distinctive flame sheet surrounding the particle, based on observations of flame characteristics in the SPR.

The predicted rate of volatilization and the time to maximum volume were compared to the measured rate and time for particles burned under a wide range of conditions. The gas temperature range was 666°C to 910°C, the gas oxygen concentration was 0% to 21% with the balance nitrogen, and the initial size was 4 mg to 60 mg.

The regression between the predicted and measured rate of volatilization had an $r^2$ of 0.72. The test to determine if there is significant lack of fit in the model yielded the result that there was no significant lack of fit, and the low $r^2$ was due to experimental error. The time to maximum volume is a combination of the drying time and the volatiles burning time. The measured time is the time it takes the drop to swell to its maximum volume. The regression between the predicted and observed time had an $r^2$ of 0.82. Again there was no significant lack of fit between the model and the data.

3. The model of the char burning stage predicts the mass, reduction ratio, and the mass of CO and $CO_2$ in the boundary layer around the particle. The time for burning pure soda liquor was accurately predicted by the model without the sulfate/sulfide cycle. Sulfur was shown, through tests with pure soda liquor and soda loaded with sulfate, to influence the char burn time in single particles. The sulfate/sulfide

cycle applies to single particle char burning. The model accurately predicted the char burn time for kraft liquor (gas temperature 800°C - 910°C, oxygen concentration 2% - 8% in nitrogen). The oxygen concentration had a large influence on the char burn time. The influence of initial char mass and gas temperature decreased as the oxygen concentration increased from 2% to 8%.

The reduction ratio was predicted to be zero throughout char burning, even with the sulfide oxidation kinetics included in the model. The reason is the high surface area to mass ratio in the highly swollen char particles and slow carbon/sulfate kinetics. Previous work used pellets with a low surface area to mass ratio and the reduction ratio was predicted to be high throughout most of char burning.[8] When those conditions used were put into the char burn model, similar predictions for the mass and reduction ratio resulted.

The mass of CO and $CO_2$ produced depended on the values selected for the parameters $f_{ox}$ and $f_{cs}$.

4. A two-color pyrometer was constructed and accurately measures the surface temperature of a burning particle to within 10°C at 500°C. The pyrometer was used to measure the surface temperature of the char particle during char burning.

## SUMMARY OF EQUATIONS AND SENSITIVITY ANALYSIS

Table 11 lists the equations solved in the three models.

Table 11. Summary of equations used in the three models, drying, volatiles burning, and char burning.

Drying

$$\frac{dm_w}{dt} = - \frac{h\,A\,(T_g - T_d) + \sigma\,A\,F_{wd}\,(T_w^4 - T_d^4)}{L_w + \left[\dfrac{39.758\,m_o\,(Cp_o\,m_o + Cp_w\,m_w)}{(m_o + m_w)^2\,\exp\,(-0.046\,T_d + 4.6)}\right]} \qquad (17)$$

$$\frac{m_w}{m_o + m_w} = 0.547\,\exp\,(-0.046\,(T_d - 100)) \qquad (13)$$

Volatiles burning

$$h\,A\,(T_g - T_d) + \sigma\,A\,F_{wd}\,(T_w^4 - T_d^4) + dm_v/dt\,H_{comb} - dm_p/dt\,H_p = m_d\,Cp_d\,dT_d/dt \qquad (18)$$

$$dm_p/dt = A_v\,m_b\,\exp\,(-E_v/RT_d) \qquad (21)$$

$$d = d_i + (d_{max} - d_i)(Tm_p/m_{po})^n \qquad (27)$$

Char burning

$$-\frac{d[C]}{dt} = 2K_1\,\frac{(1-r)\,s}{K_2 + (1-r)\,s}\,[C]\,\exp\,(-E_1/RT_d) + Kcox\,C_{O2}\,A\,P + \frac{K_3\,p_{CO2}}{1 + K_4\,p_{CO2} + K_5\,p_{CO}}\,[C]\,\exp\,(-E_3/RT_d) \qquad (53)$$

$$\frac{dr}{dt} = \frac{K_1}{s}\,\frac{(1-r)\,s}{K_2 + (1-r)\,s}\,[C]\,\exp\,(-E_1/RT_d) - Krso\,C_{O2}\,r\,A\,(1-P)/2 \qquad (54)$$

$$\frac{dm_{CO2}}{dt} = \left[\frac{2(1-f_{ox})}{2 - f_{ox}}\,ROX + \frac{4(1-f_{cs})}{2 - f_{cs}}\,RCS - RCO_2 - F_{CO2}\right] M_{CO2}\,n_{Na2} \qquad (59)$$

$$\frac{dm_{CO}}{dt} = \left[ \frac{2\, f_{ox}}{2 - f_{ox}} ROX + \frac{4\, f_{cs}}{2 - f_{cs}} RCS + 2\, RCO_2 - F_{CO} \right] M_{CO}\, n_{Na2} \qquad (60)$$

Figure 26 shows the results of the sensitivity analysis for the drying model. The base case was a 2.77 mm diameter drop drying in air at 800°C, with a gas velocity of 1.7 m/sec, the swelling factor was 1.25, and the combination view factor/emissivity was 0.65. The convective heat transfer coefficient was doubled and halved, the view factor was set at 0.95 and 0.35, and the swelling factor was 1.0 and 1.5. The convective heat transfer coefficient had a large influence on the drying time and the combination view factor/emissivity had a very small influence on the drying time. This indicates that the majority of the heat was transferred through convection.

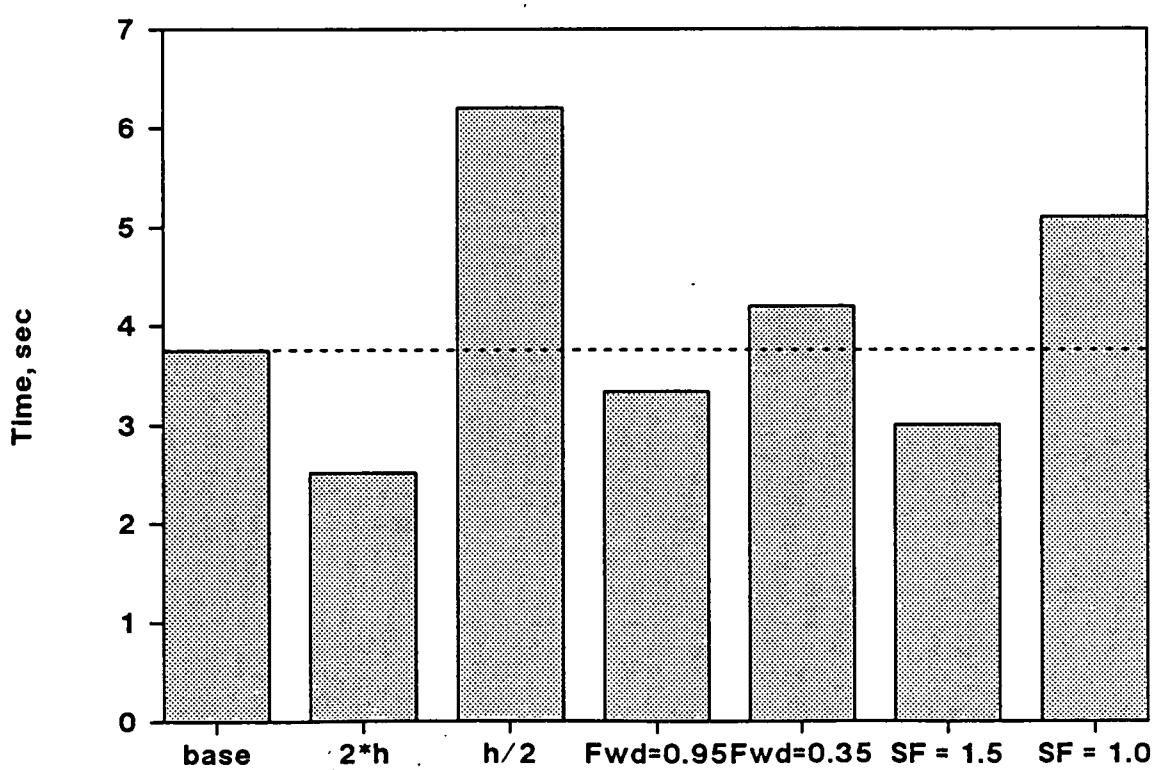


**Figure 26. Sensitivity analysis of the drying model.**

Figure 27 shows the results of the sensitivity analysis for the volatiles burning model. The base case was a 21 mg drop burning in 8% oxygen at 800°C. The gas velocity was 1.7 m/sec. The parameters varied were the heat transfer coefficient (doubled and halved), the combination view factor/emissivity (0.30, 0.78), the pyrolysis pre-exponential factor (5.035, 20.14), the pyrolysis activation energy (11000, 33000), and the order on the pyrolysis mass term, n, used in the diameter equation (0.5, 2). The base case of these parameters was 0.54 for the combination view factor/emissivity, 10.07 for the pre-exponential factor, 22000 for the activation energy, and 1 for n. The parameters with the greatest influence on the volatiles burning time were the pyrolysis pre-exponential factor and the activation energy. This points out the need for a better understanding of the pyrolysis kinetics for particles of black liquor.

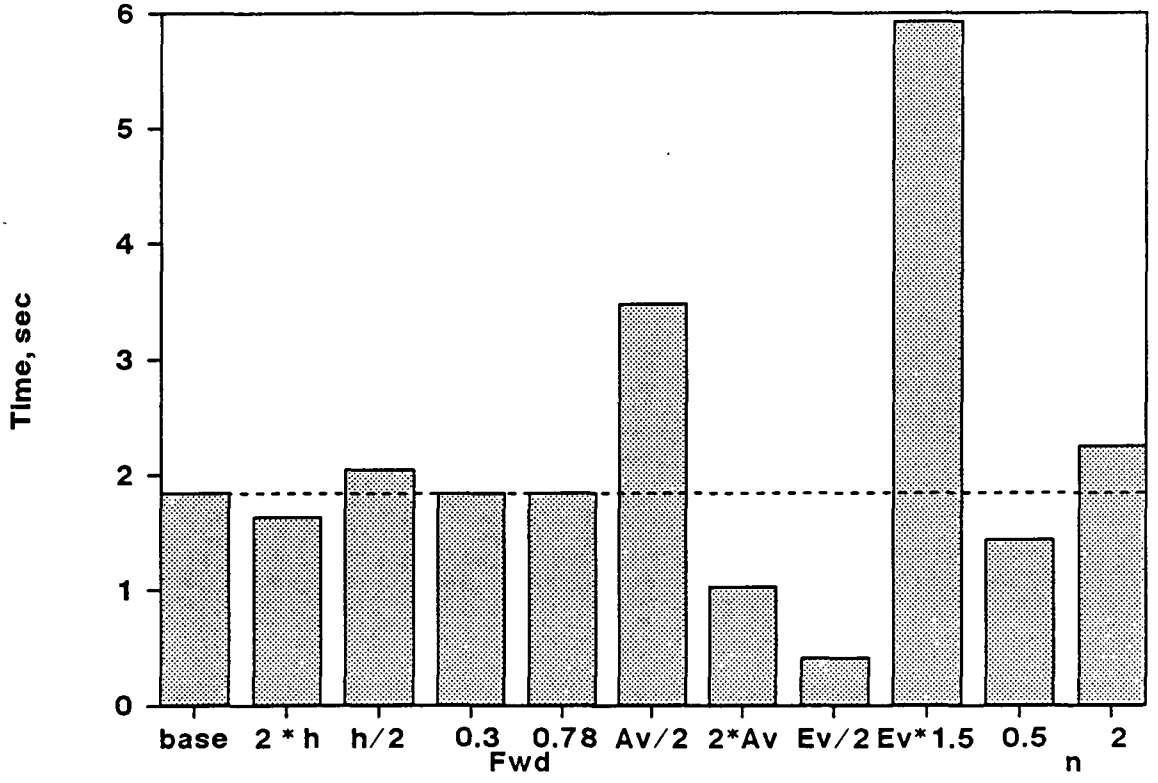


**Figure 27. Sensitivity analysis of the volatiles burning model.**

Figure 28 shows the results of the sensitivity analysis for the char burning model. The base case was 10.6 mg of char burning in 8% oxygen at 800°C. The gas velocity was 1.7 m/sec. The parameters varied were the maximum char temperature ($T_{max} \pm 50°C$), the boundary layer thickness (doubled and halved), and $f_{cs}$ and $f_{ox}$ (1, 0). The base values for $f_{ox}$ and $f_{cs}$ were 0.9, and the base value for $T_{max}$ was calculated using Equation (63). The only parameter which influenced the char burn time was $f_{ox}$ and $f_{cs}$, pointing out the need for a better understanding of the fraction of CO produced through the carbon/sulfate reaction and the carbon/oxygen reaction.

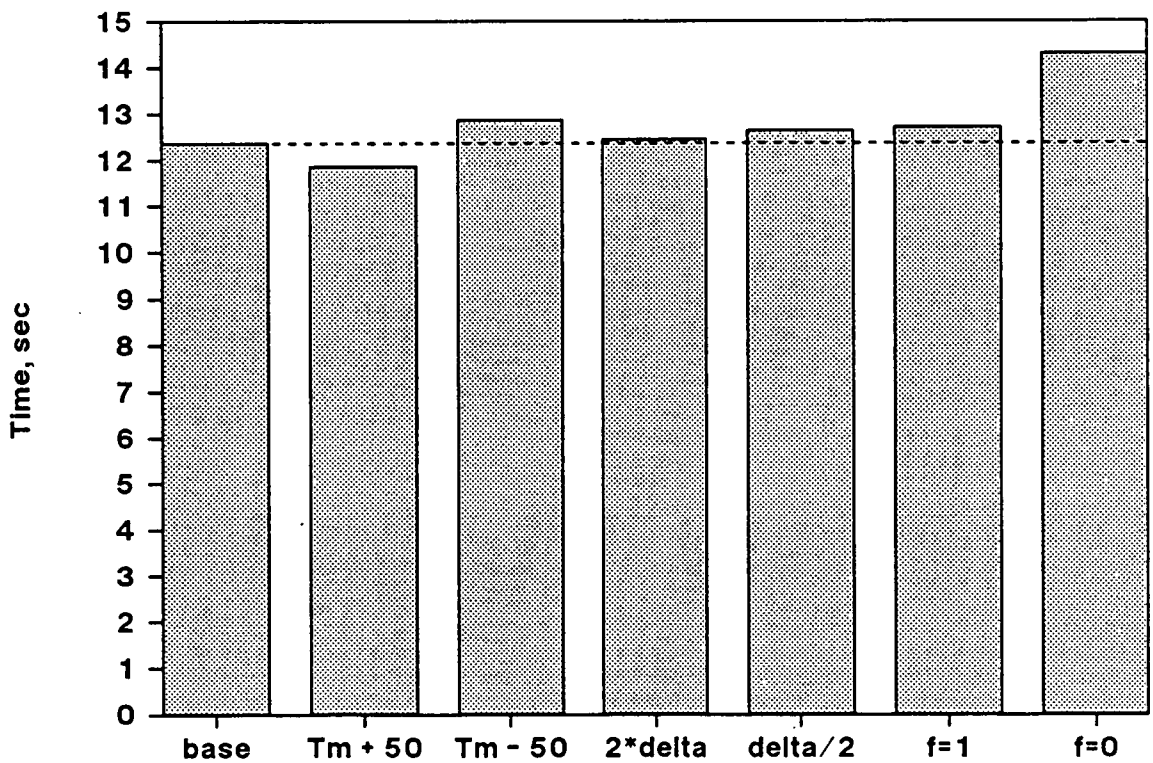


**Figure 28. Sensitivity analysis for char burn model.**

# RECOMMENDATIONS

The three models, drying, volatiles burning, and char burning, presented in this thesis are an improvement over previous models in the literature because they are verified with experimental data. However, each of the three models contains empiricism due to a lack of information in several areas which were beyond the scope of this thesis.

The boiling behavior for drops dried at high temperatures has not been investigated. The assumption of an isothermal drop is a direct result of this lack of knowledge. More detailed information on boiling is needed to eliminate the isothermal simplification in the drying model.

Particle swelling in less than 10% oxygen with the balance nitrogen has not been investigated in any detail. The swelling during drying was assumed constant in the present model, the value of the diameter increase relative to the initial diameter was a parameter used to fit the model to data. A prediction for the average amount of swelling during drying is needed to relate the swelling factor used in the model to the furnace conditions.

The swelling during volatiles burning was predicted from an empirical equation relating the maximum diameter to the initial mass of solids. This was a liquor specific relation, and only one data set was available for the correlation. The diameter increase with time was assumed to be a function of the fraction of total volatiles to evolve. A better understanding of the chemical and physical factors which drive swelling in less than 10% oxygen, and the dynamic diameter during volatiles burning is

needed for a less empirical representation of the swelling process in the volatiles burning model. It is apparent from this work that the maximum diameter can be predicted from the initial test conditions. Swelling at low oxygen concentrations does not appear to be as random an event as swelling in nitrogen. This could be due to volatiles combustion, which reduces swelling.

The kinetic mechanism for volatiles evolution is not quantified for volatiles evolution from single particles in low concentrations of oxygen. This was an area of major simplification in the present volatiles burning model. The kinetic expression used in the model treated all the volatile evolution reactions as one Arrhenius type reaction with overall kinetic constants. The constants were obtained from pyrolysis tests in the SPR.

During volatiles burning the black liquor particle was assumed to be isothermal. A temperature gradient should be included inside the particle during this stage. Volatiles evolution is an endothermic process causing the particle to act as a heat sink. The center of the particle is therefore cooler than the surface, creating a temperature gradient across the particle. The experimental techniques now available are not able to track the front of volatilization through the particle, or even to estimate the thermal conductivity, density, porosity, or heat capacity as functions of time.

The char burning model contains two major simplifications. The first is the char temperature profile in time, and the second is the relative rates of CO and $CO_2$ production from the $C/SO_4$ reaction, $f_{cs}$, and

from the $C/O_2$ reaction, $f_{ox}$. The char temperature can be measured experimentally with an optical pyrometer. However, this does not make the model useful in practical situations where the char surface temperature is not known. The equation used to predict the maximum temperature for kraft char burning as a function of gas temperature and concentration is an empirical correlation obtained from char bed studies. The solution to the temperature question is to incorporate an energy balance into the char burn model. The addition of the energy balance is not as simple as it sounds, since the combustion term is heavily dependent on $f_{cs}$ and $f_{ox}$.

$f_{cs}$ and $f_{ox}$ are difficult to measure with the experimental techniques now available. Off gas analysis of the reaction products also include gas phase oxidation of CO to $CO_2$. Ongoing research in FTIR analysis of the gases immediately above the char bed[52] at the Institute of Paper Chemistry, will hopefully be able to measure values for $f_{cs}$ and $f_{ox}$ as functions of combustion gas composition. Until this research, or other investigations which are able to directly measure $f_{cs}$ and $f_{ox}$, are completed, the char temperature and $f_{cs}/f_{ox}$ will have to be assumed.

The carbon/sulfate reaction needs to be studied in a system similar to Thorman and Macur[21] to allow a high loading of kraft char in the smelt pool. Thorman and Macur[21] obtained a kinetic expression for the carbon/sulfate reduction reaction using a large quantity of graphite, and Grace et. al[8] obtained a kinetic expression using a small quantity of kraft char. Neither kinetic expression[8,21] applies to single particle char combustion. Additional work is needed for an adaquate kinetic expression for the carbon/sulfate reaction.

The three models need to be integrated into one overall model which can then be inserted into a recovery boiler simulation. Each individual model accurately describes its respective stage of black liquor combustion. The disadvantage of three separate models lies in manually feeding the results of one model into the next model.

The three models presented in this thesis accurately predict the time to complete each combustion stage, drying, volatiles burning, and char burning. Implementation of the suggestions described in this section will lead to fine tuning of the models to an even higher degree of accuracy by removing the empiricism used in developing these models.

# NOMENCLATURE

$A$ = surface area, $cm^2$

$A_v$ = overall pre-exponential factor for volatiles evolution, $sec^{-1}$

$c_1$, $c_2$ = constants in Planck's Law

$c$ = speed of light, cm/sec

$Cp$ = heat capacity, cal/g-°C

$d$ = diameter, cm

$d_{avg}$ = average diameter during drying, cm

$d_{ign}$ = diameter at ignition, cm

$d_{max}$ = maximum swollen diameter, cm

$D_i$ = diffusivity of species i in air, $cm^2/sec$

$E$ = activation energy, J/mol

$E_v$ = overall activation energy for volatiles evolution, J/mol

$F_i$ = mass transport of species i away from boundary layer, mol i/mol $Na_2$-s

$F_{wd}$ = combination view factor and emissivity

$f_{cs}$ = mol $(CO/CO+CO_2)$ produced in $C/SO_4$ reaction

$f_{ox}$ = mol $(CO/CO+CO_2)$ produced in $C/O_2$ reaction

$h$ = convective heat transfer coefficient, $cal/cm^2$-°C-sec

$h$ = Planck's constant, J/sec, in Appendix I

$H_{comb}$ = heat of volatiles combustion, cal/g

$H_p$ = heat of pyrolysis, cal/g

$k$ = gas thermal conductivity, cal/s-cm-K

$K_i$ = mass transfer coefficient for species i, cm/sec

$K_j$ = kinetic constant j, j = 1 to 5

Kso = overall rate constant for $S/O_2$ reaction, cm/sec

Krso = kinetic rate constant for $S/O_2$ reaction, cm/sec

Kcox = overall rate constant for $C/O_2$ reaction, cm/sec

Kr = kinetic rate constant for $C/O_2$ reaction, cm/sec

Kp = reaction rate constant for $C/O_2$ reaction, $g/cm^2$-sec-atm $O_2$

$L_w$ = latent heat of water, cal/g $H_2O$

m = mass of subscript, g

$m_b$ = mass of black liquor solids at any time, g

$m_{evap}$ = mass of water evaporated, g

$m_p$ = mass of volatiles evolved, g

$m_v$ = mass of volatiles combusted, g

$M_i$ = molecular weight of species i, g/mol

$n_{O2}$ = oxygen reaching particle surface, mol/sec

Nu = Nusselt number, h d/k

P = fraction of char surface which is carbon

$p_i$ = partial pressure of species i in boundary layer, atm

Pr = Prandtl number, Cp $\mu$/k

$Q_{cond}$ = heat of conduction, cal/sec

$Q_{conv}$ = heat of convection, cal/sec

$Q_{rad}$ = heat of radiation, cal/sec

$r_f$ = flame radius, cm

r = reduction ratio, mol $(Na_2/Na_2 + Na_2SO_4)$

$r_\lambda$ = spectral intensity of radiometric quantity, $W/cm^2$ $\mu$

R = gas constant

Re = Reynolds number, d v/$\nu$

Rm = measured ratio of $r_\lambda$ at two wavelengths

Rth = theoretical ratio of $r_\lambda$ at two wavelengths

RCS = rate of $C/SO_4$ reaction, mol $SO_4$/mol $Na_2$-sec

ROX = rate of $C/O_2$ reaction, mol $O_2$/mol $Na_2$-sec

$RCO_2$ = rate of $C/CO_2$ reaction, mol C/mol $Na_2$-sec

RSO = rate of $S/O_2$ reaction, mol $Na_2S$/mol $Na_2$-sec

s = sulfidity, mol S/mol $Na_2$

Sc = Schmidt number, $\nu/D_{O2}$

Sh = Sherwood number, $K_{O2}\ d/D_{O2}$

t = time, sec

T = Temperature, K

$T_g$ = gas temperature, K

$T_{max}$ = peak temperature during char burning, K

$T_w$ = wall temperature, K

v = gas velocity, cm/s

V = volume, $cm^3$

$V_{BL}$ = volume of boundary layer, $cm^3$

[C] = carbon concentration in char, mol C/mol $Na_2$

[S] = sulfide concentration in char, mol S/mol $Na_2$

$[SO_4]$ = sulfate concentration in char, mol $SO_4$/mol $Na_2$

Greek

$\delta$ = thickness of boundary layer, cm

$\lambda$ = wavelength, cm

$\mu$ = gas viscosity, g/cm-sec

$\rho$ = density of subscript, $g/cm^3$

$\sigma$ = Stefan-Boltzmann constant, cal/sec-$cm^2$-$K^4$

$\nu$ = kinematic viscosity, $cm^2$/sec

$\Omega$ = stoichiometric limit of $O_2$ required/g. volatiles

Subscripts

c = char or char carbon

d = drop or particle

o = initial or dry

s = inorganic

w = water

$\infty$ = smelt bead

# LITERATURE CITED


1. Frederick, W.J.; Adams, T.N. Kraft Recovery Boiler - Physical and Chemical Processes. American Paper Institute. (1988).

2. Clay D.T.; Grace, T.M.; Kapheim R.J.; Semerjian, H.G.; Macek, A; Charagundla, S.R. Fundamental Studies of Black Liquor Combustion. Report No. 1 - Phase 1. DOE Report, DOE/CE/40637-T2. (1985).

3. Hupa, M.; Solin, P; Hyöty, P. Combustion behavior of black liquor droplets. TAPPI Proc. Int'l. Rec. Conf. Book 3:335-44 (April 28 - May 1, 1985) New Orleans, LA.

4. Grace, T.M.; Cameron, J.H.; Clay, D.T. Role of the sulfate/sulfide cycle in char burning. TAPPI Proc. Int'l Rec. Conf. Book 3:371-9 (April 28 - May 1, 1985) New Orleans, LA.

5. Monagham, M.T.; Siddall, R.G. The combustion of single drops of waste sulfite liquor - a preliminary investigation. TAPPI. 46(2):89-91 (1963).

6. Clay, D.T.; Ragland, K.W. Kraft black liquor combustion: sensitivity to key process variables. Presented at AIChE Annual Meeting, San Francisco, CA, 1984.

7. Kulas, K.A.; Clay, D.T. An empirical rate equation describing the volatiles burning stage of kraft black liquor. AIChE Forest Products Division, 2:53-7 (1988).

8. Grace, T.M.; Cameron, J.H., Clay, D.T. Role of sulfate-sulfide cycle in char burning: experimental results and implications. TAPPI :108-13 (Oct. 1986).

9. Robinson, M.L.; Clay, D.T. Characterization of black liquor drop drying in air. Presented at AIChE Summer National Meeting (Aug 16-20, 1987) Minneapolis, MN.

10. Merriam, R.L. KRAFT, version 2.0: Computer model of a kraft recovery furnace. Prepared for the American Paper Institute by A.D. Little, Inc., Cambridge, MA, 1980.

11. Shick, P.E. Predictive simulation of recovery furnace processes on a microcomputer. TAPPI 1986 Recovery Operations Seminar :121-33 (Feb. 9 - 14) Orlando, FL.

12. Walsh, A.R. A computer model for in-flight black liquor combustion in a kraft recovery furnace. Doctoral Dissertation, The Institute of Paper Chemistry, Appleton, WI, 1989.

13. Frederick, W.J.; Kulas, K.A.; Clay, D.T.; Hupa, M.; Noopila, T. Analysis of black liquor single droplet combustion data. TAPPI Proc. Int'l Chem. Rec. Conf. :81-88, Ottowa, CANADA, March 1989.

14. Miller, P.T.; Clay, D.T. Swelling of kraft black liquor during pyrolysis. AICHE Forest Products Division, 1:152-9 (1986)

15. Miller, P.T.; Clay, D.T.; Lonsky, W.F.W. The influence of composition on the swelling of kraft black liquor during pyrolysis. TAPPI Proc. Eng. Conf. Book 1:225 (Sept 1986)

16. Noopila, T.; Alen, R.; Hupa, M. Combustion properties of laboratory made cooking liquors. TAPPI Proc. Int'l Chem. Rec. Conf. :75-80, Ottowa, CANADA, March 1989.

17. Milanova, E.; Kubes, G.J. The combustion of kraft liquor chars. JPPS, 12(6):J187-92 (Nov. 1986).

18. Moreland, B.A.; Clay, D.T. The influence of water on black liquor combustion. Preprints of TAPPI Pulping Conf., Book 2:389 (Nov. 1985).

19. Brown, C.A.; Grace, T.M.; Lien, S.J.; Clay, D.T. Char bed burning rates - experimental results. TAPPI Proc. Int'l Chem. Rec. Conf. :65-73, Ottowa, CANADA, March 1989.

20. Smoot, D.L.; Smith, P.J. Coal Combustion and Gasification. Plenum Press, New York, NY, 1985.

21. Thorman, R.P.; Macur, T.S. Kinetics of sodium sulfate reduction by carbon in molten sodium carbonate. TAPPI Proc. Int'l Rec. Conf. Book 3:451-8 (April 28 - May 1, 1985), New Orleans, LA.

22. Grace, T.M.; Cameron, J.H.; Clay, D.T. Char Burning. Summary Technical Report to American Paper Institute Recovery Boiler Committee prepared by the Institute of Paper Chemistry, Appleton, WI (Feb. 22, 1985).

23. Aiken, G.W.; Cameron, J.H. $CO/CO_2$ ratio of kraft char burning. AIChE Forest Products Division 2:81-6 (1988).

24. Cameron, J.H.; Grace, T.M. Kinetic study of sulfate reduction with carbon. Ind. Eng. Chem. Fundam. 22:486-94 (1983).

25. Li, J.; van Heiningen, A.R.P. Mass transfer limitations in gasification of black liquor char by carbon dioxide. TAPPI Proc. Int'l. Rec. Conf. Book 3:459-64 (April 28 - May 1, 1985), New Orleans, LA.

26. Goerg, K.A.; Cameron, J.H. A kinetic study of kraft char gasification with carbon dioxide. AIChE Forest Products Division, 2:46-52 (1988).

27. Sumnicht, D.W. A computer model of the char bed. Doctoral Dissertation, The Institute of Paper Chemistry, Appleton, WI (1989).

28. Jones, A.K. A recovery furnace model. Doctoral Dissertation, The Institute of Paper Chemistry, Appleton, WI (1989).

29. Nusselt, W. Combustion process involved in firing coal dust. Ver. Dtsch. Ing. Z. 68(6):124-8 (Feb. 9, 1924).

30. Kobayashi, K. An experimental study on the combustion of a fuel droplet. 5th Int'l. Symp. on Comb. The Comb. Inst. :141-8 (1955).

31. Sakai, T.; Saito, M. Single-droplet combustion of coal slurry fuels. Comb. and Flame. 51:141-54 (1983).

32. Long, V.D. A simple theoretical model of droplet combustion. J. Inst. Fuel :522-5 (Dec. 1964).

33. Hayhurst, A.N.; Nedderman, R.M. The burning of a liquid oil droplet. Chem. Eng. Ed. :126 (Summer 1987).

34. Timothy, L.D.; Sarofim, A.F.; Beer, J.M. Characteristics of single particle coal combustion. 19th Int'l Symp. on Comb. The Comb. Inst. : 1123-30 (1982).

35. Melia, P.F.; Bowman, C.T. An analytical model for coal particle pyrolysis and swelling. Presented at Western States Section/Combustion Inst. (April 5-6, 1982) Salt Lake City, UT.

36. Jost, M.; Leslie, I.; Kringle, C. Flow-tube reactor studies of devolatilization of pulverized coal in an oxidizing environment. 20th Int'l Symp. on Comb. The Comb. Inst. :1531-7 (1984).

37. Gururajan, V.S.; Wall, T.F.; Truelove, J.S. Diffusion limited volatile combustion model. Comb. and Flame. 72:1-12 (1988).

38. Peck, R.E.; Pollock, M.A. Development of an aerodynamic levitation technique to study coal particle combustion. Fuel 60:727-31 (Aug 1981)

39. Peck, R.E.; Pollock, M.A. The thermal response of heated, levitated coal particles. J. Heat Transf. 104:788-90 (Nov. 1982).

40. Jost, M. Doctoral Dissertation, Stanford University. (1984).

41. Murdoch, P.L.; Pourkashanian, M.; Williams, A. The mechanism of combustion of coal-water slurries. 20th Int'l Symp. on Comb. The Comb. Inst. :1409-18 (1984).

42. Bird, R.B.; Stewart, W.E.; Lightfoot, E.N. Transport Phenomena. J. Wiley and Sons, New York, NY, p. 409, (1960).

43. Robinson, M.L.; Clay, D.T. Equilibrium behavior of kraft black liquor in superheated steam. Chem. Eng. Commun. 43:225-35 (1986).

44. Kuo, K.K. Principles of Combustion. Wiley Interscience Publication, J.Wiley and Sons, New York, NY (1986).

45. Stelling, O.; Vegeby, A. Corrosion on tubes in black liquor recovery boilers. Pulp and Paper Can. Mag. :51-77 (Aug. 1969).

46. Bhattacharya, P.; Vidyasekara, P.; Kunzru, D. Pyrolysis of black liquor solids. Ind. Eng. Chem. Proc. Des. Dev. 25:420-6 (1986).

47. Anthony, D.B.; Howard, J.B.; Hottel, H.C.; Meissner, H.P. Rapid devolatilization of pulverized coal. 15th Int'l Symp. on Comb. The Comb. Inst. :1303-17 (1975)

48. Hough, G. Chemical recovery in the alkaline pulping processes. TAPPI Press, Atlanta, GA (1985).

49. Sumnicht, D.W. An improved theory of char burning. Appendix for Doctoral Dissertation, The Institute of Paper Chemistry, Appleton, WI, (1989).

50. Bennett, C.O.; Myer, J.E. Momentum, Heat, and Mass Transfer. McGraw-Hill, New York, NY. (1982).

51. Bird, R.B.; Stewart, W.E.; Lightfoot, E.N. Transport Phenomena. J. Wiley and Sons, New York, NY, p142 (1960).

52. Medvecz, P. Spectroscopic evaluation of the gas phase above a burning black liquor char bed. Doctoral Dissertation, The Institute of Paper Science and Technology, Atlanta, GA. In progress.

53. Bramson, M.A. Infrared Radiation: A Handbook for Applications. Plenum Press, New York, NY, p.164 (1968).

54. Braide, K.M.; Isles, G.L.; Jordan, J.B.; Williams, A. The combustion of single droplets of some fuel oils and alternative liquid fuel combinations. J. Inst. Energy. 52:115-24. (1979)

55. Bach, J.H.; Street, P.J.; Twamley, C.S. Temperature measurement of particulate surfaces. J. of Physics E: Scientific Instruments. 3:281-6 (1970).

56. Bramson, M.A. Infrared Radiation: A Handbook for Applications. Plenum Press, New York, NY, p47 (1968).

## APPENDIX I. TWO-COLOR PYROMETER

The color temperature has been described by Bramson as the "temperature at which a blackbody would emit radiation with an energy distribution most closely matching the smoothed spectrum of a given body - radiation having the same ratio of spectral radiances at two prescribed wavelengths."[53] Many researchers have used two-color, or ratio, pyrometry to unobtrusively measure high temperatures.[34,54,55]

Two-color pyrometry is based on Planck's Formula (64) which is the general form of all the previously established blackbody radiation laws.[56]

$$r_\lambda(T) = c_1 \lambda^{-5} \left(e^{c_2/\lambda T} - 1\right)^{-1} \qquad (64)$$

$c_1 = 2 \pi c^2 h$

$c_2 = 1.4388$ cm °K

$c = 2.998 \times 10^{10}$ cm/sec

$h = 6.625 \times 10^{-34}$ J sec

$r_\lambda$ = spectral intensity of a radiometric quantity [$W/cm^2 \mu$]

T = temperature [°K]

$\lambda$ = wavelength [cm]

When the intensity from two distinct wavelengths are ratioed, the equation is

$$Rth = \frac{r_{\lambda 1}}{r_{\lambda 2}} = \left(\frac{\lambda_2}{\lambda_1}\right)^5 \exp\left(c_2/T \left[1/\lambda_2 - 1/\lambda_1\right]\right) \qquad (65)$$

taking the log of each side,

$$\ln Rth = 5 \ln\left(\frac{\lambda_2}{\lambda_1}\right) + c_2/T \left[ 1/\lambda_2 - 1/\lambda_1 \right] \qquad (66)$$

and

$$T = \frac{c_2(1/\lambda_2 - 1/\lambda_1)}{\ln R - 5 \ln (\lambda_2/\lambda_1)} \qquad (67)$$

Several assumptions are inherent in a two-color pyrometer. The first is that the emissivity of the source must vary the same with temperature at each wavelength. This assumes that the burning black liquor drop/flame envelope behaves as a gray body. The second assumption is that the background intensity is about the same at each wavelength. The closer the two wavelengths are to each other, the better this assumption is.

The schematic of the pyrometer is shown in Figure 29. The common end of the fiber optic probe is 1.5 inches from the source, the combusting drop. A 6 inch quartz rod is joined to the fiber optic with a teflon sleeve to protect it from the high temperatures in the furnace. The fibers can only withstand 440°C. The probe tip is exposed to 900°C gas temperatures. A stainless steel sheath surrounds the quartz rod and extends an additional 3/4 inch to reduce the probe's zero angle. The zero angle is a measure of how large the spot size is, or how much area the probe sees. Initially, the sheath was not used and the particle/background area ratio was too small to have good sensitivity. Now the probe only sees the particle, with a spot size of 0.5 inches. The fiber optic is bifurcated and each branch runs to a narrow bandpass filter. The filters are each 10 nm wide and are centered about 1000

nm ($\lambda_1$) and 850 nm ($\lambda_1$). The wavelengths were chosen to measure only the continuum and to avoid the elemental lines of volatilized species. Work at NBS indicated that 1000 nm and 850 nm would satisfy that criteria. The detector is a silicon photodiode which picks up the intensity of radiation passing through the filter, and sends it to a radiometer/photometer which amplifies it into a signal which the data acquisition system can recognize. The detector/radiometer/photometer was from EG&G Gamma Scientific.

Calibration was accomplished with a working standard blackbody. The pyrometer was calibrated for the temperature range of 475°C-1000°C. Below 475°, not enough light was emitted for the detectors to pick up at either wavelength. At a given temperature the theoretical ratio of the intensities, $R_{th}$, was calculated with Eqn. (65). The probe was then placed so it could only see the blackbody cavity and the intensities were measured. The measured ratio, $R_m$, was $r_{\lambda 1}/r_{\lambda 2}$. The calibration constant of the pyrometer, A, was $R_{th}/R_m$. The calibration was checked every couple months and was redone when the probe or the detector assembly was taken apart. The fiber/filter/detector assembly was housed in a light tight wooden box to keep it immobile and protected.

Temperature profiles of combusting drops were obtained in the following manner. The probe was positioned into the reaction chamber before the furnace was heated. When the gas reached the desired temperature, a drop of black liquor was formed around the wire, hung in the furnace, and the gas was allowed to flow past the drop. A video system recorded the entire event. The measured intensities were ratioed after the burn to calculate $R_m$. $R_{th}$ was calculated using the calibration constant. The temperature was then

calculated using Eqn. (67). Figure 30 shows the surface temperature as a function of time for a drop of black liquor burning in air at 800°C.

Two-color pyrometry has several advantages. It is versatile in that it can be used in many situations by employing the appropriate filters. The emissivity does not have to be known to calculate the temperature. It is nonintrusive, a good attribute for many situations where the thermocouple could introduce large errors. The disadvantages are that with the selected wavelengths, temperatures below 500°C can not be measured. The probe does not have any sighting optics (a commercial pyrometer does) making it difficult at times to be confident that the particle is being viewed. The most important disadvantage is that the source must act like a gray body for the equations to be valid.

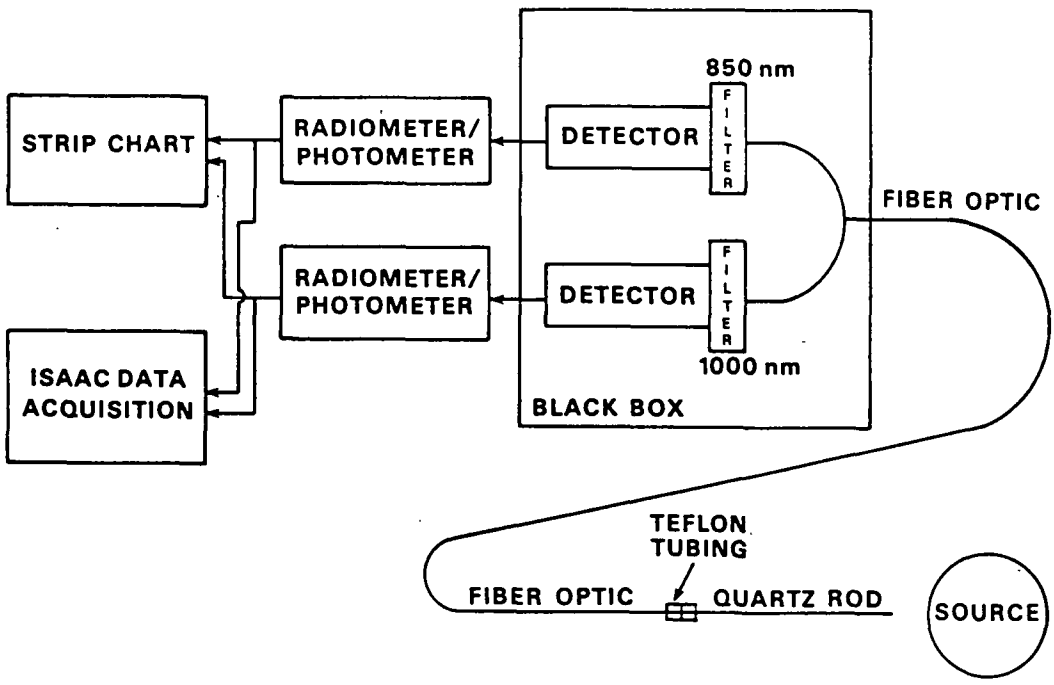


Figure 29. Schematic of two-color pyrometer

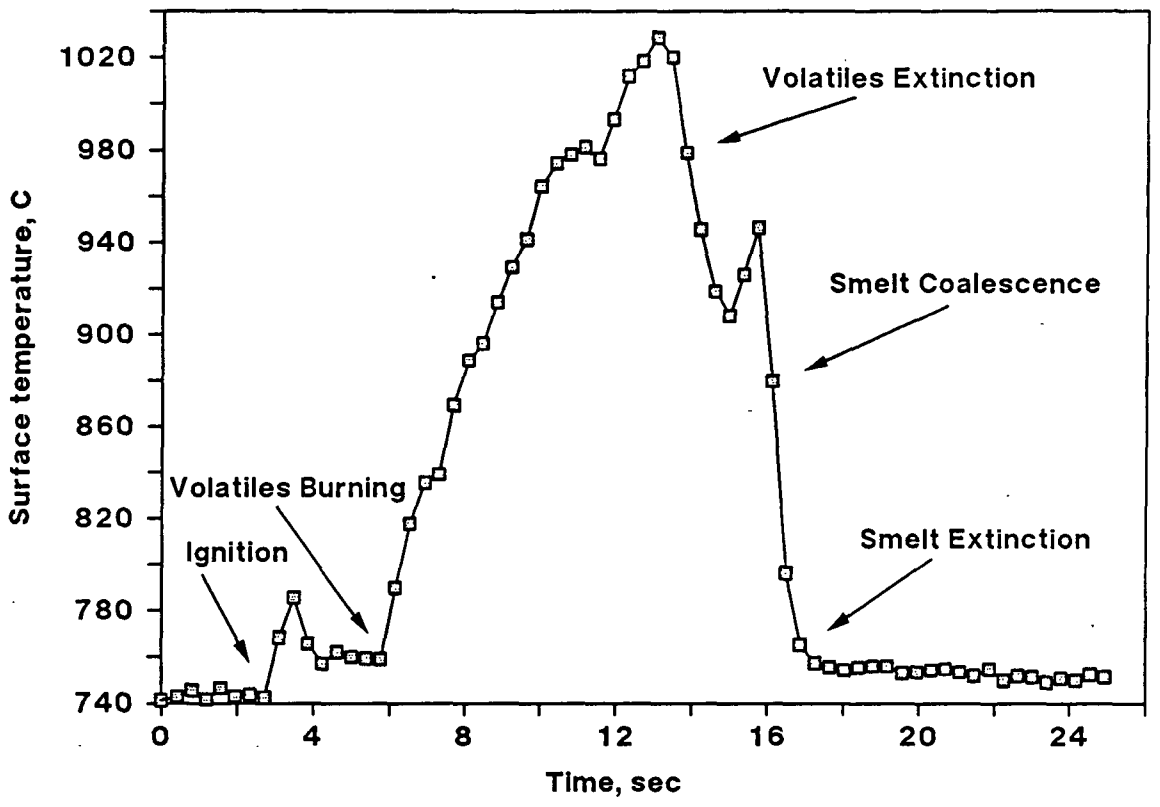


Figure 30. Surface temperature of kraft black liquor drop during burning, using two-color pyrometer, 52 mg, 700 C, air

## APPENDIX II. LIQUOR PREPARATION

All the liquors tested were concentrated to approximately 65% solids in a rotovap evaporator. Evaporation occurred under vaccuum, allowing lower temperatures to be used. This minimized volatile loss during liquor concentration. Solids determinations were done as follows. The liquor was placed in a dish with burned sand and weighed. Distilled water was added to provide uniform mixing of the liquor and the sand, and the dish was dried in a convective oven at 105°C for at least 3 hours. The dry liquor and dish were weighed and the percent solids was calculated from the water loss.

The liquor used to validate the drying model was from a lab cook for Robinson.[9] The liquor was concentrated from 16% to 65% solids. Prior to concentration, sodium carbonate (7.6% by weight) and sodium sulfate (4.1% by weight) were added to increase the dead load to normal levels for kraft liquor. The liquor analysis is shown in Table 12.

Table 12. Analysis of liquor used to validate the drying model. The concentrated liquor was analyzed.

| | Weight percent (dried basis) |
|---|---|
| Carbon | 39.4 |
| Hydrogen | 5.8 |
| Oxygen | 22.7 |
| Sulfur | 3.6 |
| Sodium | 24.5 |

The liquor used to validate the volatiles burning model was from two mills, Thilmany in Kaukana, WI, and Weyerhaeuser's Valliant mill. The Valliant liquor was used in the tests at low oxygen concentration (2% - 8%). The

Thilmany liquor was concentrated to 71.8% solids and the Valliant liquor was concentrated to 68% solids. The liquor analysis for the Valliant liquor is shown in Table 13.

Table 13. Analysis of Valliant Liquor, on dried solids basis.

| | Weight Percent (dried basis) |
|---|---|
| Carbon | 35.6 |
| Hydrogen | 3.7 |
| Oxygen | 33.7 |
| Sulfur | 4.2 |
| Sodium | 20.1 |

The soda liquor used in char burning was a lab cook. The sulfur was added as granular sodium sulfate. The liquor analysis of the concentrated liquors, SDA - SDF, are listed in Table 14. The percentages are on a dried solids basis.

Table 14. Analysis of Soda Liquors, on dried solids basis.

| Liquor ID | SDA | SDC | SDD | SDE | SDF |
|---|---|---|---|---|---|
| Carbon | 43.3 | 33.1 | 29.0 | 24.8 | 21.5 |
| Hydrogen | 3.9 | 2.7 | 2.1 | 1.9 | 1.7 |
| Oxygen | 33.7 | 35.8 | 35.5 | 39.0 | 38.6 |
| Sulfur | 0.0 | 4.0 | 6.9 | 7.4 | 8.5 |
| Sodium | 19.9 | 23.0 | 24.5 | 23.6 | 25.8 |
| Solids, % | 59.2 | 61.7 | 65.4 | 73.0 | 70.4 |

The kraft liquor used to validate the char burn model was Valliant liquor, the composition was shown in Table 13.

APPENDIX III. COMPUTER CODE FOR DRYING MODEL

This is the computer code for the drying model. The model is written in basic to be run on an IBM type PC. The inputs are the initial drop diameter, the gas temperature, the wall temperature, the original liquor solids, and the swelling factor. The swelling factor is $d_{avg}/d_i$.

```
10 ' DRYMODEL                          Kathy Kulas
20 '                                   06/29/89
30 '
40 ' This program will solve the equation for black liquor drying
50 ' using the 4th order Runge-Kutta Method
60 '
70 '   where x(i+1) = x(i) + 1/6*(K1 + 2K2 + 2K3 + K4)
80 '         K1 = h*f(t(i),x(i))
90 '         K2 = h*f(t(i)+h/2, x(i)+K1/2)
100 '        K3 = h*f(t(i) + h/2, x(i) + K2/2)
110 '        K4 = h*(f(t(i) + h, x(i) + K3)
120 '
130 'Input the parameters
140 '
180 INPUT "Output file ";BB$
190 INPUT "Initial Diameter, mm ";DI
200 INPUT "Gas Temperature, deg C ";TG1
210 INPUT "Wall Temperature, deg C ";TW1
220 INPUT "Liquor Solids, fraction ";XS
230 INPUT "Swelling Factor, i.e. 1.5 ";SF
240 '
250 T = .07              ' the initial time, corresponds to the start of data
255                      ' acquisition
260 H = .409             ' time step to correspond to data acquisition
300 '
310 ' Initialize and set initial values to constants and equations
320 '
322 VEL = 0                    'gas velocity, cm/sec, this is for no gas flow
324 KINVISC = 1.525            'kinematic viscosity of gas, cm^2/sec
326 PR = .676                                  ' Prandtl number
330 A = 3.14159 * (SF*DI)^2                    'drop surface area, mm^2
340 MO = 1.4 * 3.14159 * DI^3/ 6000            'initial liquor mass, g
350 MS = XS * MO                               'initial dry mass, g
360 MW = (1-XS) * MO                           'initial water mass, g
365 TD = (4.6 - LOG(MW/(.54678*(MS+MW))))/.046  'initial drop temperature, °C
370 TG = TG1 + 273.15                          'gas temp, K
380 TW = TW1 + 273.15                          'wall temp, K
390 CPS = .4             'heat capacity of black liquor solids, cal/g-deg
400 CPW = 1              'heat capacity of water, cal/g-deg
410 LW = 539.8           'latent heat of water, cal/g water
420 EW = 1 for Hupa tests      'emissivity of the walls, assumed
```

```
      = 0.65 for SPR
430 '
440 IF TG1 = 550   THEN HCON = 8.992E-05        'cal/s-mm-K,
450 IF TG1 = 650   THEN HCON = .0000985         'cal/s-mm-K
455 IF TG1 = 800  THEN HCON = 1.1167E-04       'cal/s-mm-K
460 '
462 K = 1.777E-05 * (TG/1173)^.68             'gas thermal conductivity
464 RE = DI/10 * SF * VEL/KINVISC                ' Reynolds number
466 HCON = K * (2 + .6*RE^.5 * PR^.33)/(SF*DI)  'convective heat coefficient
470 A1 = HCON * A
480 A2 = 4.275E-14 * A * EW/3.14159
490 A3 = 39.758 * MS^2 * CPS
500 A4 = 39.758 * MS * CPW
510 '
520 'Open output file
530 '
540 OPEN "O",#2,BB$
545 PRINT,"    "
590 '
600 ' Actual Integration
610 '
620 FOR I = 1 TO 200
640     DUM1 = A1*(TG1-TD) + A2*(TW^4-(TD+273.15)^4)
650     DUM2 = LW + (A3 + A4*MW)/((MS+MW)^2*EXP(-.046*TD+4.6))
652
655' Calculate first Runge-Kutta constant
657
660     K1 = -H * DUM1/DUM2
661'
662' Calculate new mass of water and drop temperature
663'
670     AMW = MW + K1/2
680         IF AMW <= 0 GOTO 950
685     ATD = (4.6-LOG(AMW/(.54678*(MS+AMW))))/.046
700     DUM1 = A1*(TG1-ATD) + A2*(TW^4-(ATD+273.15)^4)
710     DUM2 = LW + (A3 + A4*MW)/((MS+MW)^2*EXP(-.046*TD+4.6))
'
' Calculate second Runge-Kutta constant
'
720     K2 = -H * DUM1/DUM2
'
' Calculate new mass of water and drop temperature
'
730     BMW = MW + K2/2
735         IF BMW <= 0 GOTO 950
740     BTD = (4.6-LOG(BMW/(.54678*(MS+BMW))))/.046
745     DUM1 = A1*(TG1-TD) + A2*(TW^4-(BTD+273.15)^4)
750     DUM2 = LW + (A3 + A4*MW)/((MS+MW)^2*EXP(-.046*TD+4.6))
'
' Calculate third Runge-Kutta constant
'
760     K3 = -H * DUM1/DUM2
'
' Calculate new mass of water and drop temperature
```

```
'
770     CMW = MW + K3
775         IF CMW <= 0 GOTO 950
780     CDT = (4.6-LOG(CMW/(.54678*(MS+CMW))))/.046
790     DUM1 = A1*(TG1-CTD) + A2*(TW^4-(CDT+273.15)^4)
800     DUM2 = LW + (A3 + A4*MW)/((MS+MW)^2*EXP(-.046*TD+4.6))
'
' Calculate fourth Runge-Kutta constant
810     K4 = -H * DUM1/DUM2
'
' Calculate new mass of water and drop temperature to be used in next time
' step
'
820     MW = MW + (K1+(2*K2)+(2*K3)+K4)/6
825         IF MW <= 0 GOTO 950
827     TD = (4.6-LOG(MW/(.54678*(MS+MW))))/.046
830     MD = MS + MW
832     RAD = A2 * (TW^4-(TD+273.15)^4)        ' Q_rad
834     CONV = A1 * (TG1 - TD)                 ' Q_conv
836     MOIST = 100 * (MW/MD)                  ' drop moisture, %
840 '
845     T = T + H
850     PRINT,T;TD;MD;MW;MOIST
860     PRINT#2,T;TD;MD;MW;MOIST
870 '
880         IF MW <= 0 GOTO 950
885 IF MOIST < .02 GOTO 950
890 '
900 NEXT
910 '
920 CLOSE #2
930 GOTO 970
940 '
952 PRINT," The mass of water is below 0, the drop is dry "
960 CLOSE #2
970 '
980 END
```

## APPENDIX IV. CALCULATION OF $A_v$ AND $E_v$ FROM PYROLYSIS DATA

Kinetic constants $A_v$ and $E_v$ were estimated from several single particle pyrolysis tests in the SPR. The rate of mass loss for pyrolysis was linear with time for more than four seconds. Equation (21) can be solved at two separate times using the measured rate of mass loss, as shown in Equation (68), and substituting $dm_p/dt = dm_d/dt$. The particle temperature was obtained from an energy balance around the particle.

$$dm_p/dt = A_v\, m_b \exp\,(-E_v/RT_d) \tag{21}$$

$$dm_d/dt = m_{b1}\, A_v\, EXP(-E_v/R\, T_{d1}) = m_{b2}\, A_v\, EXP(-E_v/R\, T_{d2}) \tag{68}$$

This simplifies to

$$E_v/R = \frac{\ln(m_{b2}/m_{b1})}{1/T_{d2} - 1/T_{d1}} \tag{69}$$

and

$$A_v = \frac{dm_d/dt}{EXP(-E_v/R\, T_{d1})\; m_{b1}} \tag{70}$$

$dm_d/dt$ was measured to be 0.00287 g/sec and the initial dry mass of the particle was 0.02405 g. The mass of black liquor solids, $m_b$, was calculated at each time step by a mass balance around the particle. At the first time, $t_1$ = 1 second, $m_{b1}$ was calculated to equal 0.0158 g and $T_{d1}$ = 381°C. At the second time, $t_2$ = 2 seconds, $m_{b2}$ was calculated to equal 0.00762 and $T_{d2}$ = 527°C. Substituting the measured and calculated values listed above into Equation (69), $E_v/R$ = 2628 $K^{-1}$. Solving Equation (70), $A_v$ = 10.07 $sec^{-1}$. The gas

temperature was 800°C and the gas velocity was 1.7 m/sec.

APPENDIX V. COMPUTER CODE FOR VOLATILES BURNING MODEL

The volatiles burning model is written in basic and was run in quickbasic (on the IBM PC) to speed up the computation time. The inputs to the model are the liquor mass, liquor solids, gas temperature, wall temperature, drop temperature at the end of drying, the oxygen concentration in the gas, and the drying time. The drop temperature and the drying time are obtained from the drying model. The outputs to the model are the particle mass, diameter, and temperature.

```
10 ' COMB.BAS                                          Kathy Kulas
20 '                                                     6/29/89
30 '
40 ' This program will solve the set of simultaneous equations for black
50 ' liquor volatiles burning using the 4th order Runge-Kutta method.
60 '
70 ' where x(i+1) = x(i) + (K1 + 2*K2 + 2*K3 + K4)/6
80 '       K1 = h * f(t(i), x(i))
90 '       K2 = h * f(t(i) + h/2, x(i) + K1/2)
100 '      K3 = h * f(t(i) + h/2, x(i) + K2/2)
110 '      K4 = h * f(t(i+1), x(i) + K3)
120 '
130 ' and dx1/dt = A1 EXP (-E1/R x3) (mo - 2.857 mp)  x1 = Mass of drop
150 '     dx3/dt = temperature of drop
170 '
' Input parameters
'
180 INPUT " Output file "; BB$
190 INPUT " Initial Mass of drop, mg "; MI
200 INPUT " Initial liquor solids, fraction "; SOL
210 INPUT " Initial gas temperature, C "; TG
220 INPUT " Initial wall temperature, C "; TW1
235 INPUT " Initial drop temperature, C "; TD
236 INPUT " Start time, sec "; TIME
237 INPUT " Bulk oxygen concentration, fraction "; BULKOXY
240 '
250 ' Set constants and initial conditions
260 '
280 H = .2045                    ' Time step, sec
290 NSTEP = 50                   ' Number of time steps
300 A1 = 10.07                   ' /sec, Pre-expon. factor in volatilization
310 E1 = 22000!                  ' J/mol, activation energy for vol.
320 R = 8.314                    ' J/mol-K, gas constant
330 MO = MI * SOL / 1000                    ' g, initial dry mass
340 MD = MO                                 ' g, initial drop mass
```

```
345 DMAX = (.221 * MI * SOL + 7.2) / 10       'cm, maximum diameter
350 AMD = MD                                  ' g, initial drop mass
360 A2 = .0424                                ' mol product/g volatile gas
370 A3 = .0178                                ' mol O2/g volatile gas
380 VEL = 170                                 ' cm/sec, gas velocity
395 TW = TW1 + 273                            ' K, wall temperature
430 CPD = .4                      ' cal/g-sec, heat capacity of solids
440 KIN = .0001777                ' thermal conductivity, 1173 K, cal/s-cm-K
450 RD = 1.5 * (MI * 3 / (3.14159 * 4000 * 1.4)) ^ .33
                                  ' cm, initial drop radius
460 DI = 2 * RD                   ' initial diameter
470 SIGMA = 1.355E-12             ' cal/cm^2-K^4, Stefan-Boltzmann constant
480 EMISDP = .54                  ' view factor - emissivity between
490 FFD = EMISDP                  ' flame and drop
500 AD = 4 * 3.14159 * RD ^ 2     ' cm^2, drop surface area
510 PYRHT = 150                   ' cal/g, heat of pyrolysis
520 COMBHT = 6400 / 4.184         ' cal/g, heat of combustion
550 KINVISC = 1.525               ' cm^2/sec, kinematic viscosity
560 RE = 2 * RD * VEL / KINVISC   ' Reynolds Number
570 PR = .676                     ' Prandtl Number, independent of Tf
580 HCONV = KIN * (2 + .6 * RE ^ .5 * PR ^ .33) / 2
                                  ' convective heat coefficient
590 C = BULKOXY / (.08206 * 1173 * 1000)      'mol/cm^3, gas conc. at drop
610 '
620 '
630 ' Open output file
640 '
650 OPEN "O", #2, BB$
660 PRINT , "The dry mass is "; MO
670 PRINT , "The drop radius is "; RD
680 '
690 PRINT , TIME; MD; TD
700 PRINT #2, TIME; MD; DI; TD; DMAX
710 '
750 A8 = SIGMA * FFD
760 '
770 ' Start integration loop
775  FLAG = 0                            ' to mark when drop diameter is
                                           95% of max diameter
780 '
790 FOR I = 1 TO NSTEP
800 '
810    MB = 2.857 * MD - 1.857 * MO       ' unreacted black liquor, g
820    K = KIN * ((TG + TD + 546) / (2 * 1173)) ^ .68
830    DP = DI + (DMAX - DI) * (MO - AMD) / (.35 * MO)
840    RD = DP / 2
850    AD = 3.14159 * DP ^ 2              ' drop surface area
910    QRADDP = A8 * AD * (TW ^ 4 - (TD + 273) ^ 4)
920    RE = 2 * RD * VEL / KINVISC
930    HCONV = K * (2 + .6 * RE ^ .5 * PR ^ .33) / (2 * RD)
940    QCONV = HCONV * 4 * 3.14159 * RD ^ 2 * (TG - TD)
970    DMD = (MD - AMD)
972    DMDDT = DMD / H
973    KOX = 2.06 * (2 + .525 * RE ^ .5) / DP
```

```
      C = BULKOXY / (.08206 * (TD + 273) * 1000)
974   OX = KOX * C * AD
975   PYR = DMDDT
976   IF DMDDT = 0 THEN GOTO 978
977   IF OX < A3 * DMDDT THEN PYR = OX / A3
978   QOX = PYR * COMBHT
980 '
990 ' Calculate Runge-Kutta constant K1 for all MD, RF, TD, and TF
1000 '
1010     K11 = -H * (A1 * EXP(-E1 / (R * (TD + 273))) * MB)
1030     K13 = H * (QCONV + QOX + QRADDP - DMD * PYRHT) / (MD * CPD)
1080 '
1090 ' Increment MD, and TD
1100 '
1110     AMD = MD + K11 / 2
1130     ATD = TD + K13 / 2
1150 '
1160     MB = 2.857 * AMD - 1.875 * MO
1170     K = KIN * ((TG + ATD + 546) / (2 * 1173)) ^ .68
1180     DP = DI + (DMAX - DI) * (MO - AMD) / (.35 * MO)
1190     RD = DP / 2
1200     AD = 3.14159 * DP ^ 2
1230     QRADDP = A8 * AD * (TW ^ 4 - (ATD + 273) ^ 4)
1235     RE = DP * VEL / KINVISC
1250     HCONV = K * (2 + .6 * RE ^ .5 * PR ^ .33) / (2 * RD)
1260     QCONV = HCONV * 4 * 3.14159 * RD ^ 2 * (TG - ATD)
1290     DMD = MD - AMD
1291     DMDDT = DMD / (.5 * H)
1292     KOX = 2.06 * (2 + .525 * RE ^ .5) / DP
         C = BULKOXY / (.08206 * (ATD + 273) * 1000)
1293     OX = KOX * C * AD
1294     PYR = DMDDT
1295     IF DMDDT = 0 THEN GOTO 1297
1296     IF OX < A3 * DMDDT THEN PYR = OX / A3
1297     QOX = PYR * COMBHT
1300 '
1310 ' Calculate Runge-Kutta constant K2 for MD, and TD
1320 '
1330      K21 = -H * (A1 * EXP(-E1 / (R * (ATD + 273))) * MB)
1350      K23 = H * (QCONV + QOX + QRADDP - DMD * PYRHT) / (AMD * CPD)
1400 '
1410 ' Increment MD, and TD
1420 '
1430     AMD = MD + K21 / 2
1450     ATD = TD + K23 / 2
1470 '
1480     MB = 2.857 * AMD - 1.857 * MO
1490     K = KIN * ((TG + ATD + 546) / (2 * 1173)) ^ .68
1500     DP = DI + (DMAX - DI) * (MO - AMD) / (.35 * MO)
1510     RD = DP / 2
1520     AD = 3.14159 * DP ^ 2
1550     QRADDP = A8 * AD * (TW ^ 4 - (ATD + 273) ^ 4)
1555     RE = DP * VEL / KINVISC
1570     HCONV = K * (2 + .6 * RE ^ .5 * PR ^ .33) / (2 * RD)
```

```
1580     QCONV = HCONV * 4 * 3.14159 * RD ^ 2 * (TG - ATD)
1610     DMD = MD - AMD
1601     DMDDT = DMD / (.5 * H)
1602     KOX = 2.06 * (2 + .525 * RE ^ .5) / DP
         C = BULKOXY / (.08206 * (ATD + 273) * 1000)
1603     OX = KOX * C * AD
1604     PYR = DMDDT
1605     IF DMDDT = 0 THEN GOTO 1607
1606     IF OX < A3 * DMDDT THEN PYR = OX / A3
1607     QOX = PYR * COMBHT
1620 '
1630 ' Calculate Runge-Kutta constant K3 for all MD, RF, TD, and TF
1640 '
1650     K31 = -H * (A1 * EXP(-E1 / (R * (ATD + 273))) * MB)
1670     K33 = H * (QCONV + QOX + QRADDP - DMD * PYRHT) / (AMD * CPD)
1720 '
1730 ' Increment MD, and TD
1740 '
1750     AMD = MD + K31
1770     ATD = TD + K33
1790 '
1810     MB = 2.857 * AMD - 1.857 * MO
1820     K = KIN * ((TG + ATD + 546) / (2 * 1173)) ^ .68
1830     DP = DI + (DMAX - DI) * (MO - AMD) / (.35 * MO)
1840     RD = DP / 2
1850     AD = 3.14159 * DP ^ 2
1880     QRADDP = A8 * AD * (TW ^ 4 - (ATD + 273) ^ 4)
1890     RE = DP * VEL / KINVISC
1900     HCONV = K * (2 + .6 * RE ^ .5 * PR ^ .33) / (2 * RD)
1910     QCONV = HCONV * 4 * 3.14159 * RD ^ 2 * (TG - ATD)
1940      DMD = MD - AMD
1941      DMDDT = DMD / H
1942      KOX = 2.06 * (2 + .525 * RE ^ .5) / DP
          C = BULKOXY / (.08206 * (ATD + 273) * 1000)
1943      OX = KOX * C * AD
1944      PYR = DMDDT
1945      IF DMDDT = 0 THEN GOTO 1947
1946      IF OX < A3 * DMDDT THEN PYR = OX / A3
1947      QOX = PYR * COMBHT
1950 '
1960 ' Calculate Runge-Kutta constants K4 for all MD and TD
1970 '
1980     K41 = -H * (A1 * EXP(-E1 / (R * (ATD + 273))) * MB)
2000     K43 = H * (QCONV + QOX + QRADDP - DMD * PYTHT) / (AMD * CPD)
2050 '
2060 ' Increment MD and TD
2070 '
2080     MD = MD + (K11 + 2 * K21 + 2 * K31 + K41) / 6
2100     TD = TD + (K13 + 2 * K23 + 2 * K33 + K43) / 6
         DRAT = DP / DMAX
         VOL = MB / MO * 100
2101 '
2102   IF DP / DMAX < .975 THEN GOTO 2120
2103      IF FLAG = 1 THEN GOTO 2120
```

```
2104       TMAX = TIME
2105       FLAG = 1
2120 '
2130      TIME = TIME + H
2140 ' Print results for this time step
2150 '
2160    PRINT , TIME; TD; MD; DP; VOL; DRAT
2170    PRINT #2, TIME; TD; MD; DP; VOL; DRAT

    IF VOL < .5 THEN GOTO 2212        ' stops program execution when the mass
                                      fraction of volatiles is less than 0.5 %
2180 '
2190 ' Repeat cycle
2200 '
2210    NEXT
2212 '
     PRINT , " VOLATILES EVOLUTION IS COMPLETE AT "; TIME; " SECONDS"
2215 PRINT , TMAX; DMAX
2216 PRINT #2, TMAX; DMAX
2220 '
2230 CLOSE #2
2240 END
```

## APPENDIX VI. COMPUTER CODE FOR CHAR BURNING MODEL

This computer code is written in basic to run on an IBM PC. Using quickbasic speeds up computation time. Model results are not dependent on the step size. The model inputs are the maximum diameter, the initial char mass, the char composition (carbon, sulfur, sodium), the oxygen concentration in the gas, the gas temperature, and the char burn time. The char burn time is used in determining the char temperature vs. time profile, for tests with no char temperature measurement. The model outputs are the char mass, carbon concentration, reduction ratio, and mass of CO and $CO_2$ in the boundary layer surrounding the particle.

The code listed in this Appendix is for kraft liquor. To run it for soda liquor, several items must be changed. The kinetic constants in the carbon/sulfate reaction have to be changed to the values for soda liquor. If a pure soda liquor (no sulfur) is used, the sulfate reaction must be disabled. X2, the reduction ratio, and SULF, the sulfidity are set equal to zero. All equations involving division by SULF must be set equal to zero.

```
10 'CHAR BURN                                          Kathy Kulas
20 '                                                    6/29/89
30 '
40 'This program will solve the set of simultaneous equations for black
50 'liquor char burning using the 4th order Runge-Kutta method.
60 '
70 'where x(i+1) = x(i) + (K1 + 2*K2 + 2*K3 + K4)/6
80 '       K1 = h * f(t(i), x(i))
90 '       K2 = h * f(t(i) + h/2, x(i) + K1/2)
100 '      K3 = h * f(t(i) + h/2, x(i) + K2/2)
110 '      K4 = h * f(t(i) + h, x(i) + K3)
120 '
130 'and dx1/dt = - ( 2 * Rcs + Rox + Rco), x1 = carbon concentration
140 '     dx2/dt = Rcs/Sulf - Rso, x2 = reduction ratio
150 '     dx3/dt = Rox + 2 * Rcs - Rco - (Kco2 * x3 * area), mass of CO2
160 '     dx4/dt = 2 * Rco - (Kco * x4 * area), x4 = mass of CO in boundary
170 '
190 '
```

```
210 INPUT " Output file "; BB$
220 INPUT " Initial Diameter, cm "; DPI
230 INPUT " Initial Mass, mg "; MI
240 INPUT " Percent carbon in char "; CARB
250 INPUT " Percent sulfur in char "; SUL
260 INPUT " Percent sodium in char "; NA
270 INPUT " Bulk oxygen concentration, fraction "; BULKOXY
272 INPUT " Initial Temperature, Kelvin "; TG
274 INPUT " Char Burn Time, sec "; CBTIME
276 INPUT " Number of seconds to run "; NSTEP
280 '
290 'Input time and temperature profile
300 '
310  TMAX = 1473
320  SLOPE = (TMAX - TG) / CBTIME
340  H = .25
360  TIME = 0
380 'Initialize and set initial values to constants and equations
390 '
400 KINVISC = 1.525                ' cm^2/sec
410 VEL = 170                      ' cm/sec
450 A1 = 1310                      ' /sec
460 A2 = .0011                     ' mol SO4/mol Na2
470 A3 = 236 * TG                  ' cm/sec
480 A4 = 9.53E+07 / 44             ' mol/atm-sec-g
490 A5 = KINVISC / VEL             ' cm
500 A6 = 10.8 / 44                 ' mol/atm-g
510 A7 = 6.3 / 28                  ' mol/atm-g
520 E1 = 29200 / 1.987             ' K
530 E2 = 22492                      ' K
540 E3 = 11022                     ' K
550 GASCONS = .08206               ' l-atm/mol-K
560 CDENS = .2                     ' char density, g/cm^3
570 IDENS = 2                      ' inorganic density, g/cm^3
580 MI = MI / 1000                  ' initial mass, g
590 MC = CARB * MI / 100            ' initial mass of carbon, g
600 MS = SUL * MI / 100             ' initial mass of sulfur, g
610 MNA = NA * MI / 100             ' initial mass of sodium, g
620 '
630 SULF = 1.437 * MS / MNA        ' sulfidity, mol S/mol Na2
640 XINOR = (MI - MC) / MI         ' initial mass fraction of inorganic
650 VR = XINOR * CDENS / IDENS     ' smelt bead volume/initial volume
660 '
670 CI = MC * 46 / (MNA * 12) ' mol C/mol Na2, initially
680 X2 = .5                   ' initial reduction ratio
690 X3 = 0                    ' no CO2 initially present
700 X4 = 0                    ' no CO initially present
704 FCS = .9
708 FOX = .9
709 MREL = (106 + 36 * SULF - 64 * SULF * X2 + 12 * CI)
710 '
720 PRINT , " Initial Mass, g "; MI
730 PRINT , " Sulfidity, mol S/mol Na2 "; SULF
```

```
740 PRINT , " Volume smelt bead/initial volume "; VR
750 '
760 'Open output file and print table headings
770 '
780 OPEN "O", #2, BB$
790 PRINT , TIME; CI; X2; X3; X4
795 PRINT #2, TIME; CI; X2; X3; X4
796  X1 = CI
800 '
810 'Start Integration
820 '
825 MP = (106 + 36 * SULF - 64 * SULF * X2 + 12 * X1) * MI / MREL
830 FOR I = 1 TO NSTEP
840 '
880 '
910 'Set values for calculating Runge-Kutta constants
920 '
922  IF X2 > .999 THEN X2 = .999
924  IF X3 < 0 THEN X3 = 0
926  IF X4 < 0 THEN X4 = 0
927  IF X2 < 0 THEN X2 = 0
928  IF X1 < 0 THEN X1 = 0
929 '
930    TEMP = SLOPE * TIME + TG              ' K
935  IF TIME >= CBTIME THEN TEMP = 1473
       TF = (TEMP + TG) / 2
       DOX = 1.757 + .003103 * (TF - TG)
       DCO = 1.753 + .002753 * (TF - TG)
       DCO2 = 1.332 + .003053 * (TF - TG)
       MP = (106 + 36 * SULF - 64 * SULF * X2 + 12 * X1) * MI / MREL
       MSA = MP - (X1 * MNA * 12 / 46)
       PS = ((CDENS / IDENS) * (MSA / MC)) ^ .67
940    RCS=A1*((1-X2) * SULF / (A2 + (1 - X2) * SULF)) * X1 * EXP(-E1 / TEMP)
950    DP = DPI * ((1 - VR) * X1 / CI + VR) ^ (1 / 3)' cm
960    DELT = 5 * (A5 * DP) ^ .5                    ' cm
970    AREA = 3.14159 * DP ^ 2 * 46 / MNA           ' cm^2/mol Na2
975    BLAREA = 3.14159 * (DP + 2 * DELT) ^ 2 * 46 / MNA' cm^2/mol Na2
980    VOL=3.14159*((DP+2*DELT) ^ 3 - DP ^ 3) / (6000 * GASCONS)   ' mol-K/atm
990    P = ((X1 / CI) ^ (2 / 3)) / ((X1 / CI) ^ (2 / 3) + PS)
1000    RE = DP * VEL / KINVISC
1010    KMOX = DOX * (2 + .525 * RE ^ .5) / DP   ' cm/sec
1020    KROX = A3 * EXP(-E3 / TEMP)                          ' cm/sec
1030    KCOX = 1 / (1 / KMOX + 1 / KROX)                     ' cm/sec
1040    ROX = KCOX * BULKOXY * AREA * P * .01219 / TEMP
        KRSO = 0
        IF X2 > 0 THEN KRSO = 2250 / (X2 * SULF * 3.14159 * DP ^ 2 * (1 - P))
        IF X2 > .1 THEN KRSO = 0
        KSO = KMOX
        IF KRSO <> 0 THEN KSO = 1 / (1 / KMOX + 1 / KRSO)
1041 '
1042   X3MAX = 44 * VOL * 2 / (TG + TEMP + 273)
1046   X4MAX = 28 * VOL * 2 / (TG + TEMP + 273)
1047   IF X3 > X3MAX THEN X3 = X3MAX
```

```
1048   IF X4 > X4MAX THEN X4 = X4MAX
1049 '
1050    RCO=P*A4*X3*X1*EXP(-E2 / TEMP) / ((VOL / TEMP) + A6 * X3 + A7 * X4)
1060    RSO = KSO * BULKOXY * AREA * (1 - P) * .01219 / (2 * SULF * TEMP)
1070    KCO2 = DCO2 * (2 + .525 * RE ^ .5) / (DP + 2 * DELT)' cm/sec
1080    KCO = DCO * (2 + .525 * RE ^ .5) / (DP + 2 * DELT)   ' cm/sec
1090 '
1100 '
1140 'Calculate Runge-Kutta constant K1 for all X1,X2,X3, and X4
1150 '
1160    K11 = -H * (4 * RCS / (2 - FCS) + 2 * ROX / (2 - FOX) + RCO)
1170    K12 = H * (RCS / SULF - RSO)
1180    K13=H*44/46*MNA*(2*(1-FOX)*ROX/(2-FOX)+4*(1-FCS)/(2-FCS)*RCS
                    - RCO - (KCO2 * X3 * BLAREA * .01219 / TEMP))
1190    K14=H*28/46*MNA*(4*FCS*RCS/(2-FCS)+2*FOX*ROX/(2-FOX)
                  + 2 * RCO - (KCO * X4 * BLAREA * .01219 / TEMP))
1200 '
1230 '
1240 'Increment x's by k1/2
1250 '
1260   AX1 = X1 + K11 / 2
1270   AX2 = X2 + K12 / 2
1280   AX3 = X3 + K13 / 2
1290   AX4 = X4 + K14 / 2
1300 '
1302 IF AX2 > .999 THEN AX2 = .999
1304 IF AX3 < 0 THEN AX3 = 0
1306 IF AX4 < 0 THEN AX4 = 0
1307  IF AX1 < 0 THEN AX1 = 0
1308  IF AX2 < 0 THEN AX2 = 0
1310 '
1320 TEMP = (SLOPE * (TIME + H / 2)) + TG
1325  IF (TIME + H / 2) >= CBTIME THEN TEMP = 1473
1330 '
       TF = (TEMP + TG) / 2
       DOX = 1.757 + .003103 * (TF - TG)
       DCO = 1.753 + .002753 * (TF - TG)
       DCO2 = 1.332 + .003053 * (TF - TG)
       MP = (106 + 36 * SULF - 64 * SULF * AX2 + 12 * AX1) * MI / MREL
       MSA = MP - (AX1 * MNA * 12 / 46)
       PS = ((CDENS / IDENS) * (MSA / MC)) ^ .67
1340   RCS=A1*((1-AX2)*SULF/ (A2 + (1 - AX2) * SULF)) * AX1 * EXP(-E1 / TEMP)
1350   DP = DPI * ((1 - VR) * AX1 / CI + VR) ^ (1 / 3)
1360   DELT = 5 * (A5 * DP) ^ .5
1370   AREA = 3.14159 * DP ^ 2 * 46 / MNA
1375   BLAREA = 3.14159 * (DP + 2 * DELT) ^ 2 * 46 / MNA
1380   VOL = 3.14159 * ((DP + 2 * DELT) ^ 3 - DP ^ 3) / (6000 * GASCONS)
1390   P = ((AX1 / CI) ^ (2 / 3)) / ((AX1 / CI) ^ (2 / 3) + PS)
1400   RE = DP * VEL / KINVISC
1410   KMOX = DOX * (2 + .525 * RE ^ .5) / DP
1420   KROX = A3 * EXP(-E3 / TEMP)
1430   KCOX = 1 / (1 / KMOX + 1 / KROX)
1440   ROX = KCOX * BULKOXY * AREA * P * .01219 / TEMP
```

```
      KRSO = 0
      IF AX2 > 0 THEN KRSO = 2250 / (AX2 * SULF * 3.14159 * DP ^ 2 * (1 - P))
      IF AX2 > .1 THEN KRSO = 0
      KSO = KMOX
      IF KRSO <> 0 THEN KSO = 1 / (1 / KMOX + 1 / KRSO)
1441  '
1442    AX3MAX = 44 * VOL * 2 / (TG + TEMP + 273)
1444    AX4MAX = 28 * VOL * 2 / (TG + TEMP + 273)
1445    IF AX3 > AX3MAX THEN AX3 = AX3MAX
1446    IF AX4 > AX4MAX THEN AX4 = AX4MAX
1447  '
1450    RCO=P*A4*AX3*AX1*EXP(-E2 / TEMP) / (VOL / TEMP + A6 * AX3 + A7 * AX4)
1460    RSO = KSO * BULKOXY * AREA * (1 - P) * .01219 / (2 * SULF * TEMP)
1470    KCO2 = DCO2 * (2 + .525 * RE ^ .5) / (DP + 2 * DELT)
1480    KCO = DCO * (2 + .525 * RE ^ .5) / (DP + 2 * DELT)
1490  '
1530  'Calculate Runge-Kutta constant K2
1540  '
1550    K21 = -H * (4 * RCS / (2 - FCS) + 2 * ROX / (2 - FOX) + RCO)
1560    K22 = H * (RCS / SULF - RSO)
1570    K23 = H * 44 / 46 * MNA * (2 * (1 - FOX) / (2 - FOX) * ROX +
                          4 * (1 - FCS) / (2 - FCS) * RCS
                          - RCO - (KCO2 * AX3 * BLAREA * .01219 / TEMP))
1580    K24 = H * 28 / 46 * MNA * (2 * FOX / (2 - FOX) * ROX +
                          4 * FCS / (2 - FCS) * RCS + 2 * RCO -
                          (KCO * AX4 * BLAREA * .01219 / TEMP))
1590  '
1620  '
1630  'Increment x's by K2/2
1640  '
1650    BX1 = X1 + K21 / 2
1660    BX2 = X2 + K22 / 2
1670    BX3 = X3 + K23 / 2
1680    BX4 = X4 + K24 / 2
1690  '
1692  IF BX2 > .999 THEN BX2 = .999
1694  IF BX3 < 0 THEN BX3 = 0
1695   IF BX1 < 0 THEN BX1 = 0
1696  IF BX4 < 0 THEN BX4 = 0
1697  IF BX2 < 0 THEN BX2 = 0
      TF = (TEMP + TG) / 2
      DOX = 1.757 + .003103 * (TF - TG)
      DCO = 1.753 + .002753 * (TF - TG)
      DCO2 = 1.332 + .003053 * (TF - TG)
      MP = (106 + 36 * SULF - 64 * SULF * BX2 + 12 * BX1) * MI / MREL
      MSA = MP - (BX1 * 12 * MNA / 46)
      PS = ((CDENS / IDENS) * (MSA / MC)) ^ .67
1698  '
1700    RCS=A1*((1-BX2)*SULF/ (A2 + (1 - BX2) * SULF)) * BX1 * EXP(-E1 / TEMP)
1710    DP = DPI * ((1 - VR) * BX1 / CI + VR) ^ (1 / 3)
1720    DELT = 5 * (A5 * DP) ^ .5
1730    AREA = 3.14159 * DP ^ 2 * 46 / MNA
1735    BLAREA = 3.14159 * (DP + 2 * DELT) ^ 2 * 46 / MNA
```

```
1740   VOL = 3.14159 * ((DP + 2 * DELT) ^ 3 - DP ^ 3) / (6000 * GASCONS)
1750   P = ((BX1 / CI) ^ (2 / 3)) / ((BX1 / CI) ^ (2 / 3) + PS)
1760   RE = DP * VEL / KINVISC
1770   KMOX = DOX * (2 + .525 * RE ^ .5) / DP
1780   KROX = A3 * EXP(-E3 / TEMP)
1790   KCOX = 1 / (1 / KMOX + 1 / KROX)
1800   ROX = KCOX * BULKOXY * AREA * P * .01219 / TEMP
        KRSO = 0
        IF BX2 > 0 THEN KRSO = 2250 / (BX2 * SULF * 3.14159 * DP ^ 2 * (1 - P))
        IF BX2 > .1 THEN KRSO = 0
        KSO = KMOX
        IF KRSO <> 0 THEN KSO = 1 / (1 / KMOX + 1 / KRSO)
1801 '
1802   BX3MAX = 44 * VOL * 2 / (TG + TEMP + 273)
1804   BX4MAX = 28 * VOL * 2 / (TG + TEMP + 273)
1806   IF BX3 > BX3MAX THEN BX3 = BX3MAX
1808   IF BX4 > BX4MAX THEN BX4 = BX4MAX
1809 '
1810   RCO=P*A4*BX3*BX1*EXP(-E2 / TEMP) / (VOL / TEMP + A6 * BX3 + A7 * BX4)
1820   RSO = KSO * BULKOXY * AREA * (1 - P) * .01219 / (2 * SULF * TEMP)
1830   KCO2 = DCO2 * (2 + .525 * RE ^ .5) / (DP + 2 * DELT)
1840   KCO = DCO * (2 + .525 * RE ^ .5) / (DP + 2 * DELT)
1880 '
1890 'Calculate Runge-Kutta constant K3
1900 '
1910   K31 = -H * (4 * RCS / (2 - FCS) + 2 * ROX / (2 - FOX) + RCO)
1920   K32 = H * (RCS / SULF - RSO)
1930   K33 = H * 44 / 46 * MNA * (2 * (1 - FOX) / (2 - FOX) * ROX +
                          4 * (1 - FCS) / (2 - FCS) * RCS - RCO -
                          (KCO2 * BX3 * BLAREA * .01219 / TEMP))
1940   K34 = H * 28 / 46 * MNA * (4 * FCS / (2 - FCS) * RCS +
                          2 * FOX / (2 - FOX) * ROX + 2 * RCO -
                          (KCO * BX4 * BLAREA * .01219 / TEMP))
1950 '
1980 '
1990   TEMP = SLOPE * (TIME + H) + TG
1995  IF (TIME + H) > CBTIME THEN TEMP = 1473
2000 '
2010 'Increment x's by K3
2020 '
2030   CX1 = X1 + K31
2040   CX2 = X2 + K32
2050   CX3 = X3 + K33
2060   CX4 = X4 + K34
2070 '
2071  IF CX1 < 0 THEN CX1 = 0
2072 IF CX2 > .999 THEN CX2 = .999
2073  IF CX2 < 0 THEN CX2 = 0
2074 IF CX3 < 0 THEN CX3 = 0
2076 IF CX4 < 0 THEN CX4 = 0
       TF = (TEMP + TG) / 2
       DOX = 1.757 + .003103 * (TF - TG)
       DCO = 1.753 + .002753 * (TF - TG)
```

```
        DCO2 = 1.332 + .003053 * (TF - TG)
        MP = (106 + 36 * SULF - 64 * SULF * CX2 + 12 * CX1) * MI / MREL
        MSA = MP - (CX1 * 12 * MNA / 46)
        PS = ((CDENS / IDENS) * (MSA / MC)) ^ .67
2078 '
2080    RCS=A1*((1-CX2)*SULF / (A2 + (1 - CX2) * SULF)) * CX1 * EXP(-E1 / TEMP)
2090    DP = DPI * ((1 - VR) * CX1 / CI + VR) ^ (1 / 3)
2100    DELT = 5 * (A5 * DP) ^ .5
2110    AREA = 3.14159 * DP ^ 2 * 46 / MNA
2115    BLAREA = 3.14159 * (DP + 2 * DELT) ^ 2 * 46 / MNA
2120    VOL = 3.14159 * ((DP + 2 * DELT) ^ 3 - DP ^ 3) / (6000 * GASCONS)
2130    P = ((CX1 / CI) ^ (2 / 3)) / ((CX1 / CI) ^ (2 / 3) + PS)
2140    RE = DP * VEL / KINVISC
2150    KMOX = DOX * (2 + .525 * RE ^ .5) / DP
2160    KROX = A3 * EXP(-E3 / TEMP)
2170    KCOX = 1 / (1 / KMOX + 1 / KROX)
2180    ROX = KCOX * BULKOXY * AREA * P * .01219 / TEMP
         KRSO = 0
         IF CX2 > 0 THEN KRSO = 2250 / (CX2 * SULF * 3.14159 * DP ^ 2 * (1 - P))
         IF CX2 > .1 THEN KRSO = 0
         KSO = KMOX
         IF KRSO <> 0 THEN KSO = 1 / (1 / KMOX + 1 / KRSO)
2181 '
2182    CX3MAX = 44 * VOL * 2 / (TG + TEMP + 273)
2184    CX4MAX = 28 * VOL * 2 / (TG + TEMP + 273)
2186    IF CX3 > CX3MAX THEN CX3 = CX3MAX
2188    IF CX4 > CX4MAX THEN CX4 = CX4MAX
2189 '
2190    RCO=P*A4*CX3*CX1 * EXP(-E2 / TEMP) / (VOL / TEMP + A6 * CX3 + A7 * CX4)
2200    RSO = KSO * BULKOXY * AREA * (1 - P) * .01219 / (2 * SULF * TEMP)
2210    KCO2 = DCO2 * (2 + .525 * RE ^ .5) / (DP + 2 * DELT)
2220    KCO = DCO * (2 + .525 * RE ^ .5) / (DP + 2 * DELT)
2260 '
2270 'Calculate Runge-Kutta constant K4
2280 '
2290    K41 = -H * (4 * RCS / (2 - FCS) + 2 * ROX / (2 - FOX) + RCO)
2300    K42 = H * (RCS / SULF - RSO)
2310    K43 = H * 44 / 46 * MNA * (2 * (1 - FOX) / (2 - FOX) * ROX +
                                   4 * (1 - FCS) / (2 - FCS) * RCS - RCO -
                                   (KCO2 * CX3 * BLAREA * .01219 / TEMP))
2320    K44 = H * 28 / 46 * MNA * (4 * FCS / (2 - FCS) * RCS +
                                   2 * FOX / (2 - FOX) * ROX + 2 * RCO -
                                   (KCO * CX4 * BLAREA * .01219 / TEMP))
2330 '
2360 '
2370 'Calculate x from constants
2380 '
2390     X1 = X1 + (K11 + 2 * K21 + 2 * K31 + K41) / 6
2400     X2 = X2 + (K12 + 2 * K22 + 2 * K32 + K42) / 6
2410     X3 = X3 + (K13 + 2 * K23 + 2 * K33 + K43) / 6
2420     X4 = X4 + (K14 + 2 * K24 + 2 * K34 + K44) / 6
2422     IF X2 < 0 THEN X2 = 0
2423     MP = (106 + 36 * SULF - 64 * SULF * X2 + 12 * X1) * MI / MREL
```

```
2425   REIM = MP / MI
2427   WIC = X1 * 12 * MNA / (46 * MP) * 100
2430 '
2440 'Print results for this time step
2442  TIME = TIME + H
2450 '
2460 '
2470 PRINT #2, TIME; X1; X2; X3; X4; MP; REIM; WIC
2475 PRINT , TIME; X1; X2; X3; X4; MP; REIM; WIC
2480 '
2490 'Repeat cycle
2500 '
2510 NEXT
2520 '
2530 CLOSE #2
2540 END
```

APPENDIX VII. DATA

This appendix contains the reduced data shown in Figures 15, 16, 18, 20, 23, and 24. Table 15 shows the measured and predicted rate of volatilization using the Thilmany liquor. This uses the two programs FLOW.BAS for drying and COMB.BAS for volatiles burning.

Table 15. Thilmany data, used in Figure 20.

| Run # | Initial Mass, mg | Oxygen % | Gas Temp, C | Rate of volatilization Meas | Pred |
|---|---|---|---|---|---|
| T196 | 23 | 4.3 | 666 | 2.91 | 3.41 |
| T197 | 22 | 10.5 | 666 | 3.87 | 4.14 |
| T198 | 33 | 16.7 | 666 | 5.82 | 4.49 |
| T184 | 23 | 0 | 763 | 2.54 | 2.29 |
| T156 | 21 | 0 | 763 | 3.02 | 2.29 |
| T185 | 21 | 10.5 | 763 | 5.22 | 4.29 |
| T163 | 21 | 10.5 | 763 | 3.28 | 4.29 |
| T157 | 21 | 10.5 | 763 | 4.78 | 4.29 |
| T149 | 22 | 10.5 | 763 | 4.82 | 4.29 |
| T161 | 11 | 10.5 | 763 | 3.78 | 2.31 |
| T164 | 23 | 10.5 | 763 | 5.83 | 4.29 |
| T188 | 22 | 10.5 | 763 | 3.57 | 4.29 |
| T144 | 4 | 10.5 | 763 | 2.05 | 1.09 |
| T146 | 11 | 10.5 | 763 | 3.86 | 2.31 |
| T158 | 22 | 10.5 | 763 | 4.71 | 4.29 |
| T162 | 41 | 10.5 | 763 | 5.82 | 7.43 |
| T187 | 10 | 10.5 | 763 | 3.15 | 2.31 |
| T--- | 22 | 10.5 | 763 | 4.89 | 4.29 |
| T160 | 10 | 10.5 | 763 | 3.94 | 2.31 |
| T165 | 23 | 21.0 | 763 | 5.47 | 4.99 |
| T189 | 21 | 21.0 | 763 | 5.63 | 4.99 |
| T190 | 12 | 4.3 | 860 | 2.65 | 2.11 |
| T166 | 11 | 4.3 | 860 | 2.67 | 2.11 |
| T167 | 33 | 4.3 | 860 | 5.09 | 5.25 |
| T204 | 34 | 4.3 | 860 | 5.29 | 5.25 |
| T202 | 11 | 10.5 | 860 | 3.71 | 2.62 |
| T193 | 42 | 16.7 | 860 | 7.20 | 7.34 |
| T199 | 12 | 16.7 | 860 | 4.40 | 3.32 |
| T201 | 33 | 10.5 | 860 | 5.76 | 6.45 |
| T169 | 33 | 16.7 | 860 | 5.39 | 6.90 |
| T200 | 33 | 16.7 | 860 | 5.61 | 6.90 |

The data shown in Figure 18, the time to maximum volume, using the

Valliant liquor, is shown in Table 16.

Table 16. Time to maximum volume, Valliant liquor.

| Run # | Initial Mass (mg) | Gas Temp (C) | Oxygen Conc. (%) | Rate of Volatiles Evolution, mg/sec Meas. | Pred. | Maximum Diameter mm Meas. | Pred. |
|---|---|---|---|---|---|---|---|
| 686-H51 | 10 | 800 | 2 | 2.05 | | 10.05 | 8.71 |
| 690-H55 | 24 | 800 | 2 | 4.40 | 3.18 | 13.74 | 10.81 |
| 691-H56 | 47 | 800 | 2 | 4.73 | | 16.72 | 14.26 |
| 685-H50 | 6 | 800 | 2 | 3.52 | | 9.69 | 8.10 |
| 683-H48 | 24 | 800 | 2 | 2.81 | | 11.74 | 10.81 |
| 684-H49 | 51 | 800 | 2 | 6.67 | | 15.00 | 14.86 |
| 688-H53 | 10 | 800 | 2 | 1.75 | 1.65 | 10.18 | 8.71 |
| 689-H54 | 20 | 800 | 2 | 2.62 | | 12.03 | 10.21 |
| 687-H52 | 51 | 800 | 2 | 5.95 | 5.93 | 17.94 | 14.86 |
| 678-H43 | 47 | 800 | 5 | 8.09 | | 13.94 | 14.26 |
| 676-H41 | 51 | 800 | 5 | 7.41 | | 0.00 | 14.86 |
| 673-H38 | 51 | 800 | 5 | 5.50 | 6.87 | 0.00 | 14.86 |
| 679-H44 | 20 | 800 | 5 | 1.89 | | 10.35 | 10.21 |
| 681-H46 | 24 | 800 | 5 | 3.05 | 3.74 | 10.81 | 10.81 |
| 672-H37 | 24 | 800 | 5 | 4.39 | | 11.12 | 10.81 |
| 674-H39 | 52 | 800 | 5 | 3.70 | | 15.86 | 15.02 |
| 680-H45 | 10 | 800 | 5 | 3.35 | 2.00 | 8.20 | 8.71 |
| 682-H47 | 9 | 800 | 5 | 3.32 | | 7.44 | 8.55 |
| 666-H31 | 50 | 800 | 8 | 3.42 | 7.30 | 14.53 | 14.71 |
| 665-H30 | 10 | 800 | 8 | 2.83 | 2.15 | 7.43 | 8.71 |
| 663-H28 | 44 | 800 | 8 | 4.89 | | 12.10 | 13.81 |
| 668-H33 | 8 | 800 | 8 | 3.19 | | 6.69 | 8.40 |
| 664-H29 | 24 | 800 | 8 | 3.05 | 4.00 | 10.53 | 10.81 |
| 667-H32 | 23 | 800 | 8 | 4.01 | | 10.09 | 10.66 |
| 670-H35 | 46 | 800 | 8 | 4.30 | | 14.98 | 14.11 |
| 669-H34 | 20 | 800 | 8 | 4.17 | | 9.24 | 10.21 |
| 646-H11 | 24 | 870 | 2 | 6.57 | | 11.35 | 10.81 |
| 645-H10 | 21 | 870 | 2 | 5.03 | | 10.23 | 10.36 |
| 652-H17 | 9 | 870 | 2 | 2.11 | 1.60 | 8.21 | 8.55 |
| 650-H15 | 53 | 870 | 2 | 4.94 | | 15.01 | 15.17 |
| 649-H14 | 7 | 870 | 2 | 4.58 | | 7.41 | 8.25 |
| 648-H13 | 8 | 870 | 2 | 2.55 | | 8.77 | 8.40 |
| 647-H12 | 53 | 870 | 2 | 3.57 | | 14.77 | 15.17 |
| 651-H16 | 23 | 870 | 2 | 4.42 | 3.23 | 11.53 | 10.66 |
| 653-H18 | 52 | 870 | 2 | 4.29 | 6.11 | 15.39 | 15.02 |
| 640-H5 | 21 | 870 | 5 | 4.14 | | 9.38 | 10.36 |
| 639-H4 | 23 | 870 | 5 | 4.33 | 3.73 | 10.54 | 10.66 |
| 643-H8 | 51 | 870 | 5 | 3.36 | 6.61 | 12.51 | 14.86 |
| 636-H1 | 30 | 870 | 5 | 3.48 | | 11.71 | 11.71 |
| 637-H2 | 48 | 870 | 5 | 3.53 | | 13.02 | 14.41 |
| 638-H3 | 50 | 870 | 5 | 3.84 | | 14.77 | 14.71 |
| 641-H6 | 8 | 870 | 5 | 3.32 | 1.83 | 8.53 | 8.40 |
| 659-H24 | 24 | 870 | 8 | 3.77 | | 10.66 | 10.81 |

Table 16. Time to maximum volume, Valliant liquor, page 2.

| | | | | | | | |
|---|---|---|---|---|---|---|---|
| 657-H22 | 60 | 870 | 8 | 4.38 | | 15.80 | 16.22 |
| 661-H26 | 9 | 870 | 8 | 2.44 | 2.23 | 7.02 | 8.55 |
| 655-H20 | 24 | 870 | 8 | 3.37 | | 10.29 | 10.81 |
| 662-H27 | 7 | 870 | 8 | 2.33 | | 6.12 | 8.25 |
| 656-H21 | 9 | 870 | 8 | 1.90 | | 7.25 | 8.55 |
| 660-H25 | 23 | 870 | 8 | 5.59 | 4.29 | 12.40 | 10.66 |
| 658-H23 | 53 | 870 | 8 | 5.58 | | 16.82 | 15.17 |
| 654-H19 | 50 | 870 | 8 | 4.20 | 7.35 | 14.75 | 14.71 |
| 708-H62 | 21 | 910 | 2 | 8.30 | | 11.91 | 10.36 |
| 716-H70 | 21 | 910 | 2 | 5.65 | 3.81 | 9.95 | 10.36 |
| 719-H73 | 53 | 910 | 2 | 3.92 | | 0.00 | 15.17 |
| 717-H71 | 12 | 910 | 2 | 2.12 | | 9.91 | 9.00 |
| 718-H72 | 12 | 910 | 2 | 5.33 | 2.52 | 9.65 | 9.00 |
| 709-H63 | 41 | 910 | 2 | 8.94 | | 14.50 | 13.36 |
| 711-H65 | 24 | 910 | 2 | 4.56 | | 11.04 | 10.81 |
| 715-H69 | 43 | 910 | 2 | 4.63 | | 0.00 | 13.66 |
| 720-H74 | 53 | 910 | 2 | 4.92 | 7.81 | 14.76 | 15.17 |
| 710-H64 | 28 | 910 | 2 | 7.18 | | 10.85 | 11.41 |
| 712-H66 | 7 | 910 | 2 | 4.65 | | 8.24 | 8.25 |
| 729-H83 | 48 | 910 | 5 | 2.73 | | 14.82 | 14.41 |
| 724-H78 | 22 | 910 | 5 | 2.77 | 4.59 | 9.39 | 10.51 |
| 721-H75 | 12 | 910 | 5 | 1.66 | | 7.95 | 9.00 |
| 726-H80 | 10 | 910 | 5 | 2.51 | 2.52 | 9.43 | 8.70 |
| 731-H85 | 24 | 910 | 5 | 4.59 | | 11.31 | 10.81 |
| 728-H82 | 52 | 910 | 5 | 3.05 | 8.70 | 14.81 | 15.02 |
| 725-H79 | 23 | 910 | 5 | 4.88 | | 9.69 | 10.66 |
| 722-H76 | 54 | 910 | 5 | 5.83 | | 14.15 | 15.32 |
| 727-H81 | 14 | 910 | 5 | 3.01 | | 10.35 | 9.30 |
| 730-H84 | 21 | 910 | 5 | 4.50 | | 10.90 | 10.36 |
| 734-H88 | 24 | 910 | 8 | 4.16 | | 10.94 | 10.81 |
| 737-H91 | 22 | 910 | 8 | 6.27 | 4.86 | 11.47 | 10.51 |
| 738-H92 | 53 | 910 | 8 | 7.72 | 9.40 | 16.28 | 15.17 |
| 740-H94 | 13 | 910 | 8 | 5.95 | | 9.68 | 9.15 |
| 735-H89 | 10 | 910 | 8 | 2.71 | 2.67 | 8.14 | 8.70 |
| 739-H93 | 55 | 910 | 8 | 4.41 | | 13.90 | 15.47 |
| 732-H86 | 40 | 910 | 8 | 4.62 | | 10.36 | 13.21 |
| 733-H87 | 23 | 910 | 8 | 6.02 | | 11.29 | 10.66 |
| 736-H90 | 55 | 910 | 8 | 8.33 | | 13.69 | 15.47 |
| 741-H95 | 11 | 910 | 8 | 4.76 | | 8.08 | 8.85 |

Table 17 shows the predicted and measured diameter of a 21 mg drop burning in 10.5% oxygen at 763°C. The liquor was Thilmany.

Table 17. Predicted and measured diameter vs. time for 21 mg drop

| Time, sec | Diameter/Initial diameter Meas. | Pred. |
|---|---|---|
| 0.00 | 1.00 | 1.00 |
| 0.50 | 1.03 | 1.25 |
| 1.00 | 1.15 | 1.25 |
| 1.50 | 1.25 | 1.25 |
| 2.00 | 1.77 | 1.25 |
| 2.50 | 2.00 | 1.25 |
| 3.00 | 2.26 | 1.25 |
| 3.50 | 2.50 | 1.50 |
| 4.00 | 2.53 | 1.74 |
| 4.50 | 2.66 | 2.74 |
| 5.00 | 2.93 | 3.02 |
| 5.50 | 3.01 | 3.34 |
| 6.00 | 2.99 | 3.36 |
| 6.50 | 2.96 | 3.37 |
| 7.00 | 2.86 | 3.37 |
| 7.50 | 2.72 | 3.38 |
| 8.00 | 2.70 | 3.38 |
| 8.50 | 2.67 | |
| 9.00 | 2.50 | |
| 9.50 | 2.51 | |
| 10.00 | 2.42 | |
| 10.50 | 2.28 | |
| 11.00 | 2.26 | |
| 11.50 | 2.07 | |
| 12.00 | 1.98 | |
| 12.50 | 1.76 | |
| 13.00 | 1.71 | |
| 13.50 | 1.47 | |
| 14.00 | 1.29 | |
| 14.50 | 1.11 | |
| 15.00 | 0.88 | |
| 15.50 | 0.77 | |
| 16.00 | 0.57 | |
| 16.50 | 0.54 | |

Table 18 shows the char burn times for the soda liquor, shown in Figure 23.

Table 18. Char burn times for soda liquor.

| Run | Char Mass mg | Dmax cm | Char burn time, sec Pred | Meas |
|---|---|---|---|---|
| 0% sulfur in char | | | | |
| SDA2 | 31.55 | 2.82 | 11.9 | 13.362 |
| SDA3 | 25.01 | 2.77 | 10.45 | 10.24 |
| SDA4 | 36.17 | 3.1 | 11.6 | 13.15 |
| SDA6 | 38.48 | 3.18 | 11.1 | 11.507 |
| SDA7 | 42.33 | 3.02 | 12.18 | 13.63 |
| SDA8 | 39.25 | 3.08 | 10.74 | 12.95 |
| SDA9 | 43.48 | 3.05 | 12.07 | 13.88 |
| SDA10 | 43.48 | 3 | 13.03 | 15.08 |
| SDA14 | 21.16 | 2.7 | 7.77 | 9.54 |
| SDA15 | 28.48 | 2.66 | 9.8 | 11.78 |
| 6.2% sulfur in char | | | | |
| SDC1 | 21.66 | 2.61 | 7.31 | 8.35 |
| SDC2 | 36.9 | 2.55 | 12.35 | 10.54 |
| SDC4 | 33.29 | 3.06 | 11.3 | 9.27 |
| SDC7 | 25.27 | 2.36 | 7.86 | 9.51 |
| SDC8 | 40.11 | 3 | 9.97 | 11.74 |
| SDC9 | 39.7 | 2.99 | 9.21 | 9.84 |
| SDC10 | 36.5 | 2.95 | 9.78 | 11.05 |
| SDC12 | 44.52 | 3.04 | 9.39 | 9.98 |
| SDC13 | 18.45 | 2.71 | 5.56 | 8.992 |

Table 19 shows the char burn times for kraft liquor, Valliant, which was shown in Figure 24.

Table 19. Char burn times, kraft

| Run | Temp C | Oxygen % | Dry Mass mg | Dmax cm | Char burn time Meas sec | Pred. sec |
|---|---|---|---|---|---|---|
| V51 | 800 | 2 | 4.42 | 1.01 | 30.01 | 31.75 |
| V55 | 800 | 2 | 10.61 | 1.37 | 46.25 | 47.5 |
| V52 | 800 | 2 | 22.1 | 1.67 | 92.42 | 77.5 |
| V47 | 800 | 5 | 4.42 | 782 | 9.34 | 13 |
| V37 | 800 | 5 | 10.61 | 1.08 | 15.06 | 18.8 |
| V39 | 800 | 5 | 22.1 | 1.49 | 22.43 | 25.32 |
| V33 | 800 | 8 | 4.42 | 0.706 | 4.88 | 8.5 |
| V29 | 800 | 8 | 10.61 | 0.995 | 8.17 | 12 |
| V31 | 800 | 8 | 22.1 | 1.39 | 12.17 | 15.7 |
| V13 | 870 | 2 | 4.42 | 0.813 | 17.64 | 22.6 |
| V16 | 870 | 2 | 10.61 | 1.104 | 29.87 | 34 |
| V18 | 870 | 2 | 22.1 | 1.539 | 54.92 | 55.12 |
| V6 | 870 | 5 | 4.42 | 0.853 | 5.24 | 8.85 |
| V4 | 870 | 5 | 10.61 | 0.996 | 6.05 | 12.45 |
| V3 | 870 | 5 | 22.1 | 1.343 | 20.3 | 23.12 |
| V27 | 870 | 8 | 4.42 | 0.68 | 4.78 | 7.82 |
| V25 | 870 | 8 | 10.61 | 1.112 | 7.18 | 9.52 |
| V19 | 870 | 8 | 22.1 | 1.579 | 12.43 | 13.3 |
| V66 | 910 | 2 | 4.42 | 0.927 | 22.39 | 23.25 |
| V65 | 910 | 2 | 10.61 | 1.097 | 33.41 | 35 |
| V74 | 910 | 2 | 22.1 | 1.476 | 43.94 | 44.75 |
| V80 | 910 | 5 | 4.42 | 0.924 | 8.03 | 9.25 |
| V85 | 910 | 5 | 10.61 | 1.032 | 12.62 | 15.25 |
| V82 | 910 | 5 | 22.1 | 1.459 | 17.88 | 19.55 |
| V89 | 910 | 8 | 4.42 | 0.863 | 6.3 | 6.8 |
| V88 | 910 | 8 | 10.61 | 1.123 | 7.03 | 8.95 |
| V92 | 910 | 8 | 22.1 | 1.462 | 12.3 | 13.3 |